AD-A165 655 STRUCTURE OF HIGH-SPEED SPRAYS(U) PRINCETON UNIV NJ 1/2
DEPT OF MECHANICAL AND AEROSPACE ENGINEERING
F V BRACCO FEB 85 ARO-18333.7-EG DAAG29-81-K-0135
UNCLASSIFIED F/G 21/4 NL

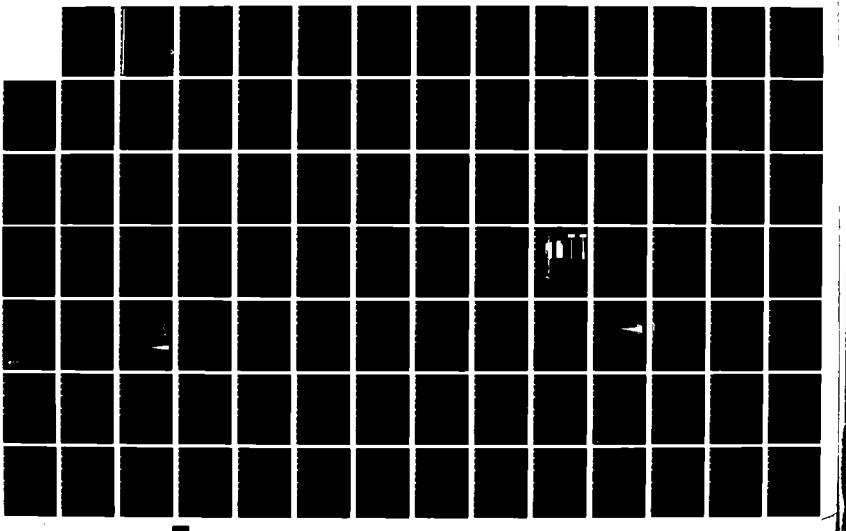

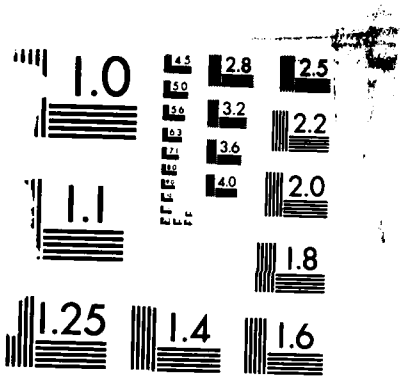

MICROCOPY RESOLUTION TEST CHART
NATIONAL BUREAU OF STANDARDS-1963-A

AD-A165 655

ARO 18333.7-EG

STRUCTURE OF HIGH-SPEED SPRAYS

Contract DAAG29-81-K-0135
U.S. Army Research Office
July 81 - June 84

FINAL TECHNICAL REPORT

By

F.V. Bracco

DTIC
ELECTE
MAR 21 1986
S D
A

DTIC FILE COPY

Princeton University
Department of Mechanical and Aerospace Engineering
Princeton, N.J. 08544

February 1985

This document has been approved for public release and sale; its distribution is unlimited.

ABSTRACT

During the 3 years of this ARO Grant we: measured and computed the drop size in the immediate vicinity of the nozzle in Diesel-type sprays [1,8]; measured (Appendix B and Ref. 9) and computed (Appendix C and Ref. 10) the drop velocities in the farfield of non vaporizing Diesel-type sprays; measured [11] (and are computing) the drop velocities in the farfield of vaporizing Diesel-type sprays. The ~~overall~~ conclusions are that: the breakup of full-cone Diesel jets is due primarily to aerodynamic interaction between the liquid surface and the chamber gas; the initial average size and velocity of the drops formed by the breakup of the outer surface of the jet can now be estimated and so can the length of the intact core but with greater uncertainty; after breakup a steady full-cone spray undergoes a development similar to that of incompressible jets; in Diesel engines it is the development region that is of importance; the major parameter in the difference between full-cone sprays and incompressible jets is the liquid-to-gas density ratio; in the absence of vaporization the most advanced of the available spray model reproduce full-cone sprays with adequate realism for applications; it is not yet known how vaporization changes the structure of these sprays and if available models adequately reproduce the changes. We also produced a number of summary papers on the mechanism of atomization (Appendix A and Refs. 12,13) and on the structure of Diesel sprays (Appendix D and Ref. 14). One student received his Ph.D. on this subject and is now at the Research Laboratories of GM (Dr. K.-J. Wu) and several staff members and visitors worked with us and have now moved on to other positions (Drs. R.D. Reitz, D.A. Santavicca, A. Coghe, Y. Onuma, and P. Felton)

QUALITY INSPECTED 3

Accession For
NTIS GRA&I
DTIC TAB
Unannounced
Justification
By
Distribution/
Availability Codes
Avail and/or
Special

REPORT

Four papers are given in the appendices. Each of the four papers is a summary of much work conducted under this Grant and the following paragraphs are a summary of the summaries.

In 1972-1976, we made some multi-dimensional computations of engine sprays (e.g., CST, Vol. 8, pp. 69-84, 1973; SAE TRANS., Vol. 84, pp. 3317-3340; 1975; CST, Vol. 12, pp. 63-74, 1976; AIAA J., Vol. 16, pp. 1053-1061, 1978). Those were the first multi-dimensional two-phase engine flow computations and from them we learned that quantitative knowledge of the mechanism of break-up of fuel jets and of the structure of dense sprays was so poor, and their effects so important, that the reliability of even the computed trends was questionable.

Vast qualitative knowledge of sprays was accumulated in the 30's, primarily at NACA, often with astute experimental techniques. But when space-resolved computations of in-cylinder events became necessary and feasible, the corresponding space-resolved quantitative spray information simply was missing.

Thus, in 1976 we started a program of detailed measurements of the break-up of fuel jets to establish its mechanism with the final objective of determining equations for the initial drop sizes and velocities. ARO provided its first 3-year support for the period July 78 - June 81. Full-cone sprays from single cylindrical orifices were injected into compressed gases in a constant-volume vessel and the spray angle and the tip penetration velocity were measured with photographic techniques in a large variety of conditions. Room temperature was employed and vaporization was negligible.

During the second 3-year ARO grant for the period July 81-June 84 drop sizes [1] were measured by photography in the immediate vicinity of the nozzle

exit. Also measured by LDV were drop velocities within nonvaporizing sprays at distances between 2.3 cm and 10 cm from the nozzle (Appendix B). The diameter of the nozzles used was between 76 and 335 mm. Although drop sizes and velocities had been measured before, they had not been measured respectively in the immediate vicinity of the nozzle exit and within very dense sprays as we did.

With the help of the new data, we sorted out the large amount of often-contradicting hypotheses that had been made about the formation of Diesel-type sprays and concluded that atomizing liquid jets are broken up by aerodynamic forces that are due to the liquid-gas relative velocity. These forces selectively amplify liquid perturbations that are generated within the nozzle. This particular mechanism was first proposed, in a quantitative way, by W.E. Ranz [2]. We now understand, or we think we do, the relationship between the many modes of breakup of liquid jets. They are different manifestations of the same forces that align themselves differently under different conditions. These forces act on perturbations of the liquid-gas interface. The perturbations, in turn, are often generated within the nozzle. At low jet velocities, the nozzle perturbations actually are not very important, but they become progressively more significant as the jet velocity increases (and the intact length decreased) and are essential components of the breakup in the atomization regime, i.e. for engine fuel jets. The mechanisms of breakup of round liquid jets are discussed in Appendix A.

Actually, as far as the formation of engine sprays is concerned, we get several lucky breaks. Practical nozzle geometries do not vary much, due to construction considerations, and influence mostly the initial angle of the spray and, possibly, the solid core length [3]. Both angle and solid core length are

influenced also, and much more markedly and importantly, by the gas-liquid-density ratio. Significantly, they are not strongly affected by any of the other many parameters (Eqs. 11 and 10a of App. A, also Eqs. 15 and 17 of App. D) except for the solid core length that is proportinal also to the nozzle diameter (Eq. 17 of App. D). The initial size of the drops that are formed by the breakup of the outer surface of the liquid jet is determined mostly by the Weber number (Eq. 12 of App. A, also Eq. 16 of App. D). The predictions of the initial angle has now been supported by numerous measurements. That of the initial drop size has been evaluated only preliminarily [1]. But the prediction of the intact core length is both weaker and largely untested. It is weaker because it is based on the questionable assumption that the stability considerations that apply to the outer surface of the liquid also apply unchanged within the jet and all the way down to its axis. It is largely untested because the length of the liquid core has been measured only once [4] and with a technique that can be criticized.

Getting back to our overview and assuming that we can estimate the initial angle of the spray, the initial size of the drops, and the shape and length of the solid core, i.e. the drop generating surface, we can then compute the subsequent development of the spray. In particular, we can compute the farfield quantities that we measured (Appendix B), that is: the axial and radial velocity distributions of the drops at all radial and axial positions within the spray and for a variety of liquid and gas conditions.

The computations and comparisons with the measured drop velocity are discussed in Appendix C. They clearly show that our model for Diesel sprays accurately predicts the average values of the sprays parameters but not the the

fluctuating component of the drop velocity. More work is now needed on the interaction between droplet motion and gas turbulence. In Appendix D, the fourth appendix, we have summarized what we have learned about the formation and structure of full-cone sprays in all of these studies.

All the measurements and computations that we have discussed so far were made under Diesel-type conditions except for the temperature that had its room value. It has been advisable to do so to avoid the trap of having too many processes to sort out simultaneously. Actually we have now completed a second round of drop velocity measurements similar to those discussed in Appendix B but in vaporizing sprays. We are in the process of studying this new experimental information and then we intend to make a second set of computations and comparisons similar to those of Appendix C.

Notice, however, that to make measurements in vaporizing sprays, first we had to modify our current experimental apparatus. It is difficult to obtain controlled, repeatable gas and liquid environments above room temperature with a closed gas vessel of limited size. Vaporization and wall heat losses cool the gas and condensation on windows limits optical access, at very least complicating repeatability. Also, the need to empty the vessel after each injection conflicts with the long time required to gather the large amount of data associated with detailed measurements. Thus we decided to build a continuous flow system and, in order to control separately liquid and gas temperature, it was also necessary to redesign the fuel injection system to allow for its water cooling.

Much work was al ɔ done on, and with, the spray model to which we have often referred. This model is important because it represents, i.e. embodies,

our current understanding of the structure of these sprays and because is already in use in several industries, including Cummins [5-7] and Komatsu.

The model computes the unsteady penetration and the steady state of axisymmetric dense sprays using information about drop sizes and velocities from the break-up of the fuel jet at the nozzle exit as input. The model solves the coupled conservation equations for the gas and liquid with an Eulerian scheme for the gas and a Lagrangian scheme for the drops. The model includes exchange functions for droplet coalescence, grazing collisions and accounts for the effect of liquid volume fraction on the rates of exchange of mass, momentum and energy between the gas drops. The functions representing these thick spray phenomena have been deduced from experimental and theoretical work in cloud physics, fluidized and packed beds, and transport processes in fixed arrays of spheres.

In the model, the gas flow-field and droplet size, velocity and temperature probability distribution functions are computed as functions of position and time in the spray. The optically thick region of the spray close to the nozzle exit is also computed. This region of dense sprays is presently inaccessible to standard probing measurements and the model offers a means to bridge the measurements of the jet break-up process at the nozzle exit to the LDV measurements of droplet velocity and size distributions within the optically-thinner downstream spray.

At present there are three advanced spray models: the CONCHAS-SPRAY of the Los Alamos National Laboratory, the RPM-SPRAY of Gosman, and ours. These models differ both in their physics and in their numerics. But they also overlap. Thus Gosman and we use k-e gas turbulence submodels whereas LANL uses a k-sub-

grid. For full-cone sprays, we all use the initial conditions from the jet break-up process determined at Princeton. We include computations of drop collisions and coalescence and of the effect of the gas-volume fraction on the gas-liquid rates of exchange of mass, momentum, and energy. Gosman does not consider such processes and LANL has recently adopted our collisions and coalescence submodel. We all use the stochastic technique of LANL for the computation of drop events, but somewhat different numerical techniques for the solution of the equations.

We believe that this diversity is very healthy. It allows for the evaluation of different approaches while tested best features are eventually adopted by all. Moreover the three efforts complement each other very well through differences in emphasis. We have concentrated on detailed testing of the physics in our model at the expense of model flexibility. LANL has adopted the greatest flexibility and its CONCHAS-SPRAY is the most general of the codes for engine computations. Gosman's model falls in between CONCHAS-SPRAY and our model.

In summary then, during the 3 years of this ARO Grant we: measured and computed the drop size in the immediate vicinity of the nozzle in Diesel-type sprays [1,8]; measured (Appendix B and Ref. 9) and computed (Appendix C and Ref. 10) the drop velocities in the farfield of non vaporizing Diesel-type sprays; measured [11] (and are computing) the drop velocities in the farfield of vaporizing Diesel-type sprays. The overall conclusions are that: the breakup of full-cone Diesel jets is due primarily to aerodynamic interaction between the liquid surface and the chamber gas; the initial average size and velocity of the drops formed by the breakup of the outer surface of the jet can now be estimated and so can the length of the intact core but with greater uncertainty; after breakup a steady full-cone spray undergoes a development similar to that of

incompressible jets; in Diesel engines it is the development region that is of importance; the major parameter in the difference between full-cone sprays and incompressible jets is the liquid-to-gas density ratio; in the absence of vaporization the most advanced of the available spray model reproduce full-cone sprays with adequate realism for applications; it is not yet known how vaporization changes the structure of these sprays and if available models adequately reproduce the changes. We also produced a number of summary papers on the mechanism of atomization (Appendix A and Refs. 12,13) and on the structure of Diesel sprays (Appendix D and Ref. 14). One student received his Ph.D. on this subject and is now at the Research Laboratories of GM (Dr. K.-J. Wu) and several staff members and visitors worked with us and have now moved on to other positions (Drs. R.D. Reitz, D.A. Santavicca, A. Coghe, Y. Onuma, and P. Felton).

REFERENCES

1. Wu, K.-J., "Atomizing Round Jets," Ph.D. Thesis No. 1612, Department of Mechanical and Aerospace Engineering, Princeton University, Princeton, NJ, July 1983.

2. Ranz, W.E., "Some Experiments on Orifice Sprays," Can. J. Chem. Eng., Vol. 36, pp. 175-181, 1958.

3. Arai, M., Tabata, M., Hiroyasu, H., and Shimizu, M., "Disintegrating Process and Spray Characterization of Fuel Jet Injected by a Diesel Nozzle," SAE Paper 840275, International Congress and Exposition, February 1984.

4. Hiroyasu, H., Shimizu, M., and Arai, M., "The Breakup of High Speed Jets in a High Pressure Gaseous Atmosphere," ICLASS-82, Madison, WI, 1982.

5. Yu, R.C., Kuo, T.-W., Shahed, S.M., and Chang, T.W., The Effect of Mixing Rate, End of Injection, and Sac Volume on Hydrocarbon Emissions from a D.I. Diesel Engine," SAE Paper 831294, International Off-Highway Meeting and Exposition, Wilwaukee, Wisconsin, September 1983.

6. Kuo, T.-W., Yu, R.C., and Shahed, S.M., "A Numerical Study of the Transient Evaporating Spray Mixing Process in the Diesel Environment," SAE Paper 831735, Fuels and Lubricants Meeting, San Francisco, California, October 1983.

7. Kuo, T.-W., "Modeling of Transient Evaporating Spray Mixing Process: Effect of Injection Characteristics," SAE Paper 840226, International Congress and Exposition, Detroit, Michigan, February 1984.

8. Wu, K.-J., Reitz, R.D., and Bracco, F.V., "Measurements of Drop Sizes at the Spray Edge Near the Nozzle in Atomizing Liquid Jets". Submitted for publication.

9. Wu, K.-J., Coghe, A., Santavicca, D.A., and Bracco, F.V., "LDV Measurements of Drop Velocity in Diesel-Type Sprays," accepted by the AIAA Journal.

10. Martinelli, L., Reitz, R.D., and Bracco, F.V., "Comparisons of Computed and Measured Dense Spray Jets", Ninth International Colloquium on Dynamics of Explosions and Reactive Systems, Poitiers, France, 1983, to appear in the AIAA Progress in Astronautics and Aeronautics Series.

11. Felton, P., Onuma, Y., and Bracco, F.V., "LDV Measurements of Drop Velocity in Vaporizing Diesel-Type Sprays", to be submitted to the AIAA Journal.

12. Reitz, R.D. and Bracco, F.V., "On the Mechanism of Atomization of a Liquid Jet," Physics of Fluids, Vol. 25, No. 10, pp. 1730-1742, October 1982.

13. Reitz, R.D. and Bracco, F.V., "Mechanisms of Breakup of Round Liquid Jets", Volume III - Gas Liquid Flows, Chapter 11, Encyclopedia of Fluid

Mechanics, 1984, to be published in Encyclopedia of Fluid Mechanics, N.P. Cheremisinoff, Editor, Gulf Publishing.

14. Bracco, F.V., "Structure of High-Speed Full-Cone Sprays", to appear in "Recent Advanced in Gas Dynamics", (C. Casci, editor), Plenum Publishing Corp., N.Y., N.Y., 1983.

MECHANISMS OF BREAKUP OF ROUND LIQUID JETS

Volume III - Gas Liquid Flows, Chapter 11
ENCYCLOPEDIA OF FLUID MECHANICS

February 9, 1984

R.D. Reitz† and F.V. Bracco
Mechanical and Aerospace Engineering Department
Princeton University
Princeton, New Jersey 08544

† Now at Fluid Mechanics Department
General Motors Research Laboratories
Warren, Michigan 48090

TO BE PUBLISHED IN

ENCYCLOPEDIA OF FLUID MECHANICS
N.P. CHEREMISINOFF, EDITOR
GULF PUBLISHING

TABLE OF CONTENTS

ABSTRACT

The mechanisms of breakup of liquid jets injected from a single hole orifice into a gaseous medium are reviewed. As the jet velocity is increased, or as other operating conditions are changed appropriately, four breakup regimes are identified. The four regimes correspond to different combinations of liquid inertia, surface tension and aerodynamic forces acting on the jet. They have been called the Rayleigh, the first wind-induced, the second wind-induced and the atomization regimes. In each of the four regimes, the outcome is also influenced by the initial state of the jet. This influence appears to grow in importance with increasing jet velocity. The existence of the regimes is consistent with a stability analysis of the liquid surface. It appears that the stability analysis can account also for the influence of the initial state of the jet but little work has been done in this area and the breakup process at high jet velocities is understood more qualitatively than quantitatively at present.

1. INTRODUCTION

The mechanisms of jet breakup discussed here result from the steady injection of a liquid through a single hole nozzle into a quiescent gas. The complexity of the breakup process is due to the unusually large number of parameters which influence it, including the details of the design of the nozzle, the jet's velocity and turbulence, and the physical and thermodynamic states of both liquid and gas. In this work we discuss a framework by means of which some of the underlying mechanisms of breakup can be organized and, eventually, be better understood.

The approach followed is to divide the jet breakup phenomena of interest into various breakup regimes. These regimes reflect differences in the appearance of the jet as the operating conditions are changed. We then attempt to relate these regimes to limiting cases of a stability analysis of liquid jets. The analysis considers the growth of initial perturbations of the liquid surface and includes the effects of liquid inertia, surface tension, viscous and aerodynamic forces on the jet. The theory is found to offer a reasonably complete description of the breakup mechanisms of low speed jets. For high speed liquid jets however, the initial state of the jet appears to be progressively more important and less understood. We will summarize the results of recent research aimed at closing this gap.

It should be pointed out that we consider only fluid-dynamic instabilities and that there are other causes of breakup such as superheating[1], electrostatic charge[2], acoustical excitation[3], and chemical reactions. Even in the field of fluid-dynamic instabilities there are difficulties; many parameters influence the outcome; the magnitude of these parameters vary over broad ranges; there are no generally accepted theories, regimes, or even terminology. Thus even comparisons of results and statements of various authors are complicated. But when conditions are properly identified and nomenclature difficulties are overcome, the framework to be presented in

this work is found to be compatible with much of the published work.

1.1 The Jet Breakup Regimes

If all other parameters are kept constant, the jet velocity becomes a convenient quantity to introduce various regimes.

Grant and Middleman[4] reviewed the behaviour of low speed jets and reported the results in the form of a breakup curve (Fig. 1) which describes the unbroken length of the jet, L_1, as a function of the jet velocity, U. Once a jet is formed (point C, Fig. 1) the jet breakup length at first increases linearly with increasing jet velocity. Thereafter it reaches a maximum (point E) and then decreases. These first two breakup regimes are reasonably well understood, as will be seen below, and here are called the Rayleigh (CD) and first wind-induced breakup (EF) regimes. A feature of breakup in these two regimes is that drops are pinched off from the end the jet and their sizes are comparable to that of the jet (see also Figs. 5a and 5b).

For higher velocity jets beyond the point F there still remains some confusion over the true shape of the breakup curve. Haenlein[1] reported that the breakup length remains constant, or decreases slightly, with increasing velocity (curve FG, Fig. 1) and then it abruptly reduces to near zero beyond point G. This suggests the existence of at least two more breakup regimes, each causing new features in the breakup curve. However, McCarthy and Malloy[4] and Grant and Middleman[4] report that the breakup length initially increases (curve FH).

It should be noted that the definition and measurement of the intact length becomes increasingly difficult as U is increased, as pointed out also by Grant and Middleman[4]. At sufficiently high velocities, the jet surface is disrupted prior to the breakup of the jet core and the use of only one breakup length is no longer a complete measure of the jet

stability. Thus we distinguish between the intact-surface length, L_1, and the intact-core length, L_2. In the Rayleigh and first wind-induced regimes the jet breaks up simultaneously over the entire cross-section and the two lengths coincide. In the second wind-induced and atomization regimes which will be described next, the disruption starts at the jet surface and eventually reaches the jet axis so that at least two lengths are necessary to identify the gross features of the breakup.

We call the atomization regime that regime in which the intact-surface length is zero (but the intact-core length is not necessarily zero) so that L_1 versus U follows the trend suggested by Haenlein[8], viz. the breakup length goes to zero beyond the point G (H) in Fig. 1. Here the jet surface appears to break up immediately at the nozzle exit and drops are formed that are much smaller than the nozzle diameter (see Fig. 5d). Although we find this definition of the atomization regime unequivocal and useful, we must point out that the term atomization has also been used by other authors in a variety of different contexts. This regime is of interest in many fuel injection applications.

For breakup in the second wind-induced regime (curve FG or FH, Fig. 1), both the intact-surface length and the intact-core length are finite and drops are formed with sizes also much smaller than the nozzle diameter (see Fig. 5c).

To introduce the four regimes we have used the injection velocity as a parameter and have kept all other parameters constant. Actually dimensionless numbers separate the various regimes as will be discussed in the following sections. Indeed the high velocity jets in jet cutting applications, for example, exhibit long intact-surface lengths even though they are faster than atomizing fuel jets, but the two families of jets differ in nozzle design, gas density, surface tension and liquid viscosity.

Attempts have been made by various authors to offer criteria with which to demarcate breakup regimes. For example, Miesse' correlated breakup

regime data and presented the results in a form suggested by Ohnesorge[9] as shown in Fig. 2. The boundaries of the regimes are represented by oblique straight lines on a graph of ln Z (a function of the physical properties of the liquid and the nozzle diameter alone) versus ln Re_l. Unfortunately, this method of correlation does not include the effect of the initial state of the jet (that is influenced, for example, by the nozzle design) nor the effect of the ambient gas density (pressure), which according to Torda[9] modifies the graph as shown by the dashed lines. These modified boundary curves show, for example, that atomization can be achieved at lower injection velocities by injecting into a compressed gas.

The effect of ambient gas density on jet breakup regimes was discussed by Ranz[10] who argued that the Weber number We_2 should be a controlling parameter. He offered the criterion $We_2 > 13$ for the onset of atomization. However, it should be noted again that his definition of the term atomization differs from ours - he does not refer to the state of the jet itself but instead refers to the process of disintegration of already formed droplets during their flight within a spray. He argued that the criteria for the formation and the subsequent further breakup of the droplets should be the same since when the inertial stresses developed by the surrounding gas exceed the surface tension stresses opposing the deformation sufficiently, the liquid drop (or ligament in the formation process) will subdivide into smaller units. But a Weber number correlation by itself is still incomplete since now the liquid viscosity is not accounted for.

This latter objection can be removed (at least conceptually) by combining Fig. 2 with a gas density parameter as is shown qualitatively in Fig. 3, taken from Reitz[11]. Still, different sets of surfaces should be given in Fig. 3 to account for the effects of different initial states of the jet. Thus completely satisfactory correlations for the regime boundaries are not yet available. Indeed many authors do not even distinguish between the two wind-induced regimes as can be seen in Fig. 2. Finally, as previously stated, we feel that part of the

difficulty in interpreting published results is due to a lack of agreed upon terminology in the field, and insufficient characterization of the injection system and the nozzle geometry.

2. LINEAR STABILITY ANALYSIS

We consider a cylindrical liquid jet issuing from a circular orifice into a stationary incompressible gas. The stability of the liquid surface to perturbations is examined using a first order linear theory which ultimately leads to a dispersion equation, Eq. (5) below. This equation relates the growth rate, ω, of an initial perturbation of infinitesimal amplitude, η_o, to its wavelength λ (wavenumber $k=2\pi/\lambda$). The relationship also includes the physical and dynamical parameters of the liquid jet and the surrounding gas. The present treatment will be seen (in Section 3) to unify the results of Levich[12], Stirling and Sleicher[13] and other authors who have treated individual jet breakup regimes.

The column of liquid is assumed to be infinite in the axial direction and a cylindrical polar coordinate system is used which moves with the jet velocity, U. Imposed on the initially steady motion is an infinitesimal axisymmetric surface displacement, one Fourier component of which, has the form

$$\eta = R(\eta_o e^{ikz+\omega t})$$

The linearized hydrodynamical equations are

$$\frac{\partial u_1}{\partial z} + \frac{1}{r}\frac{\partial}{\partial r}(rv_1) = 0$$

$$\frac{\partial u_1}{\partial t} = -\frac{1}{\rho_1}\frac{\partial p_1}{\partial z} + \nu_1\{\frac{\partial^2 u_1}{\partial z^2} + \frac{1}{r}\frac{\partial}{\partial r}(r\frac{\partial u_1}{\partial r})\} \qquad (1)$$

$$\frac{\partial v_1}{\partial t} = -\frac{1}{\rho_1}\frac{\partial p_1}{\partial r} + \nu_1\{\frac{\partial^2 v_1}{\partial z^2} + \frac{\partial}{\partial r}(\frac{1}{r}\frac{\partial}{\partial r}rv_1)\}$$

where u_1, v_1 and p_1 are small axisymmetric velocities and pressure. With the assumption that $\eta<<a$, the kinematic, tangential stress and normal stress equations are to first order

$$v_1 = \frac{\partial \eta}{\partial t}$$

$$\frac{\partial u_1}{\partial r} = -\frac{\partial v_1}{\partial z} \qquad (2)$$

$$-p_1 + 2\mu_1 \frac{\partial v_1}{\partial r} - \frac{\sigma}{a^2}(\eta + a^2 \frac{\partial^2 \eta}{\partial z^2}) + p_2 = 0 \ .$$

The inertial effects of the gas enter through the gas pressure p_2. This is found from the linearized inviscid equations of motion for the gas

$$\frac{\partial u_2}{\partial z} + \frac{1}{r}\frac{\partial}{\partial r}(r v_2) = 0$$

$$\frac{\partial u_2}{\partial t} + U(r)\frac{\partial u_2}{\partial z} + \frac{dU}{dr} v_2 = -\frac{1}{\rho_2}\frac{\partial p_2}{\partial z} \qquad (3)$$

$$\frac{\partial v_2}{\partial t} + U(r)\frac{\partial v_2}{\partial z} = -\frac{1}{\rho_2}\frac{\partial p_2}{\partial r}$$

where the mean gas motion above the liquid surface is given by $U(r)$. The boundary conditions are

$$v_2 = \frac{\partial \eta}{\partial t} + U\frac{\partial \eta}{\partial z} \quad \text{at } r = a$$

$$u_2,\ v_2,\ p_2 \to 0 \quad \text{as } r \to \infty \ .$$

Equations (1) are solved by introducing a stream function ψ_1, and a velocity potential ϕ_1 and by seeking wave solutions of the form

$$\phi_1 = \Phi_1(r)\, e^{ikz+\omega t} \text{ and } \psi_1 = \Psi_1(r)\, e^{ikz+\omega t}.$$

Solutions free from singularities on the axis r=0 are found to be $\Phi_1 = C_1 I_0(kr)$ and $\Psi_1 = C_2 r I_1(\ell r)$, where C_1 and C_2 are arbitrary constants, and the liquid pressure can then be found from the relation $p_1 = -\rho_1 \partial \phi_1 / \partial t$.

For the gas flow, Eqs. (3) can be simplified by defining a stream function $\psi_2 = (U - i\omega/k)\eta f(r)$. This leads to an Orr-Sommerfeld equation

$$\frac{d^2 f}{dr^2} + \left(\frac{2U'r}{U - i\omega/k} - 1\right)\frac{d(f/r)}{dr} - k^2 f = 0$$

with $f(r=a) = 1$, and $f(r\to\infty) = 0$. The equation for the gas pressure is

$$p_2 = -\rho_2 \eta (U - i\frac{\omega}{k})^2 \left(\frac{df}{dr} - \frac{f}{r}\right) \ . \qquad (4)$$

Here the arbitrary constant of integration has been set equal to zero. If the gas velocity profile U(r) is known, the gas pressure at the jet surface can be determined from Eq. (4) for use in Eq. (2). For the special case of slip at the gas-liquid interface, U(r)=U=constant, and the gas surface pressure is .

$$p_2 = -\rho_2(U-i\frac{\omega}{k})^2 k\eta \frac{K_0(ka)}{K_1(ka)} \quad .$$

Finally, substituting these relationships into Eqs. (2) yields

$$\begin{aligned} \omega^2 + 2\nu_1 k^2\omega[&\frac{I_1'(ka)}{I_0(ka)} - \frac{2k\ell}{k^2+\ell^2}\frac{I_1(ka)}{I_0(ka)}\frac{I_1'(\ell a)}{I_1(\ell a)}] \\ &= \frac{\sigma k}{\rho_1 a^2}(1-k^2a^2)\left(\frac{\ell^2-k^2}{\ell^2+k^2}\right)\frac{I_1(ka)}{I_0(ka)} \\ &+ \frac{\rho_2}{\rho_1}(U-i\omega/k)^2k^2\left(\frac{\ell^2-k^2}{\ell^2+k^2}\right)\frac{I_1(ka)K_0(ka)}{I_0(ka)K_1(ka)} \end{aligned} \qquad (5a)$$

which is the governing dispersion relationship. Equation (5a) may for brevity be written in nondimensional form as

$$\beta^2 + 2Z k^2a^2F_1\,\beta = ka(1-k^2a^2)F_1 + We_2\,k^2a^2F_2 \qquad (5b)$$

where $\beta=\omega\sqrt{\rho_1 a^3/\sigma}$, $Z=\mu_1/\sqrt{\rho_1\sigma d}$ and $We_2=\rho_2U^2d/\sigma$ and the F's are dimensionless ratios of Bessel functions and wave numbers.

3. BREAKUP REGIMES AND THE DISPERSION EQUATION

In this Section we attempt to relate the mechanisms of breakup in the four jet breakup regimes to limiting cases of the linear stability analysis of Section 2. This theory offers a unified approach for the organization of the jet breakup phenomena but is not complete mostly because it does not account explicitly for different initial states of the jet.

3.1 Rayleigh Breakup Regime

Rayleigh[14] made substantial contributions to the understanding of the stability of low speed jets. He obtained a dispersion equation for the growth of axisymmetric surface disturbances by equating the potential and kinetic energies of an inviscid jet. With the hypothesis that that disturbance with the maximum growth rate would lead to the destruction of the jet, he also obtained an expression for the droplet size, assuming that it would be of the order of the wavelength of this disturbance.

For the special case $Z = 0$ and $We_2 = 0$ (inviscid liquid jet at low velocity) the dispersion Equation (5a) (cf. also Eq. [5b]) becomes

$$\omega^2 = \frac{\sigma k}{\rho_1 a^3} (1 - k^2 a^2) \frac{I_1\{ka\}}{I_0\{ka\}} \qquad (6)$$

which is the same as Rayleigh's result. This equation predicts that the jet surface is unstable for all wavenumbers with $ka<1$ and the corresponding wavegrowth curve is given in Fig. 4.

This wavegrowth curve can be found experimentally by vibrating low speed jets at various frequencies and by measuring the growth rate of the axisymmetric surface oscillations. The corresponding measurements of Donnely and Glaberson[15] given in Fig. 4 show excellent agreement with the first order theory. Differentiating Eq. (6) shows that the maximum growth rate is

$$\omega_m \cong 0.34 \left(\frac{\sigma}{\rho_1 a^3}\right)^{1/2} \quad \text{at } k \cong 2\pi/9.02a$$

and if the initial disturbance η_o of the most unstable wave grows exponentially to a magnitude 'a' in time T, it follows that the breakup length of the jet (the position of the point of droplet formation) then on average will be

$$L_1 = UT = U \ln (a/\eta_o) / \omega_m \tag{7}$$

This linear dependence of L_1 on U was seen in Fig. 1 for low velocity jets in the Rayleigh breakup regime.

The parameter $\ln (a/\eta_o)$ has been determined experimentally. It lies in the range 11-16 [16] but it has been found to be weakly related to the Ohnesorge number Z [17]. The theoretical influence of the liquid viscosity is found by retaining the term involving Z in Eq. (5b). For large Z (high liquid viscosity) the maximum wavegrowth rate is

$$\omega_m = \frac{1}{2\sqrt{2}} \left(\frac{\sigma}{\rho_1 a^3}\right)^{1/2} \frac{1}{1 + 3Z} \quad \text{at } k = \frac{1}{a\sqrt{(Z+2)}}$$

where ka has been assumed to be small and the Bessel functions and their arguments have been replaced by their asymptotic values. This relationship was first obtained by Weber[18]. His analysis showed that the effect of the increased liquid viscosity is to move the most unstable wave to longer wavelengths without altering the value of the stability boundary, ka=1. The jet breakup agency remains the destabilizing combination of surface tension and inertia forces on the jet.

The above analysis predicts that the jet breakup yields droplets many nozzle diameters downstream of the nozzle. The drop diameters are larger than that of the jet and a photograph typical of jet breakup in this regime is shown in Fig. 5a, taken from Lee and Spencer[19].

To estimate the droplet size, Rayleigh assumed that all of the liquid enclosed within the wave forms the volume of the newly created drop when

the surface wave amplitude equals the jet radius. However, as pointed out by Wang[20] when the wave amplitude becomes comparable to the jet radius, the surface deformation is observed to be non-sinusoidal due to nonlinear effects. Also, mass is only conserved to first order in the first order stability analysis. Yuen[21] and Nayfey[22] retained higher order terms in their jet stability analysis and Rutland and Jameson[23] demonstrated that this improved theory also predicts the existence of satellite droplets formed between the primary drops. Interestingly, LaFrance[24] showed that the drop sizes are not influenced by the magnitude of the initial disturbances to the jet.

3.2 First Wind-Induced Breakup Regime

The second term on the right hand side of Eqs. (5) becomes important when the jet velocity (for example) is increased. In this case the inertial effects of the surrounding gas can no longer be neglected and the Weber number We_2 becomes a controlling parameter in the dispersion equation. Weber[18] showed that the effect of the environment on the jet is to enhance the growth rate of disturbances, leading to earlier breakup of the jet. He obtained the result

$$\omega^2 + 3\nu_1 k^2 \omega = \frac{\sigma}{2\rho_1 a^3}(1 - k^2a^2)\, k^2a^2 + \frac{\rho_2}{\rho_1}\,\frac{U^2k^2a^2}{2a^2}\,\frac{K_0(ka)}{K_1(ka)} \qquad (8)$$

which can also be found from Eqs. (5) in the limit $ka < 1$. Computations of the maximum wave growth rate now show that the jet breakup length equation, Eq. (7), becomes a nonlinear formula which must be solved numerically. It indeed predicts that the breakup length L_1 decreases with increasing jet velocity (Fig. 1, curve EF). However the predicted value of the maximum in the breakup curve (Fig. 1, point E) fails to agree with experimental results, since Weber's theory is found to overestimate the aerodynamic effect of the gas. This has led many investigators to attempt modifications to Eq. (8).

Fenn and Middleman[25] argued that the viscosity of the gas should also be

considered in a more complete analysis. The effect of the gas viscosity enters through the normal and tangential stress boundary conditions Eqs. (2) and was neglected by Weber (also in the linear stability analysis of Section 2). The inviscid gas approximation implies slip at the gas liquid interface.

Benjamin[24] showed that if the gas boundary layer is thin compared to the surface wave wavelength (high gas Reynolds numbers) then the energy transmitted between the gas and the liquid by normal stresses (aerodynamic effect) is large compared to that transmitted by shear stresses (viscous effect) , and their ratio is independent of the Reynolds number. However, for finite Reynolds numbers the magnitude of the fluctuating pressure component p_2 which is in phase with the wave elevation (the part responsible for energy transfer) becomes reduced. Based on these results, Sterling and Sleicher[13] introduced an attenuation coefficient C, multiplying p_2 with $C = 1-h(ka,Re_2)$. The function, h, increases as k increases and decreases to zero as the Reynolds number becomes large. They found that C could be replaced by a constant, noticing that the wavenumber and the Reynolds number move in opposite directions as the aerodynamic effects increase.

This modification of Weber's theory with C = 0.175 multipying the second term on the right hand side of Eqs. (5) agrees well with experimental results. The numerical results of Sterling and Sleicher[13] then show that the point E in Fig. 1 is reached when $We_2 = 1.2 + 3.41Z^{0.9}$. In this regime the jet breakup still occurs many nozzle diameters downstream of the nozzle and produces droplets whose diameters are still comparable to that of the jet as was seen in Fig. 5a for jets in the Rayleigh breakup regime (see Fig. 5b). The breakup is still due to the destabilizing influence of surface tension, but it is now augmented by the aerodynamic interaction between the liquid and gas.

Sterling and Sleicher[13] also pointed out that relaxation of the jet's exit velocity profile to a uniform flow beyond the nozzle can influence the jet breakup process. In their analysis (which was quoted

above) they considered the case where l_r/L is small (l_r is the jet profile relaxation length). For large l_r/L they suggest that jet instability could be enhanced by velocity profile rearrangement effects but they offered no details of the mechanism by which this would occur. The profile relaxation phenomenon was also alluded to by Grant and Middleman[4] who found a dependence of L_1 on the nozzle passage length. In particular, nozzles of short length produced more stable jets than those produced from long tubes. They argued that this implies a coupling between the velocity profile and the mechanism of instability in this breakup regime. Parenthetically, their experiments also showed that the breakup length in the Rayleigh regime (Section 3.1) is not influenced by nozzle design details.

Another example of the influence of the initial state of the jet is discussed by Phinney[27] who proposed that liquid turbulence also enhances the jet breakup process. He reasoned that the effect of the jet turbulence is to increase the initial disturbance level η_o. He noted that, even in the abscence of aerodynamic effects, the jet breakup length L_1 is reduced once a critical value of the jet Reynolds number is reached. Furthermore, this critical Reynolds number is of the same order as that for transition to turbulence in the nozzle. However the influence of jet turbulence on the magnitude of the initial disturbance level is still quantitatively unclear.

3.3 Second Wind-Induced Breakup Regime

With further increases in We_2 , Eq. (8) predicts that the maximum wave growth rate occurs at progressively larger wavenumbers (shorter wavelengths). An inspection of Eq. (8) (or Eqs. [5]), shows that the first term on the right hand side changes sign at ka=1, after which the surface tension forces oppose the breakup process. Jet breakup is now due to the unstable growth of short wavelength surface waves (ka>1) which are induced by the relative motion between the jet and the ambient gas. An analysis of Eq. (8) shows that the maximum wave growth rate occurs at ka=1 when $We_2 \geq 12$ for inviscid jets. This estimate was made

using the numerical results of Sterling and Sleicher[13]. The estimate also agrees well with the experimentally obtained criterion of Ranz[10], We_1=13, for the onset of short wavelength waves.

An expression for the growth rate of short wavelength surface waves was presented by Levich[12] and Levich and Krylov[28], who examined Eqs. (5) in the limit ka >> 1 and deduced, neglecting the liquid viscosity, that

$$\omega^2 = (\rho_2 k^2 U^2 - \sigma k^3)/\rho_1 \ . \qquad (9)$$

This result implies the existence of unstable surface waves when $k < \rho_2 U^2/\sigma$. The maximum growth rate is given by

$$\omega_m \cong 0.4 \frac{U^3}{\sigma} \left(\frac{\rho_1^2}{\rho_2}\right)^{1/2} .$$

Equation (9) shows that the dispersion relation Eq. (5) becomes independent of the jet radius in this limit. Consequently, for ka >> 1 jet curvature effects are unimportant. Similarly, the Weber number We_2 can no longer appear as a controlling parameter.

The influence of the liquid viscosity is seen by retaining the second term on the left hand side of Eqs. (5). In the limit $ka \to \infty$ this reduces to

$$(\omega + 2\nu_1 k^2)^2 + \sigma k^3/\rho_1 - 4\nu_1^2 k^3 \sqrt{(k^2 + \omega/\nu_1)} + (\omega + iUk)^2 \rho_2/\rho_1 = 0 \ .$$

This result is identical to that of Taylor[29] who performed an analysis of the unstable growth of 2-dimensional planar surface waves due to the relative motion between a liquid and a gas. He considered the limit ka >> 1 and, assuming $\rho_2 << \rho_1$ he found that the wave growth rate is

$$\omega/kU = 2 \left(\frac{\rho_1}{\rho_2}\right)^{1/2} x g(\Gamma, x) \ .$$

The function g is a correction to the result of Levich[12] which now accounts for the effect of the liquid viscosity. It is shown as a function of the new parameter

$$\Gamma = \frac{\rho_1}{\rho_2}\,\frac{\sigma^2}{\mu_1^2 U^2} = \frac{\rho_1}{\rho_2}\left\{\frac{Re_1}{We_1}\right\}^2$$

and the nondimensional wavelength $x = \rho_2 U^2/\sigma k$ from Taylor's work in Fig. 6. The figure shows that the disturbance growth rate increases with increasing Γ, and that the maximum growth rate occurs at larger wavenumbers (shorter wavelengths) as Γ increases.

Taylor[21] also estimated the intact-core length, L_2, by computing the rate at which droplets remove mass from the liquid core. Here the droplet sizes were assumed to be proportional to the unstable surface wave wavelengths. This analysis gives (see also Reitz and Bracco[20])

$$L_2 = B_1\, a\, \left(\frac{\rho_1}{\rho_2}\right)^{1/2} f(\Gamma) \qquad (10a)$$

where B_1 is a constant of order unity. The function $f(\Gamma)$ corresponds to the maximum wavegrowth rates of Fig. 6, and it is shown in Fig. 7. The intact-surface length L_1 can be estimated using similar arguments to those which led to the development of Eq. (7) (where the jet radius 'a' is replaced by some characteristic wave height at breakup, say). In this case we find that

$$L_1 = B_2\ \ L_2\ /\ We_2 \qquad (10b)$$

where B_2 is another constant which would be dependent weakly (logarithmically) on drop size.

Equation (10a) predicts that the intact-core breakup length L_2 remains constant with increasing jet velocity until the parameter Γ becomes small (i.e. for high velocity jets). L_2 then decreases with increasing jet velocity. The intact-surface length L_1 from Eq. (10b) is predicted to decrease as the inverse square of the velocity and then to decrease even faster when Γ becomes small. This prediction is not inconsistent with the form of breakup curve of Haelein[3] for jets in the second wind-induced regime and, possibly, even in the atomization regime once L_1 becomes of the order of the wavelength of the surface waves.

A photograph typical of jet breakup in this regime is shown in Fig. 5c from Reitz[11]. The photograph shows that the jet breakup starts some distance downstream of the nozzle exit and yields droplets whose average diameters are much less than the jet diameter. Droplet formation results from the unstable growth of short wavelength surface waves on the jet. This wave growth is caused by the relative motion between the jet and the ambient gas, and surface tension forces oppose the wave growth process.

3.4 Atomization Regime

In this regime the breakup appears to commence at the nozzle exit (see Fig. 5d). The spray takes the form of a cone with its vertex within the nozzle. Various authors have suggested possible jet breakup agencies for jets in the atomization regime and some of these are considered below, but a complete and tested theory is not yet available.

Experiments were made to study atomization in Reitz and Bracco[21,22] and Wu et al.[2,23]. The range of conditions of these studies has been extensive and includes the operating conditions of fuel injection systems in Diesel and stratified charge internal combustion engines. The experiments were made under steady conditions with injections into a semi-infinite gas. The test conditions include: Constant liquid injection pressures in the ranges 3.4-17.0 MPa[21] and 10.8-90.5 MPa[23]; Constant gas pressures in the range 0.1-4.1 MPa with air, nitrogen, helium and xenon (different molecular weights to isolate effects of gas density and pressure[21]); Water and water + glycerol injections (10^3 range in liquid viscosity[21]). Hexane, water and tetradecane (factor of 10 in viscosity, 4 in surface tension, 1.5 in liquid density[23]. Pentane, hexane and ethanol (factor of 3 surface tension, 1.5 liquid density[1]; 21 nozzles: sharp edge inlet tube nozzles (length to diameter ratio range 0.5-85.0 (diameter 0.35 mm), rounded inlet[21] and rounded exit nozzles and cavitation free nozzles, and a factor of 2.5 in nozzle exit diameter[23,1]; Liquid temperature: room temperature[21,23]: 100-200 C[1].

Certain trends were found from photographs of jet breakup in the experiments. For example, the spray angle (divergence angle of the jet) was found to increase with increasing (isothermal) gas compression. Moreover, it was established that this is due to increases in the gas density, not pressure[33]. The spray angle was also found to increase with decreasing liquid viscosity.

Another trend concerns the boundary between the atomization and the second wind-induced regimes. It was found that the breakup starts progressively closer to the nozzle exit as the gas density is increased, until it reaches the exit with no evidence of an abrupt change. This trend is also shown in Fig. 8 in which the measured spray angle is plotted against the gas-liquid density ratio for sharp edge inlet nozzles with a length to diameter ratio of 4.0. The solid data points are in the second wind-induced regime - jets intact before diverging. The open points show atomizing jets - divergence begins at the nozzle exit. It was also found that atomization is reached once the liquid viscosity is decreased below a certain level, again with no abrupt change in the appearance of the jet.

Other results were: The spray angle decreases with increased nozzle passage length for nozzle length to diameters greater than 10 or 20. (For shorter nozzles there is more scatter in the results and the trends are not yet fully established, Wu et al.[33]); For the same length, rounded inlet nozzles produce less divergent jets than sharp edge inlet nozzles; Atomization commences at different gas density and liquid viscosity levels as the nozzle design is changed.

With these results it is possible to examine previously proposed theories for atomization in detail. For example, DeJuhasz[34] and Schwietzer[35] proposed that liquid turbulence causes atomization. But if pipe turbulence were the only mechanism, turbulent jets (from the nozzles with large length to diameter ratios[34]) would have been the most unstable flows - contrary to the experiments. Similarly, cavitation phenomena were proposed Bergwerk[37] to lead to atomization. But jets were

found to atomize even when the cavitation free nozzles of Wu et al.[33] were used.

In fact, an evaluation of other proposed atomization mechanisms has revealed that none of the theories taken alone, is able to explain the results fully[31]. These theories include proposals that atomization is caused by: Aerodynamic surface wave growth[38,39] - the results would be independent of the nozzle geometry; Rearrangement of the jet's velocity profile[40] - the high viscosity jets would be the most unstable; Liquid supply pressure oscillations[41] - atomization would not have occurred since the pressure was constant in the experiments; and Wall boundary layer velocity profile relaxation[42] - atomization would have been independent of the gas density; all of these contrary to the experiments.

However, the aerodynamic surface wave growth theory was found to predict many of the trends in tests with a given nozzle. Thus it is useful to consider its predictions in more detail. In this case, the appropriate limit of the dispersion Equation (5) is $ka \to \infty$, as in the second wind-induced regime above. Ranz[43] argued that the spreading angle of the atomizing jet could be predicted by combining the radial velocity of the fastest growing of the unstable surface waves with the axial injection velocity:

$$\tan(\theta/2) = \frac{V}{U} = \frac{2\pi\omega}{AkU}_m = 4\pi\,(\rho_2/\rho_1)^{1/2} f(\Gamma)/A \qquad (11)$$

where the proportionality constant A is obtained from experiment.

In Eq. (11) the spray angle increases with increasing gas density and decreases with increasing liquid viscosity and increasing velocity. This is consistent with tests with a given nozzle. Notice also from Fig. 7 that for $\Gamma > 1$ the function $f(\Gamma)$ becomes asymptotically equal to $\sqrt{3}/6$. Equation (11) then predicts that the spray angle depends only on the gas-liquid density ratio - which is surprising considering the many parameters that could effect it. This behaviour is also generally borne

out by the measurements with a given nozzle.

Ranz[43] determined that A ≃ 18 or 20, but he pointed out that the data of Schweitzer[44] give A ≃ 3. Results given in Reitz and Bracco[31] indicate that the predicted variation of the spray angle with gas density is followed if A has a different value for each different nozzle. Also other results show that agreement is found with respect to liquid viscosity variations by using (for each nozzle) the same value of A as that obtained from the gas density best fit. Figure 9 shows spray angle measurements and the predictions of Eq. (11) with respect to gas density and jet velocity variations. Again the measurements follow the predicted trend, but the results do exhibit a mild opposite trend at low gas densities, indicating that the theory only complies with the most pronounced, and practically important, of the measured trends.

There is additional evidence in support of the aerodynamic theory. For example, the data of Hiroyasu et al.[45] agree with the prediction of the intact-core length of Eq. (10a) with respect to injection velocity and gas density changes. Their experiments were based on measurements of electrical resistance between the nozzle and a screen that could be moved axially within the spray; thus detecting any continuous liquid connection between the nozzle and the screen. However, a connected ligament could give the same signal as a solid liquid core free of gas. Consequently there is still some uncertainty about the structure of the core.

Drop sizes have been measured at the edge of the spray in the vicinity of the nozzle exit[46]. In the surface wave growth theory the drop size would be related to the wavelength of the unstable surface waves i.e.

$$r \simeq c\, 2\pi\sigma\chi/\rho_g U^2 \qquad (12)$$

where c is a constant of order unity. The predictions of Eq. (12) with regard to liquid properties, jet velocity and lack of sensitivity to nozzle design are found to be in agreement with experiment. However a discrepancy has been found with the dependence on gas density but it

appears that a reasonable explanation for this disagreement exists[47].

Based on the definition that atomization occurs when the intact surface length approaches zero, Eq. (10a) can be used to predict that atomization occurs if:

$$(\rho_1/\rho_2)^{1/2} < K \qquad \text{for } \Gamma > 1$$

$$\text{and} \quad \left(\frac{\rho_1 We_1}{\rho_2 Re_1}\right)^{1/3} < K \qquad \text{for } \Gamma < 1 \tag{13}$$

where the constant, K, depends on the nozzle geometry. For the nozzles in Fig. 8 (length to diameter ratio 4), K is found empirically to be equal to 9.2.

The stability analysis does not include the details of the flow field within the nozzle. This shortcoming was also mentioned for the first and second wind-induced breakup regimes in Sections 3.2 and 3.3. Thus, it appears that the stability analysis can explain many of the experimental results in the atomization regime (and also in the second wind-induced regime) if it is supplemented by additional information pertaining to the initial state of the jet since such information is not included explicitly in the theory. In particular, the nozzle geometry obviously effects the initial state of the jet. The simplest way of accounting for the initial state of the jet is through the magnitude of the initial perturbation η_o which could have a different value for different nozzle geometries, for example. However, even if this is eventually found to be a sufficient modification, the magnitude of the perturbation is known at best only empirically. All that can be said at present is that η_o depends in some complex manner on the details of the initial jet flowfield that in turn is influenced by the nozzle geometry and possibly by other parameters, such as the flowfield just upstream of the nozzle.

However, a physical picture of the atomization process can now be proposed which is consistent with the available data. The surface of the liquid jet emerges from the nozzle already perturbed by events that

occur within the nozzle itself and are affected by its geometry. The perturbations are rapidly and selectively amplified by aerodynamic interaction with the gas until the outer surface of the jet breaks into drops. The size of the drops and the intact-surface length is much smaller than the diameter of the nozzle. The depth from the surface of the jet to which the above drop formation mechanism would apply is not known. But the core eventually breaks up too since only isolated drops are found far downstream.

Other aspects of atomization still remain unresolved besides the influence of the nozzle. Not predicted by the stability theory, and therefore unknown, are the size and size distribution of the unstable waves at the moment of breakup and also the time between successive ruptures. Away from the nozzle exit, as the generating surface regresses towards the axis of the jet, there are questions as to what gas velocities are seen by the liquid surface. The velocity of the entrained gas certainly approaches that of the liquid surface. Thus the breakup process should be coupled with the two-phase flow field that exists between the presumed intact-core and the unperturbed outer gas. As the relative velocity between the liquid and gas decreases inside the jet, larger drops or ligaments or blobs should be formed; just as larger drops are found when the injection velocity is decreased, as in going from Fig. 5d to Fig. 5a.

An additional factor to be considered is coalescence of the liquid fragments which can be expected where locally large values of the liquid volume fraction exist. In fact, the net outcome of atomization may be the result of a small difference between large droplet formation and coalescence rates[40]. Thus it is clear that Eqs. (10) to (13) may provide some information about the outcome of the breakup, but in no way do they give all that is necessary.

ACKNOWLEDGMENTS

This work was supported under grants NSF-RANN, AER 75-09538, and ARO DAAG 29-77-G-0146.

REFERENCES

1. Wu, K.-J., Steinberger, R.L. and Bracco, F.V. "On the Mechanism of Breakup of Highly Superheated Liquid Jets." The Combustion Institute Central States Meeting, March 23-24, General Motors Research Laboratories, Warren, Michigan, 1981.

2. Kelly, A.J. "The Electrostatic Atomization of Hydrocarbons." Proceedings of the Second International Conference on Liquid Atomization and Spray Systems, June 20-24, Maidison, Wisconsin, 1982.

3. Topp, M.N. "Ultrasonic Atomization - A Photographic Study of the Mechanism of Disintegration." J. Aerosol Sci., Vol. 4, 1973, p. 17.

4. Grant R.P. and Middleman, S. "Newtonian Jet Stability." A.I.Ch.E., Vol. 12, 1966, p. 669.

5. Haenlein, A. "Uber den Zerfall eines Flussigkeitsstrahls" (On the disruption of a Liquid Jet), N.A.C.A., TM 659, 1932.

6. McCarthy, M.J. and Malloy, N.A. "Review of Stability of Liquid Jets and the Influence of Nozzle Design." The Chem. Eng. J., Vol. 7, 1974, p. 1.

7. Miesse, C.C. "Correlation of Experimental Data on the Disintegration of Liquid Jets", Indust. Engng. Chem., Vol. 47, 1955, p. 1690.

8. Ohnesorge, W. von "Die Bildung von Tropfen an Dusen und die Auflosung Flussiger Stralen" (Formation of Drops by Nozzles and the Breakup of Liquid Jets), Z. Angew. Math. Mech., Vol. 16, 1936, p. 355.

9. Torda, T.P. "Evaporation of Drops and the Breakup of Sprays." Astronautica Acta., Vol. 18, 1973, p. 383.

10. Ranz, W.E. "On Sprays and Spraying." Dept. Engng. Res. Penn. State University, Bulletin 65, 1956.

11. Reitz, R.D. "Atomization and Other Breakup Regimes of a Liquid Jet." Ph.D. Thesis, AMS Department, Princeton University, 1978.

12. Levich, V.G. "Physicochemical Hydrodynamics." Prentice-Hall, New Jersey, 1962.

13. Stirling, A.M. and Sleicher, C.A. "The Instability of Capillary Jets." J. Fluid Mech., Vol. 68, 1975, p. 477.

14. Rayleigh, W.S. "On the Instability of Jets." Proc. Lond. Math. Soc., Vol. 4, 1878, p. 10.

15. Donnely, R.J. and Glaberson, W. "Experiments on the Capillary Instability of a Liquid Jet." Proc Royal Society London A, Vol. 290, 1965, p. 547.

16. Meister, B.J. and Scheele, G.F. "Prediction of the Jet Length in Immiscible Systems." A.I.Ch.E. J., Vol. 15, 1969, p. 689.

17. Phinney, R.E. "Stability of a Laminar Viscous Jet - The Influence of the Initial Disturbance Level." A.I.Ch.E. J., Vol. 18, 1972, p. 432.

18. Weber, C. "On the Breakdown of a Fluid Jet." Z.A.M.P., Vol. 11, 1931, p. 136.

19. Lee, D.W. and Spencer, R.C. "Photomicrographic Studies of Fuel Sprays." N.A.C.A. TR. 454, 1933.

20. Wang, D.P. "Finite Amplitude Effect on the Stability of a Jet of Circular Cross-section." J. Fluid Mech., Vol. 34, 1968, p. 299.

21. Yuen, M.C. "Non-linear Capillary Instability of a Liquid Jet." J. Fluid Mech., Vol. 33, 1968, p. 151.

22. Nayfey, A.H. "Capillary Jet Instabilities." The Physics of Fluids, Vol. 13, 1968, p. 841.

23. Rutland, D.F. and Jameson, G.J. "Theoretical Prediction of the Size of Drops Formed in the Breakup of Capillary Jets." Chem. Eng. Science., Vol. 25, 1970, p. 1689.

24. LaFrance, P. "Non-linear Breakup of a Liquid Jet." The Physics of Fluids, Vol. 18, 1975, p. 428.

25. Fenn, R.W. and Middleman, S. "Newtonian Jet Stability - The Role of Air Resistance." A.I.Ch.E. J., Vol. 15, 1969, p. 379.

26. Benjamin, T.B. J. Fluid Mech., Vol. 6, 1959, p. 161.

27. Phinney, R.E. "The Breakup of a Turbulent Liquid Jet in a Gaseous Atmosphere", J. Fluid Mech., Vol. 60, 1973, p. 689.

28. Levich, V.G. and Krylov, V.S. "Surface Tension Driven Phenomena." Annual Review of Fluid Mech., Vol. 1, 1969, p. 293.

29. Taylor, G.I. "Generation of Ripples by Wind Blowing over a Viscous Fluid." Collected Works of G.I. Taylor, Vol. 3, 1940.

30. Reitz, R.D. and Bracco, F.V. "On the Dependence of Spray Angle and Other Spray Parameters on Nozzle Design and Operating Conditions." SAE paper 790494, 1979.

31. Reitz, R.D. and Bracco, F.V. "Mechanism of Atomization of a Liquid Jet." The Physics of Fluids, Vol. 25, 1982, p. 1730.

32. Reitz, R.D. and Bracco, F.V. "Ultra High Speed Filming of Atomizing

Jets." The Physics of Fluids, Vol. 22, 1979, p. 1054.

33. Wu, K.J., Su, C.C, Steinberger, R.L., Santavicca, D.A. and Bracco, F.V. "Measurements of the Spray Angle of Atomizing Jets." J. Fluids Engng., Vol. 105, 1983, p. 406.

34. DeJuhasz, K.J. "Dispersion of Sprays in Solid Injection Oil Engines." Trans. A.S.M.E. (OGP), Vol. 53, 1931, p. 65.

35. Schweitzer, P.H. "Mechanism of Disintegration of Liquid Jets." J. Applied Physics, Vol. 8, 1937, p. 513.

36. Hinze, J.O. "Turbulence." McGraw Hill, New York, 1st ed., 1959, p. 514.

37. Bergwerk, W. "Flow Pattern in Diesel Nozzle Spray Holes." Proc. Instn. Mech. Engrs., Vol. 173, 1959, p. 655.

38. Castleman, R.A. "Mechanism of Atomization Accompanying Solid Injection." N.A.C.A. Report, 440, 1932.

39. Castleman, R.A. "Mechanism of Atomization of Liquids." U.S. Natl. Bureau Std. J. Res., Vol. 6, 1931, p. 281.

40. Rupe, J.H. "On the Dynamic Characteristics of Free-Liquid Jets and a Partial Correlation with Orifice Geometry." J.P.L. Tech. Report, No. 32, 1962, p. 207.

41. Giffen, E. and Muraszew, A. "The Atomization of Liquid Fuels." John Wiley, New York, 1953.

42. Shkadov, V.Ya. "Wave Formation on the Surface of a Viscous Liquid due to Tangential Stress." Fluid Dynamics, Vol. 5, 1970, p. 473.

43. Ranz, W.E. "Some Experiments on Orifice Sprays." Canad. J. Chem.

Engng., Vol. 36, 1958, p. 175.

44. Schweitzer, P.H. "On the Formation and Dispersion of Oil Sprays." Penn. State University, Bulletin 40, 1932.

45. Hiroyasu, H., Shimizu, M. and Arai, M. "The Breakup of a High Speed Jet in a High Pressure Gaseous Atmosphere", Proceedings of the Second International Conference on Liquid Atomization and Spray Systems, June 20-24, Maidison, Wisconsin, 1982.

46. Wu, K.-J. "Atomizing Round Jets." Ph.D. Thesis, MAE Department, Princeton University, 1983.

47. Wu, K.-J, Reitz, R.D. and Bracco, F.V. "Drop Sizes of Atomizing Jets." to be published.

48. O'Rourke, P.J. and Bracco, F.V. "Modeling of Drop Interactions in Thick Sprays and Comparisons with Experiments." Proc. Instn. Mech. Engrs., Publication No. 085298-469, 1980.

NOMENCLATURE

a	liquid jet or nozzle exit radius
A	nozzle constant Eq. (11)
$B_{1,2}$	breakup length constants Eqs. (10)
c	drop size constant Eq. (12)
$C_{1,2}$	constants of integration in stability analysis
C	attenuation coefficient
d	nozzle exit diameter = 2a
f	Orr-Sommerfeld parameter, Eq. (4)
f	maximum growth rate parameter, Eq. (10) and Fig. 7
$F_{1,2,3}$	dimensionless ratios of Bessel functions in Eq. (5b)
g	Taylors wave growth function Fig. 6
i	$\sqrt{-1}$
I_n	nth order modified Bessel function of the first kind
k	wave number $2\pi/\lambda$
K_n	nth order modified Bessel function of the second kind
K	nozzle constant Eq. (13)
ℓ	wave number $\sqrt{(k^2+\omega/\nu_1)}$
l_r	velocity profile relaxation length
L_1	intact-surface breakup length
L_2	intact-core breakup length
p	pressure
r	radial coordinate, drop radius
R	real part of a complex quantity
Re	Reynolds number $\rho Ud/\mu$
t	time

T	jet breakup time
u	axial velocity component
U	jet exit velocity (averaged over jet cross-section)
v	radial velocity component
We	Weber number $\rho U^2 d/\sigma$
x	dimensionless wave length $\rho_2 U^2/\sigma k$
z	axial coordinate
Z	Ohnesorge number $\mu_1/\sqrt{(\rho_1 \sigma d)}$
β	dimensionless wavegrowth $\omega\sqrt{(\rho_1 a^3/\sigma)}$
Γ	Taylor parameter $=\rho_1 \sigma^2/(\rho_2 \mu_1^2 U^2)$
ΔP	effective injection pressure P_1-P_2
η	surface wave amplitude
θ	jet divergence or spray angle
λ	wave length
μ	kinematic viscosity
ν	dynamic viscosity $= \mu/\rho$
ρ	fluid density
σ	surface tension coefficient
ϕ	velocity potential
ψ	stream function
ω	wave growth rate $=R(\omega)$

Subscripts

1,L	liquid phase
2,g	gas phase
m	maximum value

FIGURES

1. Jet surface breakup length L_1 as a function of jet velocity: ABC Drip flow; CD Rayleigh breakup regime; EF First wind-induced breakup regime; FG (FH) Second wind-induced breakup regime; Beyond G (H) Atomization regime.

2. Jet breakup regime boundaries of Miesse[7], Ohnesorge[8] and Torda[9].

3. Schematic chart of influence of gas density on breakup regime boundaries, Reitz[11].

4. Wave growth rate with wave number for jets in Rayleigh breakup regime. Line: theory Eq. (6). Symbols: measured wave growth rates of Donnely and Glaberson[18].

5. Examples of jets in the four breakup regimes [11,19]. a.) Jet breakup in the Rayleigh regime. Droplet sizes of the order of the jet diameter and breakup occurs many nozzle diameters downstream of the nozzle. b.) Jet breakup in the first wind-induced regime. Droplet sizes are still of the order of the jet diameter and breakup occurs many nozzle diameters downstream of the nozzle. c.) Jet breakup in the second wind-induced regime. Droplet sizes much smaller than the jet diameter and the breakup starts some distance downstream of the nozzle. d.) Jet breakup in the atomization regime. Droplet sizes much smaller than the jet diameter and the breakup starts at the nozzle exit.

6. Theoretical wave growth rate as a function of dimensionless wave length parameter, $x = \rho_2 U^2/\sigma k$ for jets in the second wind-induced breakup regime, Taylor[19].

7. Dependence of the maximum growth rates in Fig. 6 on Taylor's parameter $\Gamma = (\rho_1/\rho_2)\{Re_1/We_1\}^2$.

8. Measured spray angle versus gas-liquid density ratio for nozzle

length to diameter ratio of 4 [11,33]. Nozzle diameter 0.34 mm. Nozzle ΔP=10.0-14.0 MPa. Liquid: water. Gas: nitrogen. Solid symbols: jets intact before diverging (second wind-induced regime). Open symbols: jet divergence starts at the nozzle exit (atomization regime). Partially solid symbols: Marginal breakup at the nozzle exit. Line: aerodynamic theory prediction Eq. (11) with A = 4.0.

9. Measured spray angle versus liquid jet velocity for different gas-liquid density ratios[33]. Liquid: n-hexane. Gas: nitrogen. Straight tube nozzle length to diameter ratio 4. Open symbols: data at ΔP = 15.3, 38.0, 64.9 and 91.8 MPa (U = 1.5, 2.3, 3.0 and 3.6×10^4 cm/s, respectively). Closed symbols: repeated measurements at ΔP=15.3 MPa made after the high injection pressure (ΔP=91.8 MPa) runs.

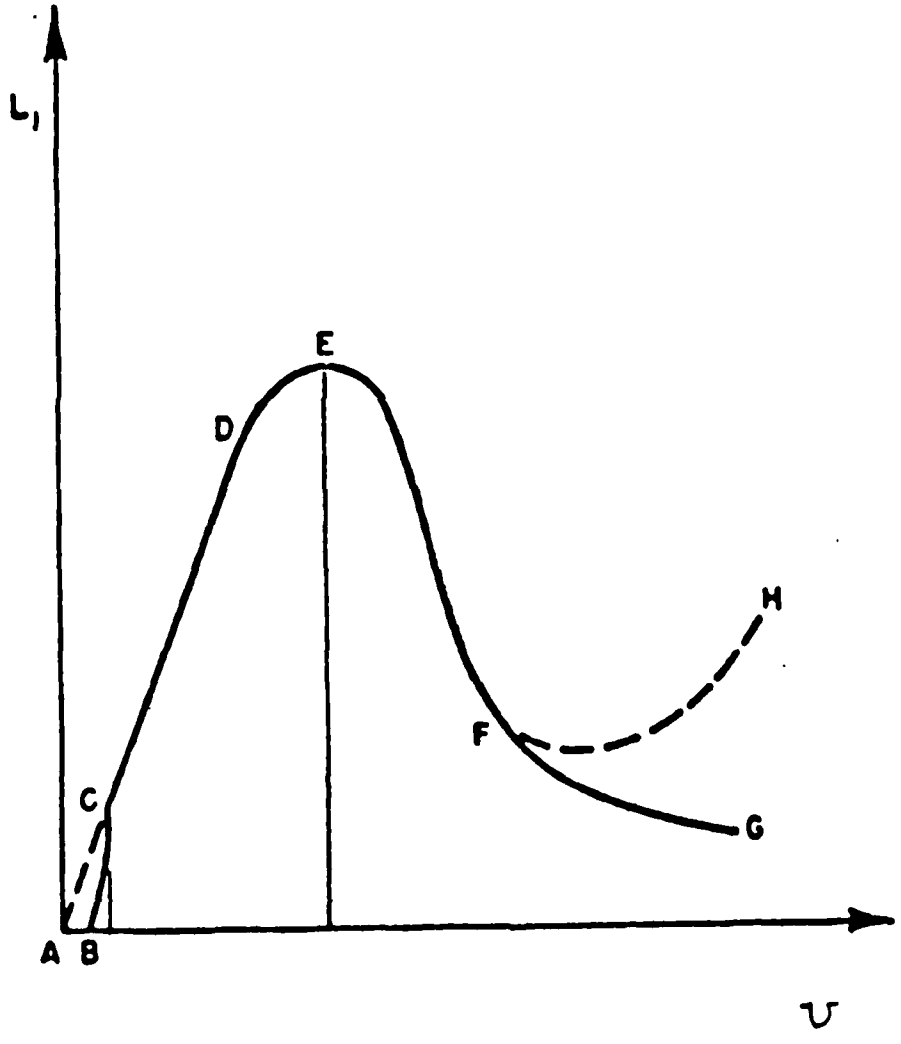

FIG 1

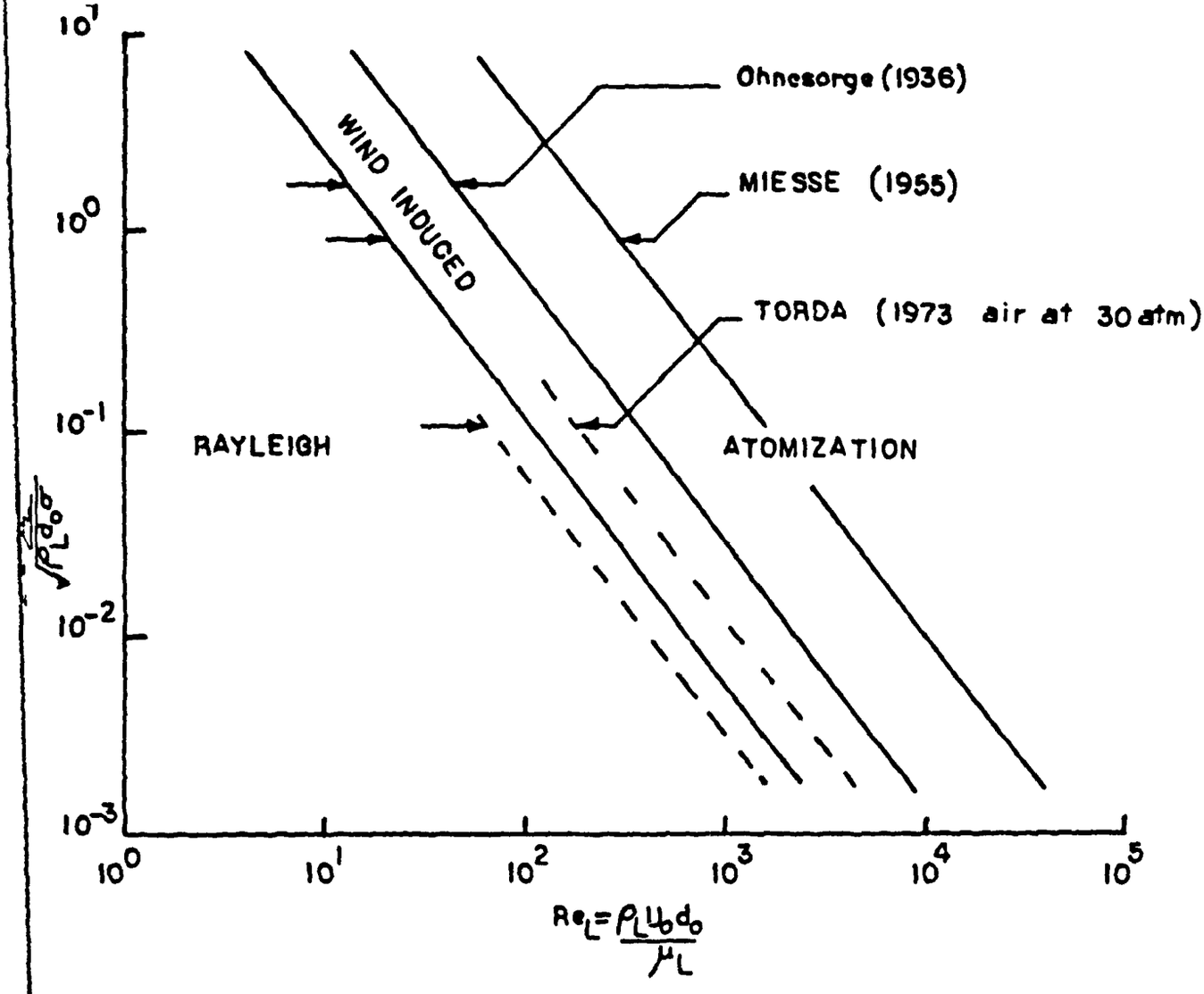
Ohnesorge (1936)
MIESSE (1955)
TORDA (1973 air at 30 atm)
WIND INDUCED
RAYLEIGH
ATOMIZATION
10^{1}
10^{0}
10^{-1}
10^{-2}
10^{-3}
10^{0}
10^{1}
10^{2}
10^{3}
10^{4}
10^{5}
$\frac{\mu_L}{\sqrt{\rho_L d_o \sigma}}$
$Re_L = \frac{\rho_L U_b d_o}{\mu_L}$

FIG 2

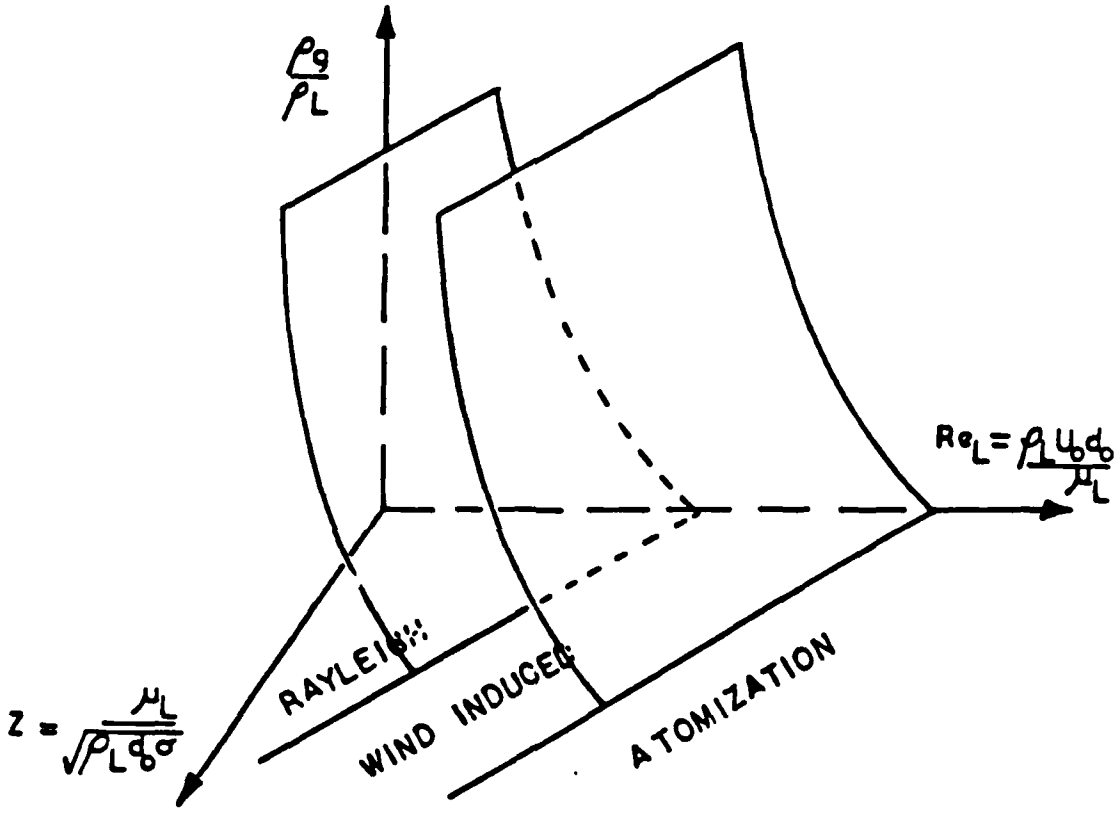
$\frac{\rho_g}{\rho_L}$
$Re_L = \frac{\rho_L U_0 d_0}{\mu_L}$
$Z = \frac{\mu_L}{\sqrt{\rho_L d_0 \sigma}}$
RAYLEIGH
WIND INDUCED
ATOMIZATION

FIG 3

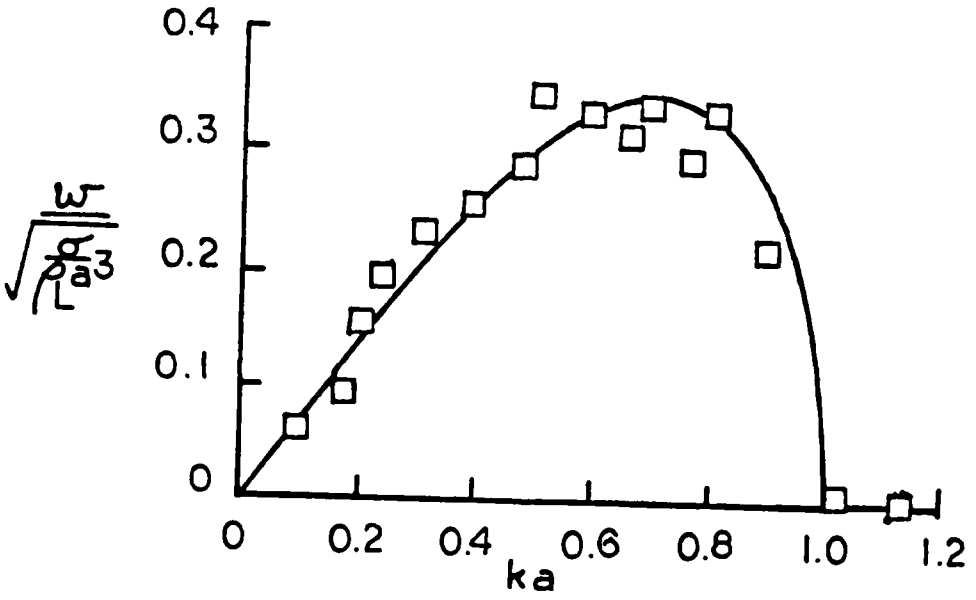

FIG 4

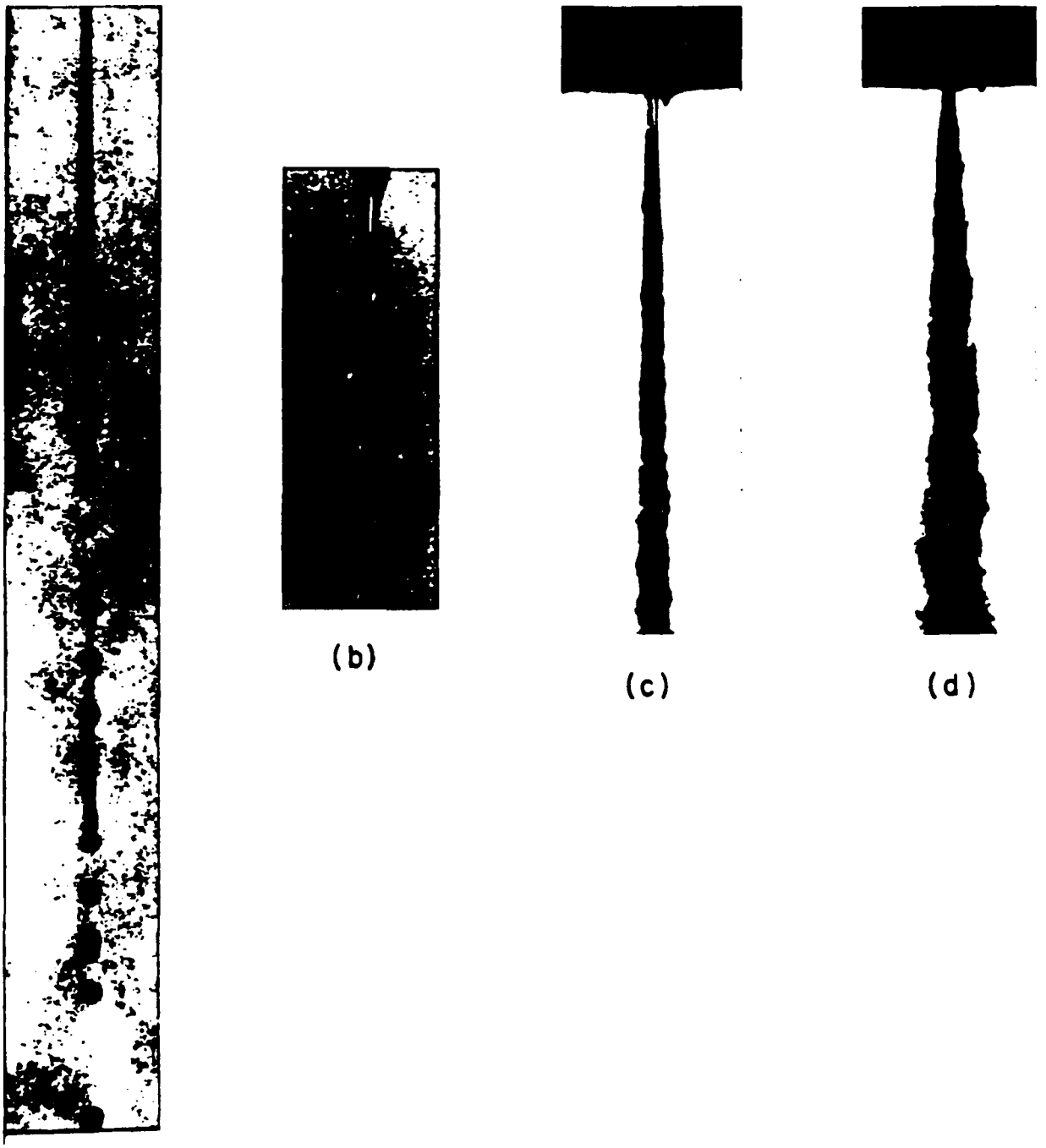

FIG 5

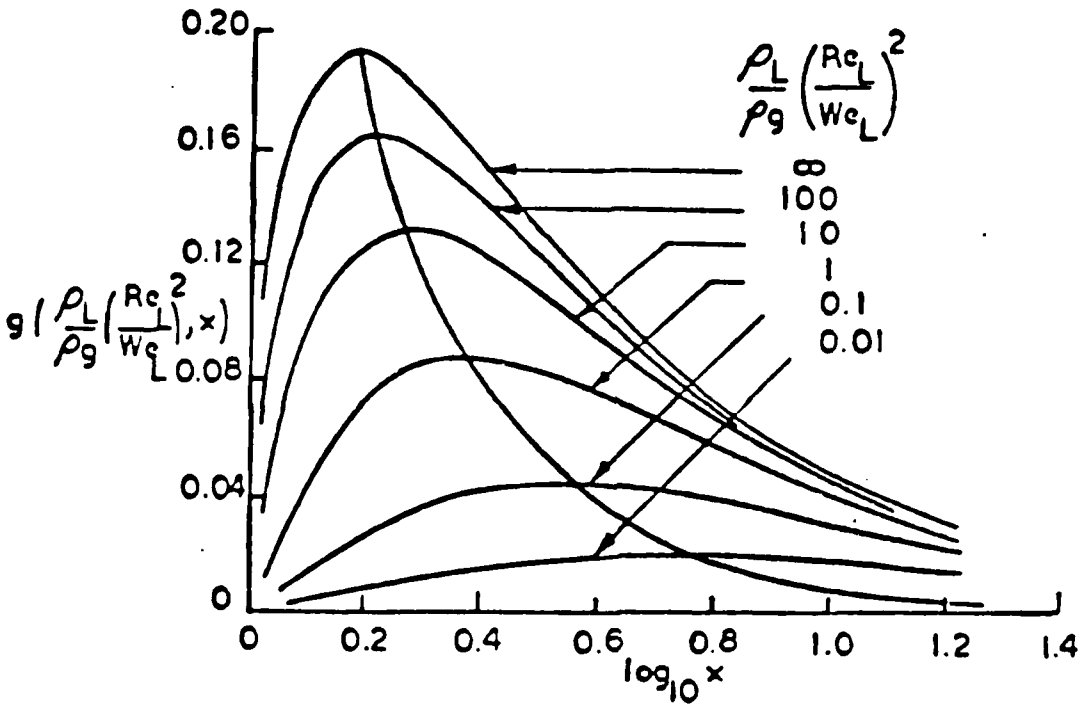
0.20
0.16
0.12
0.08
0.04
0
$g\left(\frac{\rho_L}{\rho_g}\left(\frac{Re_L^2}{We_L}\right), x\right)$
$\frac{\rho_L}{\rho_g}\left(\frac{Re_L}{We_L}\right)^2$
∞
100
10
1
0.1
0.01
0
0.2
0.4
0.6
0.8
1.0
1.2
1.4
$\log_{10} x$

FIG 6

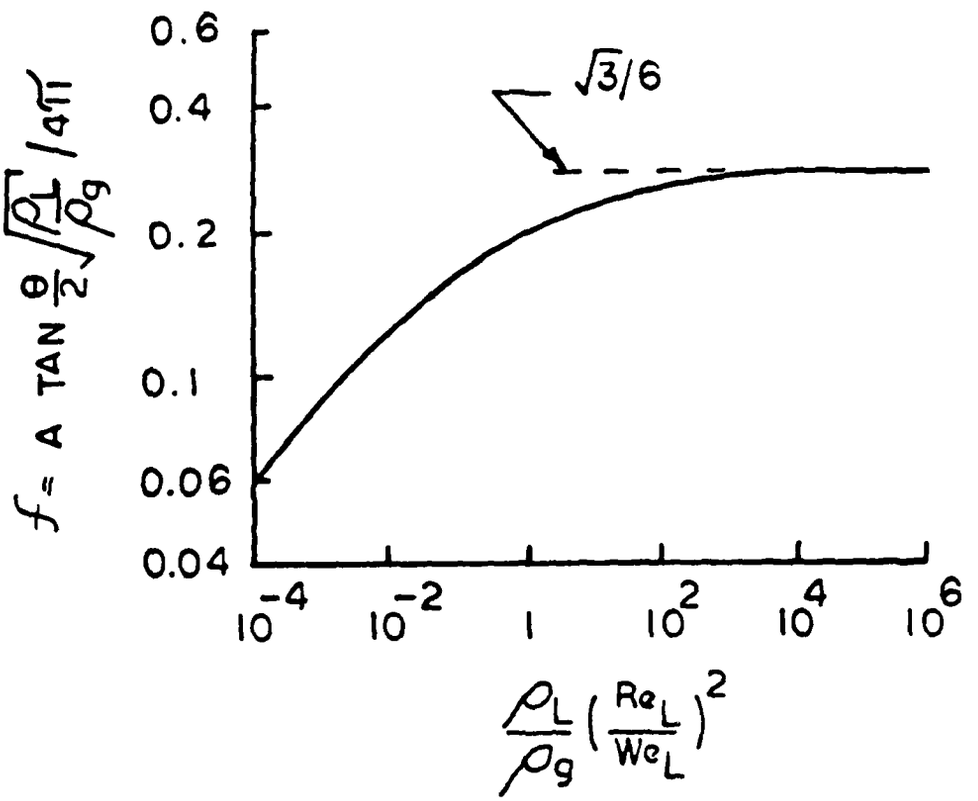
0.6
0.4
0.2
0.1
0.06
0.04
$\sqrt{3}/6$
$f = A \tan\frac{\theta}{2}\sqrt{\frac{\rho_L}{\rho_g}}/4\pi$
10^{-4}
10^{-2}
1
10^{2}
10^{4}
10^{6}
$\frac{\rho_L}{\rho_g}\left(\frac{Re_L}{We_L}\right)^2$

FIG 7

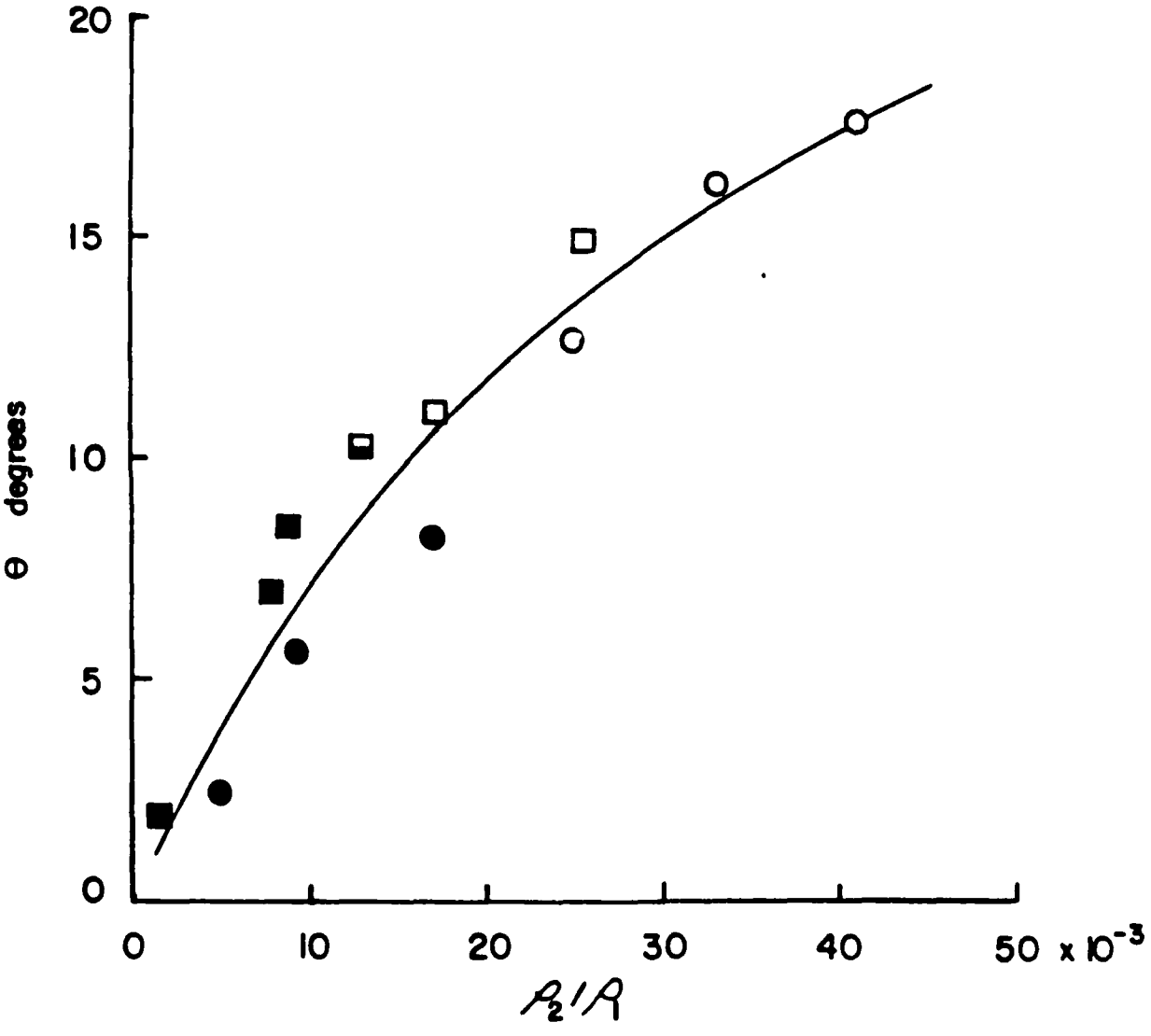
20
15
10
5
0
θ degrees
0
10
20
30
40
50 x 10⁻³
R₂/R

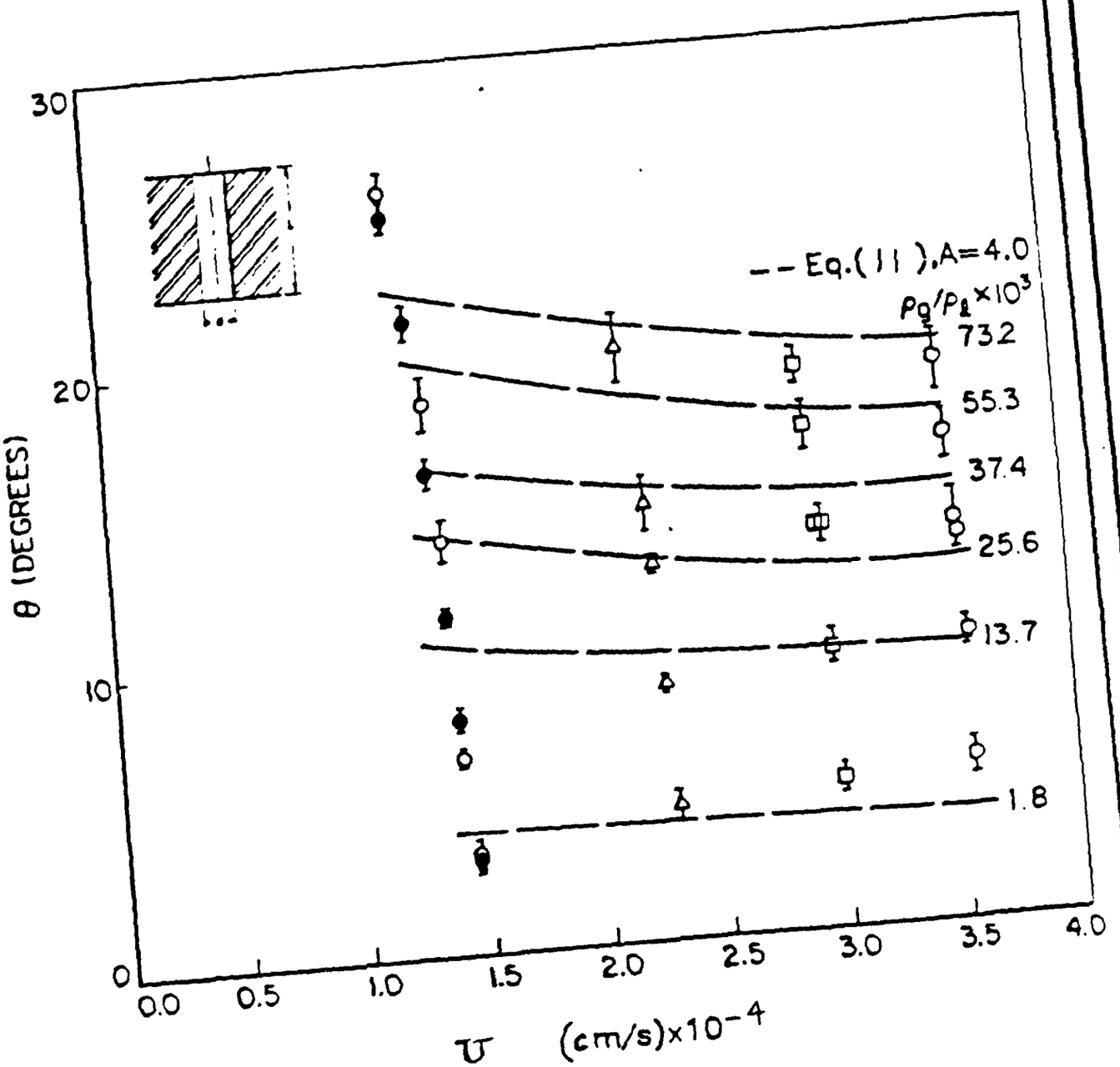
30
20
10
0
θ (DEGREES)
-- Eq.(11), A=4.0
$\rho_g/\rho_l \times 10^3$
73.2
55.3
37.4
25.6
13.7
1.8
0.0
0.5
1.0
1.5
2.0
2.5
3.0
3.5
4.0
U (cm/s)×10⁻⁴

FIG 9

APP B

LDV Measurements of Drop Velocity in Diesel-Type Sprays

K.-J. Wu, D. A. Santavicca, F. V. Bracco, A. Coghe

Reprinted from

AIAA Journal Volume 22, Number 9 September 1984 Page 1263

AMERICAN INSTITUTE OF AERONAUTICS AND ASTRONAUTICS • 1633 BROADWAY • NEW YORK, N.Y. 10019

LDV Measurements of Drop Velocity in Diesel-Type Sprays

K.-J. Wu,* D. A. Santavicca,† and F. V. Bracco‡
Princeton University, Princeton, New Jersey
and
A. Coghe§
Centro Ricerche Propulsione e Energetica CNR, Milan, Italy

Axial and radial components of the drop velocity were measured by laser Doppler velocimetry (LDV) within n-hexane-into-nitrogen sprays from single-hole cylindrical nozzles at room temperature. The gas-to-liquid density ratio, the injection velocity, and the nozzle length and diameter were varied. The LDV system included an argon-ion laser, dual beam LDV optics with frequency shifting and 90-deg collection, a counter processor, and minicomputer data acquisition. The total error in the measured mean and fluctuation drop velocities was less than 10% from the centerline to the half-radius (half-the-width at half-the-depth) and larger and more uncertain beyond it. Velocity bias was the most difficult error to quantify. It is found that beyond 300 nozzle diameters from the nozzle so much ambient gas has been entrained by the drops that the subsequent structure of the spray is dominated by the entrained ambient gas, and the fully developed incompressible jet structure and drop-gas equilibrium are being approached. This conclusion is supported by all the measured drop velocity parameters: jet half radius, centerline velocity decay, axial mean velocity distribution, axial and radial velocity fluctuation distributions, and independence of drop velocity on drop size. Large uncertainties about the magnitude of errors at the outer edges of jets using both laser Doppler velocimetry and hot-wire anemometry suggest that this region is still poorly characterized even for incompressible jets.

Nomenclature

C, C_p, C_i = constants of Eqs. (1) and (2)
d = nozzle orifice diameter, μm
$F_{t,r}, F_{t,x}$ = flatness = $\overline{V_r^4}/[\overline{V_r^2}]^2$, $\overline{V_x^4}/[\overline{V_x^2}]^2$
L = nozzle passage length, μm
p_g = chamber gas pressure, MPa
r = radial coordinate, cm
$r_{0.5}$ = half-radius (half-the-width at half-the-depth) of the drop axial velocity profile, cm
$RFA_{t,x}$ = relative fluctuation amplitude (standard deviation) of the axial velocity of the drops, $= \sqrt{\overline{V_x'^2}}/V_x$
$S_{t,r}, S_{t,x}$ = skewness = $\overline{V_r^3}/[\overline{V_r^2}]^{3/2}$, $\overline{V_x^3}/[\overline{V_x^2}]^{3/2}$
U_r, U_x = radial and axial components of the gas velocity, m/s
$U_{x,cl}$ = axial velocity of the gas at the centerline of the jet, m/s
V_r, V_x = radial and axial components of the drop velocity, m/s
$\bar{V}_{inj}$ = mass mean injection velocity, m/s
$V_{x,cl}$ = axial velocity of the liquid at the centerline of the spray, m/s
X, Y, Z = spatial coordinates (X is from the nozzle exit, see Fig. 3), cm
X_0 = virtual origin, cm
Δp = effective injection pressure, MPa
θ = gas volume fraction
μ_l = liquid dynamic viscosity, kg/m·s
ρ_g = chamber gas density, kg/m^3
ρ_l = liquid density, kg/m^3
σ_l = liquid surface tension coefficient, kg/s^2

Superscripts

$(\bar{\ })$ = mean value
$(\ )'$ = fluctuating component

Introduction

THE breakup of liquid jets is achieved through a large variety of atomizers for an even larger variety of applications.[1,2] Its purpose is to increase the surface-to-volume ratio of the liquid, thus increasing the specific rates of mass, momentum, and heat transfer and the vaporization rate. Even restricting ourselves to injectors used in diesel engines, many designs exist but the most common consists of a group of cylindrical holes 100-300 μm in diameter.[3,4]

When a liquid is forced through a cylindrical hole into a gas, many modes of breakup are observed. In the one relevant in internal combustion engines, no outer intact length is seen and the jet starts diverging at the nozzle exit. All other parameters being the same, this regime, which has been called the atomization regime, is reached at high injection velocities—of the order of 100 m/s for the fuels and conditions of engine applications.[5]

Because of their practical importance, many aspects of atomizing jets have been studied extensively. In the 1930's significant data were collected on such global quantities as downstream drop sizes, tip penetration rates, and average spray angles.[1-4] More recent efforts have attempted to determine the structure of atomizing jets. For example, the outer part in the immediate vicinity of the nozzle exit[5,6] and the inner part in the same region [7] are being studied in detail. Recently, laser techniques have been used to measure drop velocity, drop size, and liquid volume concentrations at ambient pressure in gas turbine-type, dilute sprays from air blast atomizers in which more than 90% of the light is transmitted.[8]

In this paper we report drop velocity measurements within nonvaporizing, steady, diesel-type, fast, dense sprays from single-hole cylindrical nozzles into compressed nitrogen at room temperature in regions so close to the injector that light transmissivity was as low as 2%.

Received June 25, 1983; revision submitted Nov. 4, 1983. Copyright © American Institute of Aeronautics and Astronautics, Inc., 1984. All rights reserved.

*Graduate Student, Department of Mechanical and Aerospace Engineering.
†Research Engineer, Department of Mechanical and Aerospace Engineering.
‡Professor, Department of Mechanical and Aerospace Engineering.
§Research Scientist.

Conditions, Apparatus, and Procedure

n-hexane was injected into quiescent nitrogen at room temperature but at such pressures that the ratio of the gas density to the liquid density was 0.0256 and 0.0732. Three single-hole round nozzles with sharp inlet and outlet and two injection pressures (Δp 11.0 and 26.2 MPa) were used. The effect of nozzle geometry was explored by varying the diameter, 127 and 76.2 μm, and the length-to-diameter ratio, 1 and 4. These parameters, summarized in Table 1, were chosen because earlier work[5] had shown the gas-to-liquid density ratio and the nozzle geometry to be the most important variables in the initial formation of the spray and the injection velocity is important in the subsequent development and propagation of jets. Using the LDV system in the 90-deg scatter mode, it was found that reliable drop velocity measurements were possible at locations characterized by very high drop number densities ($\geq 10^{11}/m^3$) and high velocity gradients (up to 5m/s/mm). Thus, measurements were made across the jet as close as 2.3 cm from the nozzle exit.

The experimental apparatus consisted of a spray chamber, a liquid pressurization system, a nozzle assembly, and LDV optics and instrumentation. A schematic diagram of the spray chamber with the liquid pressurization system and the nozzle assembly is shown in Fig. 1 and details are available in Refs. 6 and 10.

The spray chamber was constructed from several cylindrical steel sections, 19-cm i.d. and 90 cm in total length. The window section has four quartz windows 10 cm in diameter. The liquid pressurization system was designed to maintain constant pressures up to 207 MPa during injection. The liquid pressure before injection was measured with an AMINCO 47-18340 gage and during injection with a Kistler 307A transducer with a frequency response of up to 240 kHz, a Kistler 504 charge amplifier, and a Tektronix 7313 storage oscilloscope. During data acquisition the pressure changed by less than 1%.

The single-hole round nozzles were drilled directly into the nozzle units, whic were made of AISI 303 stainless steel, and examined under a scanning electron microscope to assure that the desired inlet sharpness was obtained and not altered during the tests. Surface roughness was less than 5% of the diameter. The nozzle unit and a typical spray are shown in Fig. 2.

The liquid injection velocity was calculated from the measured injection duration, the area of the nozzle, and the total amount of liquid injected [$\bar{V}_{inj}$ = volume/$\pi(d/2)^2\Delta t$]. This volume (mass) mean velocity was reproducible to within $\pm 1\%$. The velocity profile within the nozzle was not measured due to the nozzle's smallness and the very high velocity of the liquid, but is expected to have been flat, except near the nozzle walls, because the upstream liquid was essentially quiescent and the length-to-diameter ratio of the nozzle was much too small for transition to turbulence away from the nozzle walls. Using the measured $\bar{V}_{inj}$ and assuming ideal velocity except near the walls, we estimate the injection momentum to have been $C_i\rho_l \bar{V}_{inj}^2 \pi(d/2)^2$ with $C_i = 1.0 \pm 10\%$.

Two LDV systems were used. Both systems employed a Lexel 95-2 argon-ion laser operated at powers between 0.1 and 1 W and TSI dual beam focusing and 90-deg scatter collection optics. The two LDV systems used different laser wavelengths, 514.5 and 488.0 nm; fringe spacing, 6.17 and 2.45 μm; and focusing optics focal lengths, 600 and 250 mm, respectively. The second system (Fig. 3) was superior because of its capability to measure flow reversal with the TSI 9180 frequency shift unit and its smaller probe volume ($0.2 \times 0.2 \times 0.2$ mm^3 vs $0.2 \times 0.2 \times 0.7$ mm^3). When using the system with the Bragg cell the LDV signal was electronically downmixed to 0 Hz for the axial velocity component measurements in the core region where the drop velocity fluctuations were small compared to the mean velocity and to 5 MHz near the outer edge of the spray and for all the measurements of the radial velocity. The beam crossing angle was measured both with and without the Bragg cell to an accuracy of $\pm 0.5\%$. The parallelness of the two beams before the focusing lens was also measured and found to be within 0.03 deg. The effect of this on the beam crossing location was estimated to be negligible. The distance from the beam waist to the beam crossing was also calculated and found to be smaller than the beam waist length. Therefore, it was assumed that the beams crossed at their beam waist.

To allow for precise and repeatable positioning of the probe volume within the spray, the entire optical system was mounted on an X,Y,Z tranversing table while the spray chamber remained fixed. The reported axial drop velocities were measured along the $-Z$ axis and the radial drop velocities along the $-Y$ axis (see coordinate system in Fig. 3). At each axial location, first the axis of the spray was located, based on the symmetry of the measured velocity profiles, and the radial distances were referred to it. A minimum of five measurements were made between the centerline and the half-

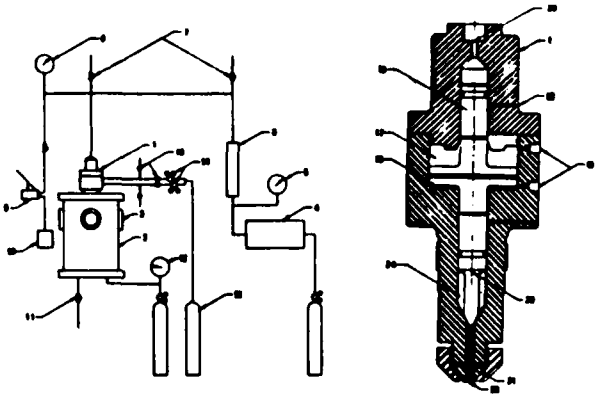

Fig. 1 Spray apparatus and details of the injection cylinder: 1) injection cylinder, 2) spray chamber, 3) window, 4) gas reservoir, 5) driver gas pressure gage, 6) liquid reservoir, 7) bleeding valves, 8) test liquid pressure gage, 9) hand pump, 10) test liquid tank, 11) drain, 12) chamber gas pressure gage, 13) nitrogen cylinder, 14) regulators, 15) solenoid valves, 16) valve unit, 17) upper control gas chamber, 18) lower control gas chamber, 19) control gas ports, 20) test liquid conduit, 21) nozzle piece, 22) leak off, 23) nozzle, 24) test liquid.

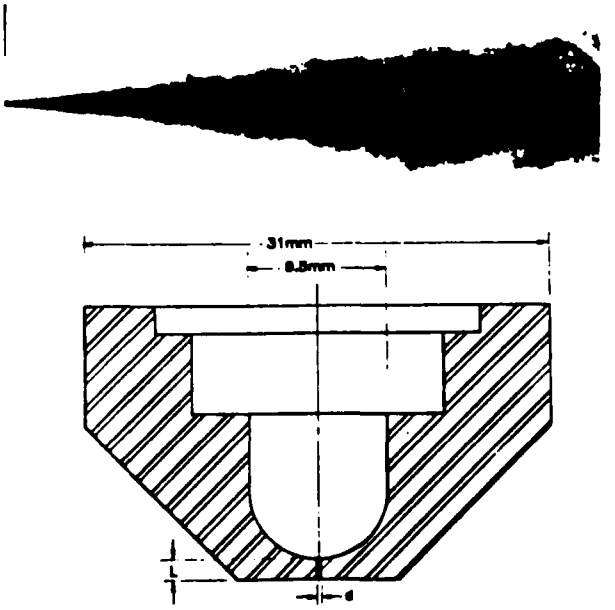

Fig. 2 Nozzle piece and typical spray (length of the field 270d).

Table 1 Spray conditions[a]

Series	p_g, MPa	ρ_g/ρ_l	Δp, MPa	$\bar{V}_{inj}$, m/s	Nozzle, $d(\mu m)$-L/d	X/d
A	1.48	0.0256	11.0	127	127-4	600,800
B	4.24	0.0732	11.0	127	127-4	300,400,500,600
C	4.24	0.0732	26.2	194	127-4	400,500,600
D	4.24	0.0732	11.0	149	76-4	300,600,700,800
E	1.48	0.0256	11.0	125	76-1	300

[a]Liquid: n-hexane, $\rho_l = 665$ kg/m^3, $\mu_l = 3.2 \times 10^{-4}$ N·s/m^2, $\sigma_l = 1.84 \times 10^{-2}$ N/m. Gas: nitrogen. Room temperature.

Table 2 Errors in LDV measurements[10]

Source	Type	Estimated error and correction
LDV optics	Beam-crossing angle	0.5%
	Fringe spacing	No error due to refraction index
	Bragg cell	<1%
LDV electronics	Clock counting	<1% based on an intrinsic accuracy of 1 ns
	Noise	<3% with SNR = 10 and $N_{fr} = 4$
Spray	Velocity gradient	≤2% for the mean value ≤5% for fluctuation amplitude based on the maximum velocity gradient of 5(m/s)/mm
	Effect of drop size distribution	No sensible effect on velocity distribution was found for $X \geq 300d$
	Spray-to-spray variation	Negligible
	Velocity biasing	Correction applied for $RFA_{v,x} \leq 30\%$
Statistics	Axial component	≤2% for the mean value ≤3% for fluctuation amplitude based on 2000 data and 50% relative fluctuation amplitude
	Radial component	No data reported for the mean value due to large error

radius; therefore, the uncertainty in the positioning at an axial location of $300d$ is no more than ±8.3% of the half-radius and at axial positions further downstream the positioning error is an even smaller percentage of the half-radius.

The frequency was measured with a TSI 1990 counter processor interfaced to a Hewlett-Packard 21 MX minicomputer. The number of fringes set on the counter processor over which the frequency was measured was eight or four. Such a small number of fringes was used primarily to increase the data rate in the region of high drop number density. The use of fewer fringes also reduces the trajectory bias that can occur when a large number of fringes are used which favors drop trajectories normal to the fringe planes.[9]

The same initiation signal that operated the valve unit (item 16 in Fig. 1) was used, through a control module, to enable the counter to transmit data. The control module was also used to insert a prefixed delay between spray initiation and the start of data transmission and to program the data acquisition period for each test. The delay was necessary to allow the spray to reach a steady-state condition as determined from the time history of the liquid pressure.

All the measurements were made in steady sprays. Even though the data were taken in a 0.5-1.0 s period to prevent recirculation inside the chamber from affecting the spray, the velocity of these sprays was so high, and their size so small, that their characteristic times are much shorter than 1.0 s. The longest time would be the convection time at the farthest axial station ($800d$) for the largest of the nozzles (127 μm) and the slowest of the injection velocities (127 m/s). This time is less than 0.03 s. As previously stated, during the measurements liquid and gas pressure were constant to better than 1%. Far downstream, the 0.5-1.0 s window was long enough to collect more than 2000 data points during one injection, but going upsteam the rate of acquisition of acceptable data decreased and up to 30 injections were necessary to obtain the same total number of velocity data. For each set of measurements, the number of rejected data, based on the criterion that the data should fall within 3.5σ of the mean, was always less than 1% of the total.

Error Analysis

An extensive analysis of experimental errors was carried out. A detailed discussion is available in Ref. 10. Sources of error, their estimated magnitudes, and possible corrections are summarized in Table 2. Only the discussion of the effects of drop size distribution and velocity biasing is given here.

No direct measurement of the drop size distribution was made from which the possible correlation between drop size and velocity could be determined. However, along the axis it was found that for $X/d \geq 300$ the velocity distribution is not affected by varying the laser power or by limiting the observed range of drop sizes to which the counter processor responded (achieved by reducing the upper limit of the dc component of the Doppler signals accepted by the LDV counter processor). Figure 4 shows the effect on the mean velocity and the fluctuation amplitude at $X/d = 800$ of a variation of the amplitude limit setting on the counter processor from 100 to 2. No significant change is seen in either $\bar{V}_x$ or fluctuation amplitude whereas the data rate changed drastically, indicating a large selectivity in drop size. It was estimated that

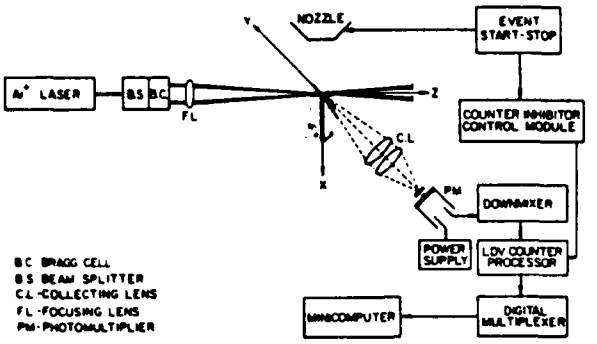

Fig. 3 LDV setup.

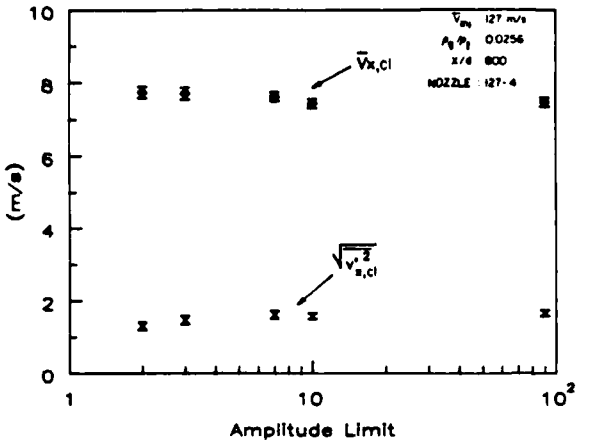

Fig. 4 Variation of mean and fluctuating components of the drop axial velocity vs amplitude limit setting of the counter processor.

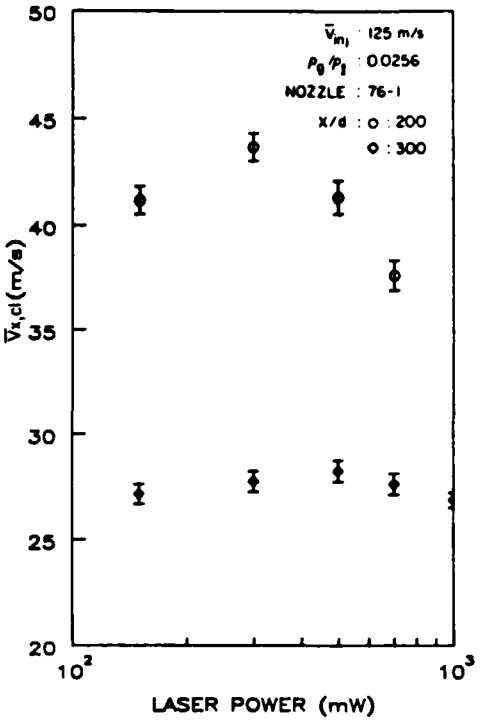

Fig. 5 Variation of mean drop axial velocity vs laser power.

at least 90% of the total number of observable drops were rejected with the lower setting.[10] However, upstream of $X/d = 300$, the mean velocity begins to show sensitivity to variations of the laser power (equivalent to changing the amplitude limit setting) and at $X/d = 200$ change in $\bar{V}_x$ is quite large, as shown in Fig. 5. For this reason only the measurements for $X/d \geq 300$ are reported and discussed. From the point of view of the structure of these sprays, the fact that, for $X/d \geq 300$, the drop velocity is independent of the drop size along the axis implies that drop and gas velocities there are the same; that is, the equilibrium limit has been reached. For $X/d < 300$, along the spray axis it is concluded that the drop and gas velocities are different.

The major source of uncertainty in the estimates of errors was the velocity bias effects. A velocity bias error can occur in fluctuating flows since, with uniform particle concentration, more particles are sampled per unit time when the gas velocity is higher.[11,12] The magnitude of the velocity bias error depends on the local fluctuation amplitude. Buchhave[13] calculated the velocity bias errors of the mean and the fluctuating velocities for three-dimensional Gaussian isotropic turbulence, for relative turbulence intensities up to 80%, including the effects of trajectory bias but without frequency shifting and showed that the errors increase monotonically with the turbulence intensity. At 30% turbulence intensity the velocity bias errors were between 5 and 10% for the mean velocity, and between 3 and 7% for the fluctuation amplitude, depending on the ratio of the minimum number of fringe crossings required for a measurement to the maximum number of fringe crossings available.

The determination of unbiased averaged quantities from velocity biased data can be achieved only if the time each particle remains in the probe volume is known exactly.[9] A simplified one-dimensional a posteriori correction can be applied by weighting each individual measurement with a weighting factor inversely proportional to the measured velocity component.[11] This correction method can reduce the velocity bias error when the relative fluctuation amplitude is small. For example, after correction, at 30% turbulence intensity, the velocity bias errors are less than 4.3% for the mean velocity and between 2 and 5.5% for the fluctuation amplitude.[13] For our sprays the one-dimensional correction method was considered acceptable and was applied as long as the relative fluctuation of the drop velocity was less than or equal to 30%. Above 30%, the residence time can no longer be approximated by the measured velocity component and the one-dimensional correction overcorrects the mean velocity and introduces errors that can be larger in magnitude, and opposite in sign, than those of the uncorrected data. Thus, the correction does not improve the accuracy of the data and the uncorrected data may be in error by as much as 22% for the mean velocity and 10% for the fluctuation amplitude at 80% turbulence intensity if the angular dependence is minimized by frequency shifting.[13]

Besides the drop velocity distribution, the half-radius as determined from the drop axial mean velocity is also affected by the velocity bias error because at the half-radius location the fluctuation amplitude is about 45%. The half-radius was derived both from data which had been velocity bias corrected around the half-radius location (fully corrected) and from data to which no velocity bias correction had been applied around the half-radius location (partially corrected). In both cases the one-dimensional velocity bias correction was applied for relative fluctuations smaller than 30%, i.e., near the spray centerline. The two sets of half-radius results differ from each other by 10%. Buchhave[13] showed that without correction the half-radius is overestimated and with correction it is underestimated. Thus, based on half the difference of these

results the uncertainty in the half-radius due to the velocity bias error is about ±5%. But when all other sources of error are considered, the total uncertainty in the half-radius becomes ±6.6%.

The velocity bias correction is strictly valid only if the drop number density can be assumed to be uncorrelated with the local velocity and provided no other limitations on the mean sampling rate interfere and further complicate the problem. The drop concentration also must be sufficiently low so that most of the time there is only one drop in the probe volume.[11] This condition was only marginally satisfied.

In summary, the one-dimensional correction was applied on the drop velocity data as long as the relative fluctuation amplitude was less than or equal to 30%. The result was that the total maximum error of the reported mean velocity was estimated to be less than 10% up to the half-radius and increasingly larger outward where it can be as large as 40% for a relative drop velocity fluctuation amplitude of 80%. The total error of the reported fluctuation amplitudes is, in general, smaller than that of the mean velocity.

Results and Discussion

The parameters varied in the experiment are listed in Table 1. Five conditions were examined with different combinations of two gas-to-liquid density ratios, two injection pressures, and three nozzle geometries. For each condition, the axial and radial components of the drop velocity were measured by LDV at several axial and radial locations. The measurements discussed in this section were taken with 300-800 nozzle diameters from the nozzle exit (2.29-10.16 cm).

We will consider, first, average drop velocities; then, fluctuations of the drop velocities; and, finally, the implications of the measurements about the structure of these sprays. In the figures, the corresponding fluid quantities measured by Wygnanski and Fiedler[14] by hot-wire anemometry in isothermal, low Mach number (incompressible) air-into-air jets are shown for reference and comparison, but without implying that they constitute definitive measurements of incompressible jets.

Figure 6 shows that, at sufficient distance from the injector, the ratio of the centerline velocity to the injection velocity tends to depend only on $X/d\,(\rho_l/\rho_g)^{1/2}$. In this figure, data other than ours are from Ref. 15. According to Hinze,[18] this scaling was first proposed by Thring and Newby,[19] but was also obtained analytically by Kleinstein.[20]

To understand the possible reasons for the scatter of the data in Fig. 6, consider a steady injection of a fluid l into a second fluid g. At sufficient distance from the injector the flow rate of the injected mass becomes negligible with respect to that of the entrained mass and the subsequent development of the jet depends on the ambient fluid entraining more ambient fluid as in "incompressible" jets. This fully developed incompressible jet limit must eventually be reached independently of the nature of the fluids and of the structure of the development region. Then, neglecting viscous stresses and pressure gradients, conservation of axial momentum gives

$$C_l \rho_l \bar{V}_{0,cl}^2 d^2/4 = C_g \rho_g \bar{U}_{x,cl}^2 r_{0.5,g}^2 \tag{1}$$

$$\frac{\bar{U}_{x,cl}}{\bar{V}_{0,cl}} = \left(\frac{C_l}{4C_g C^2}\right)^{1/2} \frac{d(\rho_l/\rho_g)^{1/2}}{X - X_0} \tag{2}$$

where C_g relates the self-preserving distributions of the mean axial velocity and velocity fluctuations to the mean centerline velocity and is equal[14,16,23] to 0.846 ± 2.9%; $C = 0.0868 \pm 7.9\%$ relates the half-radius to the distance from X_0, the virtual origin[14,21-23]; and C_l relates the injection momentum to the injection centerline velocity. For uniform injection velocity profile $C_l = 1$ and the coefficient of Eq. (2) is 6.3 ± 9% (Capp

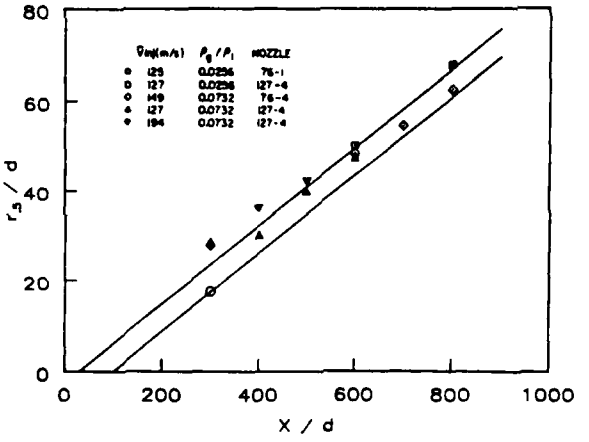

Fig. 7 Dimensionless half-radius of the drop axial velocity vs dimensionless axial distance.

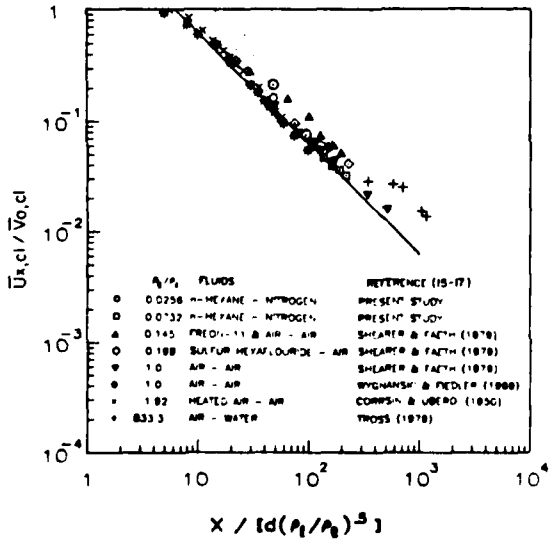

Fig. 6 Centerline velocity decay of different jets vs dimensionless axial distance.

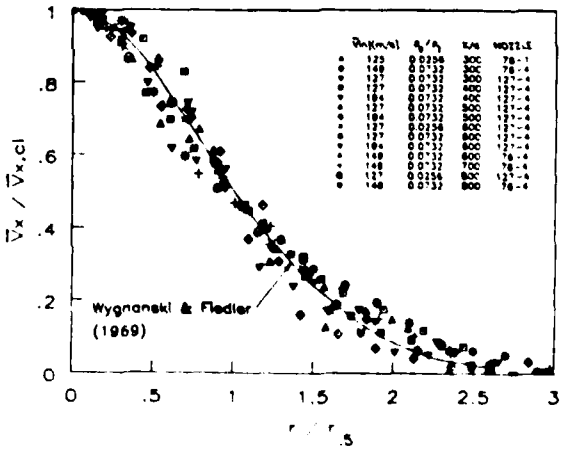

Fig. 8 Self-similar profile of the dimensionless mean drop axial velocity.

and George,[23] for example, give 5.8). In Fig. 6 the continuous line corresponds to $X_0 = 0$ whereas the two dotted lines correspond to $(X_0/d)/(\rho_l/\rho_g)^{1/2} = 30/(13.7)^{1/2}$ and $100/(39.1)^{1/2} = 8.12$ and 16.0, respectively. The X_0 values of 30 and 100 will be explained later. The three lines show that, at sufficient distance from the injector, the structure and length of the development region become immaterial.

Often there is uncertainty about the value of C_i for different experiments because the injection momentum generally is not measured and because different authors may use velocities other than the centerline velocity as reference injection velocity. As previously stated, we did not measure the injection velocity profile. We measured the mass mean injection velocity, $\bar{V}_{inj}$, and estimated that the injection momentum was equal to $C_i \rho_l \bar{V}_{inj}^2 \pi d^2/4$ with $C_i = 1 \pm 10\%$. Thus, using V_{inj} for $V_{0,cl}$ in Fig. 6 far from the injector our data must fall on the continuous line. For data other than ours we used the injection velocity given by the various authors. We believe that the main reason for the scatter of the data at large values of $X/d\,(\rho_l/\rho_g)^{1/2}$ is the uncertainty about the injection momentum, i.e., about the value of C_i.

Another factor could be that the fully developed local equilibrium condition was not reached by all the jets of the figure, as suggested by Shearer and Faeth.[15] For $X/d \geq 300$, earlier it was shown that drop and gas velocity tend to be the same along the axis and, presently, it will be shown that mean and fluctuating components of the drop velocity have reached self-preserving profiles. Thus, the conditions for convergence to the solid line of Fig. 6 are met and our data tend to fall on it.

Finally, accurate measurements in these jets continue to be difficult and experimental errors may be present. For example, the data of Wygnanski and Fiedler are seen to tend to a different slope in Fig. 6, but Capp and George[23] report that their faster decay may be due to wall effects.

Equation (2) can now be used to determine somewhat more precisely the virtual origin. If $\bar{V}_{inj}/\bar{U}_{x,cl}$ is plotted vs X in linear scales, our far-field data must converge on straight lines of known slope, corresponding to the continuous line of Fig. 6. By extrapolating backward, the intersections of these lines determine the virtual origins. We found $X_0 = 30d$ for $\rho_l/\rho_g = 13.7$ and $X_0 = 100d$ for $\rho_l/\rho_g = 39.1$, the other variables having no clear effect on X_0 within the accuracy of our data. Obviously, the convergence to fully developed jets occurs further downstream in our sprays than in incompressible jets ($\rho_l/\rho_g = 1.0$) for which the reported X_0/d is always smaller than 10. Having the virtual origins, the value of C was determined by curve fitting the measured half-radius data (Fig. 7), and found to agree with the value obtained from incompressible jet data.

Another implication of Eq. (2) is that the tip penetration rate of sprays for constant pressure injection into a stationary unconfined gas can be estimated using the injection momentum and the nozzle diameter, and without detailed knowledge of their structure. The estimate is only rough near the injector but becomes accurate far from it. This is because under such conditions the velocity of the tip of a transient spray is close to 70% of the local steady-state centerline velocity.[24,25]

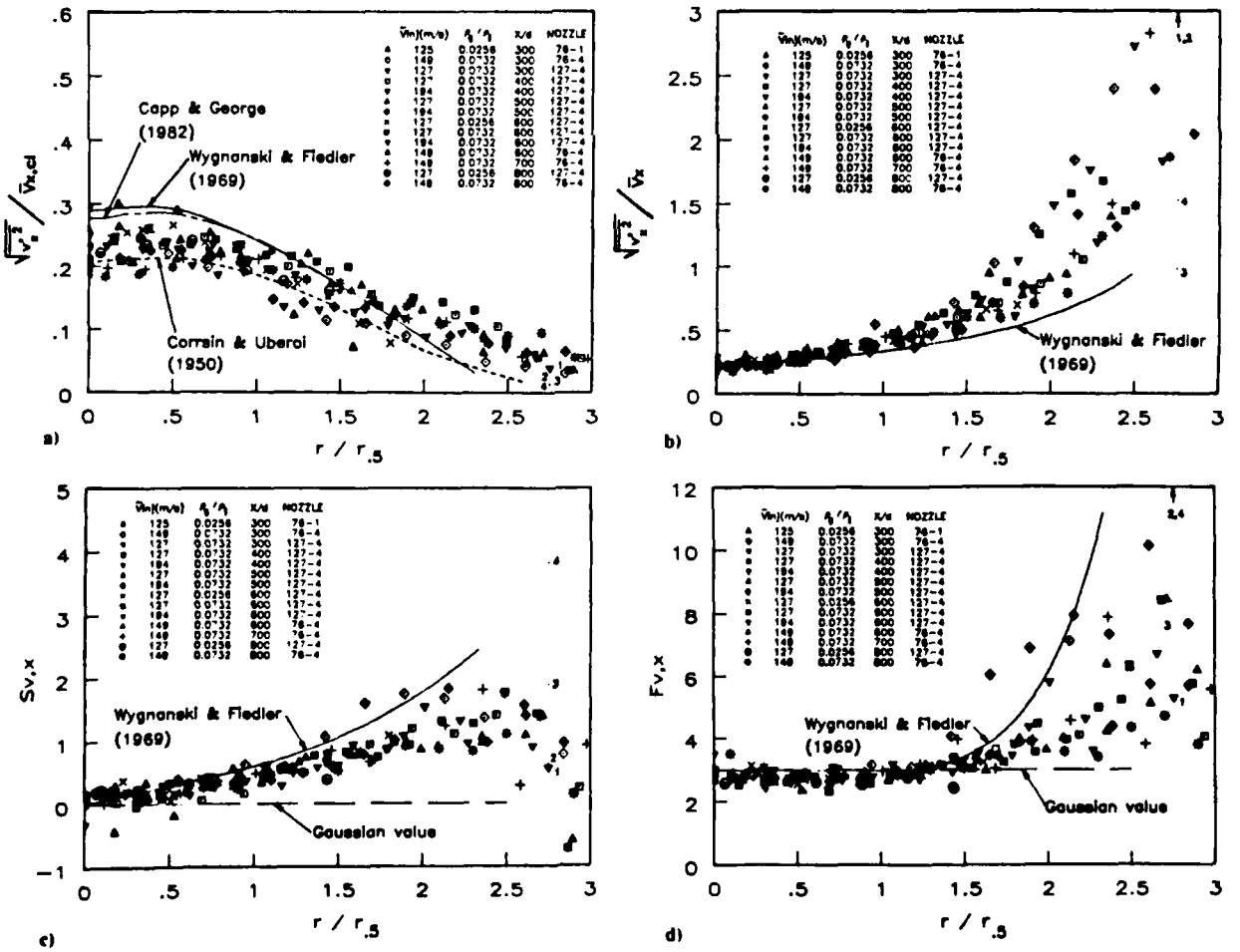

Fig. 9 Self-similar profiles of the dimensionless fluctuation of the drop axial velocity: a) dimensionless fluctuation amplitude, b) relative fluctuation amplitude, c) skewness, and d) flatness.

So far we have considered only the mean centerline velocity and the half-radius. Figure 8 shows that for $X/d \geq 300$ the parallel between the mean axial drop velocity in our sprays and the mean axial fluid velocity of incompressible jets extends to all axial and radial locations and all conditions.

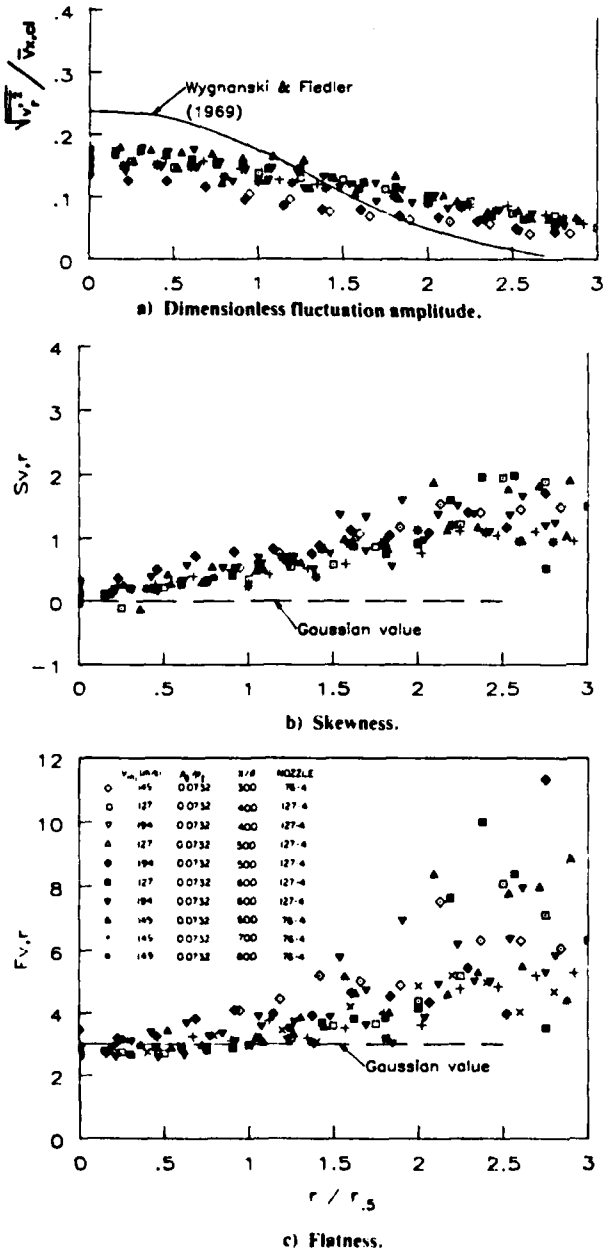

a) Dimensionless fluctuation amplitude.

b) Skewness.

c) Flatness.

Fig. 10 Self-similar profiles of the dimensionless fluctuation of the drop radial velocity.

The parallel extends also to the fluctuating components of drop and fluid velocities but with increasing uncertainty. At each axial and radial location the measured axial and radial components of the drop velocity show a distribution of values. The standard deviation and skewness and flatness of these distributions are shown in Figs. 9 and 10. It is seen that near the axis, the amplitude of the velocity fluctuation of the drops falls into the lower part of the range of incompressible jets and appears to be larger at the edge. Near the axis the distribution of the drop velocity is also Gaussian, as indicated by the skewness and flatness. At the edge of the sprays the shapes of the spray drop and incompressible jet velocity distributions appear to differ. Those of the drops tend to remain more Gaussian.

The effects of corrections and differences between experimental techniques on the disparity between the drop velocities at the edge of our sprays and the fluid velocity at the edge of incompressible jets were evaluated for the case $\Delta p = 26.2$ MPa, $p_g = 4.24$ MPa, nozzle 127-4, $X/d = 400$, and $r = 2.75 r_{0.5}$. Results are shown in Fig. 9 (numbered 1-4 at $r/r_{0.5} = 2.75$) and Table 3. The measured drop velocity distribution is nearly Gaussian without the one-dimensional correction (results 1 in the skewness and flatness graphs) but if the one-dimensional correction is applied it becomes much narrower (test 2 in Table 3) and its parameters move closer to the incompressible jet values (results 2 in flatness graph). Since the real quantities are most likely between the corrected and the uncorrected ones, there is a tendency toward better agreement.

The influence of the measuring technique appears to be even stronger and to tend to further close the gap between our results and those of the incompressible jet. It is recalled that most of the incompressible jet data, including those of Wygnanski and Fiedler, were taken with hot-wire anemometry. We can approximate the spray data that would have been obtained by hot-wire anemometry by disregarding the direction of the drop velocity as determined by the Bragg cell. The spray data thus obtained would move closer to the corresponding incompressible jet data as shown by results 3 and 4 in Table 3 and Fig. 9. Intermittency can also contribute to explaining the differences. Our drops come to the edge of the spray primarily with the gas from the core and reflect the fluctuations of this gas. Fluctuations that are averaged also over the potential fluid would be of smaller amplitude.

Thus, it is likely that the difference between our drop velocity at the edge of our sprays and the corresponding fluid velocity at the edge of incompressible jets is less than shown in Fig. 9. However, correct values cannot be established at this time.

In summary, indications are that for $X/d \geq 300$, drops and gas are nearly in equilibrium. As a further elaboration of the question of equilibrium, estimates of the characteristic relaxation times of drop velocity[26] and gas turbulence[27] were considered.[10] It was concluded that at $X = 300d$ the condition for local equilibrium should be met at least by the more numerous, smaller drops. Downstream of $X = 300d$, the drop relaxation time does not increase appreciably, because collisions and coalescence are no longer numerous at low liquid-volume fractions,[28] whereas the turbulent eddy time continues to increase as X^2. Thus, a station is reached at

Table 3 Effects of the Bragg cell and the one-dimensional correction on the drop velocity distribution

Test	Bragg cell	Correction	$\bar{V}_x$, m/s	$\sqrt{V_x'^2}$, m/s	$S_{v,x}$	$F_{v,x}$
1	Yes	No	0.024	0.503	0.57	5.32
2	Yes	1-D	0.003	0.198	0.63	18.44
3	No	No	0.360	0.351	1.89	7.63
4	No	1-D	0.109	0.166	3.82	25.16

which most of the drops are in equilibrium with most of the eddies.

Finally, it is recalled that for $X < 300d$ all indications are that local equilibrium is not present. This lack of equilibrium near the injector and a successive but selective equilibration process downstream are in general agreement with those described by Faeth.[29]

Summary and Conclusions

Axial and radial components of the drop velocity were measured by LDV at numerous radial and axial locations ($300 \le X/d \le 800$) within diesel-type n-hexane sprays but at room temperature, under steady injection pressure, and into initially quiescent nitrogen. Five configurations were employed that differed in gas-to-liquid density ratio (0.0256, 0.0732), injection velocity (127, 149, and 194 m/s), and nozzle geometry (straight cylindrical holes with sharp inlet and outlet, diameters of 76 and 127 μm, and length-to-diameter ratio of 4 and 1). The LDV system was made up of an argon-ion laser, TSI dual beam LDV optics with a Bragg cell, 90-deg scatter collection optics, counter processor, and minicomputer.

In the error analysis we considered errors related to the LDV optics, LDV electronics, velocity gradient broadening, drop size distribution, drop number density, probe volume position, finite sample size, and velocity bias. The magnitude of the velocity bias error was particularly difficult to estimate but it was concluded that for the reported data the total error is less than 10% from the centerline to the half-radius and progressively greater and more difficult to evaluate beyond the half-radius. Significant uncertainties about the magnitude of errors at the outer edge of jets with either LDV or hot-wire anemometry suggest that this region is still poorly characterized even for incompressible jets.

It was found that at sufficient distance from the nozzle so much gas has been entrained that the subsequent structure of the spray is dominated by the entrained gas and that the fully developed incompressible jet structure and the equilibrium limit are reached. This condition is being approached 300 nozzle diameters from the nozzle as shown by all the measured drop velocity parameters: jet half-radius, centerline velocity decay, axial mean velocity distribution, axial and radial velocity fluctuation distributions, and independence of drop velocity on drop size. However, the condition is not verified at distances smaller than 300 nozzle diameters.

For engine applications, the distance up to 300 nozzle diameters, i.e., the first 3-12 cm, is the one of prime interest. If it is true that vaporization should speed up the achievement of the fully developed state, it is also true that neither the ambient gas nor the injection pressure are steady during fuel injection and, therefore, accurate computations of engine sprays are likely to require knowledge of the non-equilibrium developing region.

On the other hand, under steady conditions it is possible to estimate the steady-state centerline velocity and the tip penetration rate for a broad range of density ratios using only the injection momentum and the nozzle diameter. The estimate becomes accurate far from the injector.

Acknowledgments

Support for this work was provided by the Army Research Office (DAAG29-81-K-0135), the Department of Energy (DE-AC-04-81AL16338), General Motors, and Cummins Engine. We are grateful to the anonymous reviewers of this article whose unusually precise comments helped us improve its clarity.

References

[1] Giffen, E. and Muraszew, A., *The Atomization of Liquid Fuels*, John Wiley and Sons, New York, 1953.

[2] Dombrowski, N. and Mundy, G., "Spray Drying," *Biochemical and Biological Engineering Science*, Vol. 22, Academic Press, New York, 1968.

[3] Taylor, C. F., *The Internal Combustion Engine in Theory and Practice*, MIT Press, Cambridge, Mass., 1966.

[4] Obert, E. F., *Internal Combustion Engines*, International Textbook Co., Scranton, Pa., 1973.

[5] Reitz, R. D. and Bracco, F. V., "Mechanism of Atomization of a Liquid Jet," *Physics of Fluids*, Vol. 25, Oct. 1982, pp. 1730-1742.

[6] Wu, K.-J., Su, C.-C., Steinberger, R.L., Santavicca, D. A., and Bracco, F. V., "Measurements of the Spray Angle of Atomizing Jets," *Journal of Fluids Engineering*, Vol. 105, Dec. 1983, pp. 406-415.

[7] Hiroyasu, H., Shimizu, M., and Arai, M., "The Breakup of High Speed Jet in a High Pressure Gaseous Atmosphere," ICLASS-82, Madison, Wis. 1982.

[8] Yule, A. J., Ah Seng, C., Felton, P. G., Ungut, A., and Chigier, N. A., "Sprays, Drops, Dusts, Particles: A Study of Vaporizing Fuel Sprays by Laser Techniques," *Combustion and Flame*, Vol. 44, Jan. 1982, pp. 71-84.

[9] Buchhave, R., George, W. K. Jr., and Lumley, J. L., "The Measurement of Turbulence with the Laser-Doppler Anemometer," *Annual Review of Fluid Mechanics*, 1979, pp. 443-503.

[10] Wu, K.-J., "Atomizing Round Jets," Ph.D. Thesis 1612-T, Dept. of Mechanical and Aerospace Engineering, Princeton Univ., N.J., Aug. 1983.

[11] McLaughlin, D. K. and Tiederman, W. G., "Biasing Correction for Individual Realization of Laser Anemometer Measurements in Turbulent Flows," *Physics of Fluids*, Vol. 16, No. 12, 1973, pp. 2082-2088.

[12] Dimotakis, P. E., "Single Scattering Particle Laser-Doppler Measurements of Turbulence," AGARD CP-193, Saint-Louis, France, 1976.

[13] Buchhave, P., "Biasing Errors in Individual Particle Measurements with the LDA-Counter Signal Processor," *Proceedings of the LDA Symposium*, Copenhagen, 1975, pp. 258-278.

[14] Wygnanski, I. and Fiedler, H., "Some Measurements in the Self-Preserving Jets," *Journal of Fluid Mechanics*, Vol. 38, Sept. 1969, pp. 577-612.

[15] Shearer, A. J. and Faeth, G. M., "Evaluation of a Locally Homogeneous Model of Spray Evaporation," NASA CR-3198, 1979.

[16] Corrsin, S. and Uberoi, M. S., "Further Experiments on the Flow and Heat Transfer in a Heated Turbulent Air Jet," NACA TR998, 1950.

[17] Tross, S. R., "Characteristics of a Submerged Two-Phase Free Jet," M.S. Thesis, The Pennsylvania State Univ., University Park, Pa. 1974.

[18] Hinze, J. O., *Turbulence*, second ed., McGraw-Hill, New York, 1975.

[19] Thring, H. W. and Newby, M. P., "Combustion Length of Enclosed Turbulent Jet Flames," *4th Symposium on Combustion*, Williams and Wilkins Co., Baltimore, Md., 1953, pp. 789-796.

[20] Kleinstein, G., "Mixing in Turbulent Axially Symmetric Free Jets," *Journal of Spacecraft and Rockets*, Vol. 1, July 1964, pp. 403-408.

[21] Hoesel, W. and Rodi, W., "New Biasing Elimination Method for Laser-Doppler Velocimeter Counter Processing," *Review of Scientific Instruments*, Vol. 48, July 1977, pp. 910-919.

[22] Schlichting, H., *Boundary Layer Theory*, seventh ed., McGraw-Hill, New York, 1979.

[23] Capp, S. P. and George, W. K. Jr., "Measurements in an Axisymmetric Jet Using a Two-Color LDA and Burst Processing," International Symposium on Applied LDA to Fluid Mechanics, Lisbon, Portugal, 1982.

[24] Kuo, T.-W. and Bracco, F. V., "On the Scaling of Transient Laminar, Turbulent, and Spray Jets," SAE Paper 820038, Warrendale, Pa., Feb. 1982.

[25] Whitehouse, N. D. and Sareen, B. K., "Prediction of Heat Release in a Quiescent Chamber Diesel Engine Allowing for Fuel/Air Mixing," SAE Paper 740084, Warrendale, Pa., Nov. 1974.

[26] Owen, P. R., "Pneumatic Transport," *Journal of Fluid Mechanics*, Vol. 39, Nov. 1969, pp. 407-432.

[27] Launder, B. E. and Spalding, D. B., *Lectures in Mathematical Models of Turbulence*, Academic Press, London, 1972.

[28] O'Rourke, P. J. and Bracco, F. V., "Modeling of Drop Interactions in Thick Sprays and Comparison with Experiments," *Institute of Mechanical Engineers*, Pub. ISBN 0 85298 4693, Nov. 1980, pp. 101-116.

[29] Faeth, G. M., "Evaporation and Combustion of Sprays," *Progress in Energy and Combustion Science*, Vol. 9, 1983, pp. 1-76.

AIAA PROGRESS IN ASTRONAUTICS AND
AERONAUTICS, VOL. 95, 1984

Comparisons of Computed and Measured Dense Spray Jets

L. Martinelli* and F. V. Bracco†
Princeton University, Princeton, New Jersey
and
R. D. Reitz‡
General Motors Technical Center, Warren, Michigan

Abstract

Steady spray jets are considered from single cylindrical orifices under conditions of direct fuel injection in internal combustion engines, but at room temperature. Computations were made with a two-dimensional unsteady model that uses atomization results as nozzle exit boundary conditions, a k-ε submodel for gas turbulence, and a stochastic algorithm to compute drop events, including collisions and coalescence. Centerline velocity decay, spray width, average drop velocity distributions and standard deviation and skewness and flatness of the drop velocity distribution are compared at several axial and radial locations with corresponding laser Doppler velocimetry data from sprays at three different conditions. Agreement is very good with mean quantities, but the computed standard deviation of the drop velocity distribution (i.e., the drop velocity fluctuation) is generally smaller than the measured one. These nonvaporizing sprays achieve a structure that is very similar to that of fully developed incompressible jets, but 5-10 times further downstream. After development, the drops have little influence on the gas, but the gas controls the motion of the drops.

Presented at the 9th ICODERS, Poitiers, France, July 3-8, 1983.
Copyright American Institute of Aeronautics and Astronautics, Inc., 1984. All rights reserved.
*Graduate Student, Department of Mechanical and Aerospace Engineering.
†Professor, Department of Mechanical and Aerospace Engineering.
‡Research Engineer, Department of Fluid Mechanics, Research Laboratories.

Nomenclature

C_1 = turbulence model constant = 1.5
C_2 = turbulence model constant = 1.9
C_3 = turbulence model constant = −1.0
C_4 = turbulence model constant = 0.09
C_a = drop size constant = 0.86
C_d = drag coefficient
c_p = gas specific heat at constant pressure
C_θ = nozzle spray angle constant = 5.2
d = nozzle diameter
d^* = numerical nozzle diameter at $\theta = 0.9$
D = molecular diffusivity
D_t = turbulence diffusivity
f = drop number distribution, $f(\underline{x}, \underline{v}, r, t)$
F_{v_x} = flatness, $\overline{v_x'^4} / \overline{v_x'^2}^2$
$\underline{g}$ = gravity acceleration
h_g = enthalpy of the gas
$\underline{\underline{I}}$ = unit tensor
k = turbulence kinetic energy
L = nozzle length
p = pressure
Pr = Prandtl number, $Pr_k = 1.0$, $Pr_\varepsilon = 1.3$
r = droplet radius; radial coordinate
$r_{0.5,g}$ = spray half-radius using half the average gas centerline velocity, $r_{0.5,g}(x,t)$
$r_{0.5,\ell}$ = spray half-radius using half the average drop centerline velocity, $r_{0.5,\ell}(x,t)$
R = universal gas constant
Re_r = drop Reynolds number $= 2\rho_g|\underline{u} + \underline{u}' - \underline{v}|r/\mu_g$
Re_j = liquid jet Reynolds number $= \rho_\ell \bar{U}\, d/\mu_\ell$
SMR = Sauter mean radius
S_{v_x} = skewness, $\overline{v_x'^3} / \overline{v_x'^2}^{3/2}$
t = time
T_g = temperature of the gas (and of mixture)
$\underline{u}$ = gas velocity vector of components $u_x(x,r,t)$ and $u_r(x,r,t)$
$\bar{U}$ = mass mean injection velocity

U^* = numerical uniform axial velocity of gas and drops at $\theta = 0.9$

$\underline{v}$ = drop velocity vector of components $v_x(x,r,t)$ and $v_r(x,r,t)$

$\dot{\underline{v}}$ = drop acceleration

W = molecular weight

We_j = jet Weber number = $\rho_\ell \overline{U}^2 d/\sigma$

$\underline{x}$ = space coordinate

x = axial coordinate

δ = Dirac delta function

Δ = numerical increment

ϵ = rate of dissipation of turbulence kinetic energy

η_c = coalescence efficiency

ν_{ab} = collision frequency

θ = gas volume fraction; spray angle

λ_t = turbulence length scale

μ_g = gas viscosity

μ_ℓ = liquid viscosity

σ = surface tension

σ_{ab} = transition probability function

σ_{v_x} = standard deviation of the fluctuation of the drop axial velocity, $\sigma_{v_x}(x,r,t)$

ρ_g = mass of gas per unit volume of gas

$\rho_{\beta g}$ = mass of gas per unit volume of mixture = $\theta\rho_g$

ρ_ℓ = mass of liquid per unit volume of liquid

$\underline{\underline{\tau}}_t$ = turbulence stress tensor

τ_c = drop-turbulence correlation time

Superscripts

$()'$ = fluctuation

$(-)$ = mean

Introduction

The family of sprays considered in this work is characterized by small length scales, high velocities, and complete or very high opacity. Because of the latter property, these sprays are loosely termed dense. Typically, the nozzle is a straight cylindrical hole 100-300 μm in diameter, the field of interest is 10 cm, the injection velocity is 100 m/s, the average drop radius is 10-30 μm, and, without evaporation, the light transmissivity through the core is still negligible hundreds of nozzle diameter

downstream. An example is shown in Fig. 1. They are used primarily in Diesel and stratified charge engines in which fuel injection, vaporization, mixing, and combustion occur in small chambers and must be completed in less than 10 ms.

In such applications, neither the injection pressure nor the chamber gas are steady during injection. The comparisons discussed in this paper are with drop velocity data taken 4-10 cm from the nozzle in non vaporizing, room temperature, steady sprays (Wu et al. 1984). No spatially resolved, accurate measurements within such sprays closer to the nozzle or under transient conditions are available. Although similar comparisons do not seem to have been previously reported, recent reviews of closely related subjects are available (Faeth 1983; Sirignano 1983). The model is outlined first and then the comparisons are discussed.

The Model

The equations of the model for the transient and steady state of non evaporating and evaporating dense sprays are those of O'Rourke and Bracco (1980). In the application of

Fig. 1 Typical high velocity spray (n-hexane, $\overline{U}$ = 222 m/s, ρ_ℓ/ρ_g = 73, d = 0.343 mm, L = 1.72 mm).

and, without evaporation, the light transmissivity through the core is still negligible hundreds of nozzle diameter

this paper, droplet vaporization and temperature effects are negligible and the corresponding terms have been dropped from the more general equations, thus obtaining the following:

Spray equation

$$\frac{\partial f}{\partial t} + \nabla\cdot(f\underline{v}) + \nabla_{\underline{v}}\cdot(f\dot{\underline{v}}) = \frac{1}{2}\iint_{ab} \nu_{ab}\{\sigma_{ab} - \delta(r-r_a)\delta(\underline{v}-\underline{v}_a) - \delta(r-r_b)\delta(\underline{v}-\underline{v}_b)\}\, dr_a\, d\underline{v}_a\, dr_b\, d\underline{v}_b \quad (1)$$

Gas mass equation

$$\frac{\partial \beta_g}{\partial t} + \nabla\cdot(\beta_g \underline{u}) = 0 \quad (2)$$

Gas momentum equation

$$\frac{\partial \beta_g \underline{u}}{\partial t} + \nabla\cdot(\beta_g \underline{u}\,\underline{u}) + \nabla p = \nabla\cdot\underline{\underline{\tau}}_t - \iint \frac{4}{3}\pi r^3 \dot{\underline{v}}\,\rho_\ell f dr d\underline{v} \quad (3)$$

Gas energy equation

$$\frac{\partial \beta_g h_g}{\partial t} + \nabla\cdot(\beta_g h_g \underline{u}) = \theta\left(\frac{\partial p}{\partial t} + \underline{u}\cdot\nabla p\right) + \nabla\cdot(\beta_g c_p D_t \nabla T_g) - \iint f\rho_\ell \frac{4}{3}\pi r^3 \dot{\underline{v}}_a\cdot(\underline{u} + \underline{u}' - \underline{v})\, dr d\underline{v} + \underline{\underline{\tau}}_t : \nabla\underline{u} \quad (4)$$

where

$$\underline{\underline{\tau}}_t = \beta_g D_t (\nabla\underline{u} + \nabla\underline{u}^T - \frac{2}{3}\nabla\cdot\underline{u}\,\underline{\underline{I}})$$

Turbulence kinetic energy

$$\frac{\partial \beta_g k}{\partial t} + \nabla\cdot(\beta_g \underline{u} k) = \nabla\cdot\left(\frac{\beta_g D_t}{Pr_k}\nabla k\right) + G - \beta_g\varepsilon \quad (5)$$

Rate of turbulent energy dissipation

$$\frac{\partial \beta_g \varepsilon}{\partial t} + \nabla\cdot(\beta_g \underline{u}\varepsilon) = \nabla\cdot\left(\frac{\beta_g D_t}{Pr_\varepsilon}\nabla\varepsilon\right) + \frac{\varepsilon}{k}(C_1 G - C_2 \beta_g \varepsilon) + C_3 \beta_g \varepsilon \nabla\cdot\underline{u} \quad (6)$$

where

$$G = D_t\left\{2\left[\left(\frac{\partial u_x}{\partial x}\right)^2 + \left(\frac{\partial u_r}{\partial r}\right)^2 + \left(\frac{u_r}{r}\right)^2\right] + \left(\frac{\partial u_x}{\partial r} + \frac{\partial u_r}{\partial x}\right)^2\right\}$$

$$D_t = D + C_4 k^2/\varepsilon$$

Momentum exchange rate and state equations

$$\dot{\underline{v}}_a = \frac{3}{8}\frac{\rho_g}{\rho_\ell}\frac{|\underline{u} + \underline{u}' - \underline{v}|}{r}(\underline{u} + \underline{u}' - \underline{v})C_d$$

$$\dot{\underline{v}} = \dot{\underline{v}}_a - (\nabla p)/\rho_\ell - g \quad (7)$$

$$p = \rho_g R T_g/W \quad (8)$$

$$h_g = c_p T_g \quad (9)$$

Equation (1) is Williams' (1962) spray equation plus a term that accounts for drop collisions and coalescence (the integral on the right-hand side). The collision frequency between drops with subscript a and those with subscript b is

$$\nu_{ab} = f_a f_b \pi (r_a + r_b)^2 |\underline{v}_a - \underline{v}_b| \quad (10)$$

In Eq. (1), the portion of the integrand within the brackets gives the sources (given by the transition probability function σ_{ab}) and the sinks (given by the delta functions δ) of drops of velocity $\underline{v}$ and radius r due to collisions between drops of classes a and b.

The transition probability function determines whether the outcome of a collision is coalescence or separation. Its mathematical expression is given by O'Rourke (1981). The criterion for drop separation after collision is that the rotational energy of the coalesced drop pair exceeds the surface energy required to reform the original drops from the coalesced pair. For the resulting coalescence efficiency η_c, which is the probability of coalescence given that collison has occurred, O'Rourke and Bracco (1980) give the expression

$$\eta_c = \min(2.4\, g(\xi)/We_c,\ 1.0) \quad (11)$$

where $We_c = \rho_\ell | \underline{v}_a - \underline{v}_b |^2 r_a / \sigma$, $r_a < r_b$, $\xi = r_b/r_a$

and $g(\xi) = \xi^3 - 2.4\xi^2 + 2.7\xi$

In the present application, most of the colliding drops have radii of similar magnitudes so that We_c is important, the coalescence efficiency is generally < 1.0, and drop reseparation (grazing collision) is significant.

In the gas-phase momentum and energy conservation equations, the integrals on the right-hand sides represent the exchange functions. They are the sum over all drops at point $\underline{x}$ and time t of the rate of momentum and energy exchanges between each drop and the gas.

The drop acceleration $\underline{\dot{v}}$, given by Eq. (7), has a contribution due to aerodynamic drag and one due to the mean pressure gradient that has been shown to be important in some applications (O'Rourke 1981). In Eq. (7) there is the drag coefficient C_d. After a detailed survey of experimental and theoretical studies, O'Rourke and Bracco (1980) proposed the following correlations to account for the effect of the gas volume fraction θ:

$$C_d(\theta, Re_r) = 24\,(\theta^{-2.65} + Re_r^{2/3}\theta^{-1.78}/6)/Re_r \qquad (12)$$

The effect of turbulence on the gas phase is accounted for by the terms involving D_t in Eqs. (3) and (4), where D_t is the turbulent diffusivity found from the turbulent kinetic energy and its rate of dissipation as shown in Eqs. (5) and (6). The turbulence effects on the drops are calculated by adding to the mean gas velocity $\underline{u}$ a fluctuating component $\underline{u}'$ when computing the aerodynamic drag force. $\underline{u}'$ is chosen randomly from an isotropic Gaussian distribution with mean square deviation 2/3k, where k is the turbulence kinetic energy. For each drop, after a turbulent correlation time τ_c, a new value of $\underline{u}'$ is chosen and τ_c is given by

$$\lambda_t = \int_t^{t+\tau_c} | \underline{v}(t') - \underline{u}(t') | \, dt' \qquad (13)$$

where $\underline{u}(t')$ is the mean gas velocity at the drop position at time t' and λ_t is the eddy size

$$\lambda_t = C_4^{3/4} k^{3/2}/\varepsilon \qquad (14)$$

A detailed derivation and discussion of the equations of the dense spray model is given by O'Rourke (1981).

All the computations were initiated at that axial location of the spray where the gas volume fraction θ is approximately 0.9 (eight nozzle diameters downstream of the nozzle in our case). At that axial location, gas and liquid are given equal axial velocity U* computed by using conservation of momentum. U* is somewhat lower than the experimentally measured mass mean liquid injection velocity U and the equivalent numerical nozzle diameter d* is somewhat larger than the actual nozzle diameter because of the divergence of the spray. The procedure to compute U* and d* is explained by O'Rourke (1981).

The initial spray angle and mean size of the drops was computed using correlations proposed by Reitz and Bracco (1982) for the atomization process. They were able to show that under the condition of $(\rho_\ell/\rho_g)(Re_j/We_j)^2 \gg 1$, the measured initial spray angle θ is correlated well by

$$\tan \theta/2 = (1/C_\theta)[4\pi(\rho_g/\rho_\ell)^{1/2}\sqrt{3}/6] \qquad (15)$$

where the proportionality constant C_θ depends on the geometry of the nozzle. Reitz and Bracco argued that the corresponding initial mean drop size should be correlated by

$$SMR = C_a\,[4\pi(\sigma/\rho_g \bar{U}^2)(3/2)] \qquad (16)$$

where the constant C_a is independent of the nozzle geometry and of order one. Note that in Eq. (16) the initial mean drop size is predicted to decrease when the chamber gas density increases. However, the computed downstream mean drop size is found to increase with increasing gas density due to collisions and recombinations and in agreement with measurements (Kuo and Bracco 1982b).

The computer code LDEF (Lagrangian Drop, Eulerian Fluid) developed by O'Rourke (1981) was employed with some modifications. This code incorporates the stochastic parcel method of Dukowicz (1980). The two-dimensional unsteady deterministic Eulerian equations for the gas and the stochastic Lagrangian equations for the drops are solved fully coupled with an implicit pressure iteration technique. In the present study, the k-ε model of turbulence was also included to describe the gas turbulence. The initial value of k in the injection cell was $k = 0.03\,U^{*2}$ and ε was found from Eq. (14) with $\lambda_t = 0.2d$. The initial values of k and ε

in the rest of the domain were set equal to small values and the resulting diffusivity was nearly the laminar one.

In the computational mesh, the cells were smaller near the nozzle exit where $\Delta y = 0.05$ cm and $\Delta x = 0.1$ cm. Away from the nozzle exit, the size of the cells increases in both the axial and radial direction with corresponding expansion factors of 4 and 7%. A total of 44 cells in the axial direction and 26 cells in the radial direction were used, giving the computational domain a length of 9.5 cm and width of 3.2 cm.

The top and right boundaries were treated as open boundaries, the left boundary as a solid wall, and the drops and gas injected from the cell of the left boundary next to the axis of symmetry. The condition on the top boundary allows for free entrainment from the surroundings. The pressures at the top and right boundaries were assumed to be uniform and equal to the ambient value to simulate a spray in a semi-infinite gas.

At any given time, the numerical solution of Eqs. (1-16) gives a distribution of the drop sizes and, for a given drop size, of the drop velocity in each elemental volume (practically, the numerical cell volume) around any point in the two-dimensional space. Also obtained are the instantaneous properties of the gas within the same volume. Even in steady state, the computed quantities fluctuate in time as they do in actual sprays, because of the stochastic nature of the atomization process reflected in the stochastic technique used to solve the spray equation. To compare with the measurements, many events are computed and then averaged, after which the fluctuating components of the various quantities are evaluated. Equivalently, one can let a steady spray run and sample the computations at appropriate time intervals and then again calculate the averages and fluctuating components. The latter was the technique used to obtain the results reported here.

The accuracy of the numerical solution of the equations is checked indirectly by reducing spatial and temporal increments and increasing the particle injection rate until the results become acceptably insensitive to them (O'Rourke 1981; Kuo 1982). The accuracy of the model is checked by comparisons with measured data. Thus, comparisons were made by O'Rourke and Bracco (1980) of the computed tip penetration rate and downstream drop size distribution with those measured by Hiroyasu and Kadota (1974) in one Diesel-type injection; by O'Rourke (1981) of the drop size and velocity distributions with those measured by Groeneweg (1967) at several locations within a spray from a swirl atomizer; and by Kuo and Bracco (1982b) with more of the penetration and drop size data of Hiroyasu and Kadota (1974) and with traditional spray tip penetration rate correlations.

Details on the model, the method of solution, comparisons with measured data, and computed structure of dense sprays are given by O'Rourke (1981) and Kuo (1982).

Comparison and Discussion

For clarity and future reference, it is useful first to give a brief description of the structure that sprays and other "compressible" jets must attain far from the injector.

In a steady nonvaporizing spray, the mass flow rate of the drops is the same at all axial locations but that of the entrained gas increases almost linearly with increasing distance from the nozzle. A station is reached where the mass and the momentum of the drops are negligible with respect to those of the entrained gas.

Downstream of this station, it is entrained gas that entrains more gas, as in "incompressible" jets. Fully developed incompressible jets exhibit self-preserving velocity profiles and relationships between fluctuating and mean components that can be used to express the total axial momentum in terms of the centerline velocity. Then, momentum conservation gives

$$C_\ell \rho_\ell \, \bar{v}^2 (0, 0, \infty) \pi d^2/4$$

$$= C_g \rho_g \, \bar{u}^2 (x, 0, \infty) \pi r^2_{0.5,g}$$

$$= C_g \rho_g \, \bar{u}^2 (x, 0, \infty) \pi C^2 (x - x_o)^2$$

or

$$\frac{\bar{u}(x,0,\infty)}{\bar{v}(0,0,\infty)} = \left(\frac{C_\ell}{C^2 C_g 4} \right)^{1/2} \frac{d(\rho_\ell/\rho_g)^{1/2}}{x - x_o} \qquad (17)$$

where ℓ is any injected fluid and g any ambient fluid; C_ℓ is defined by the injection velocity and velocity fluctuation profiles and C_g by the fully developed velocity and velocity fluctuation profiles; and C relates the half-radius (i.e., half-the-width at half-the-depth) to the distance from the virtual origin x_o. Equation 17 shows that, at sufficient distance from the nozzle, the ratio of the centerline velocity to the injection velocity becomes a function only of $x/d(\rho_\ell/\rho_g)^{1/2}$. This is true for all jets that have the same injection velocity profiles. If not, to the same injection

centerline velocity there correspond different momenta and C_ℓ is different. Figure 2 shows this relationship and the departure from the single line for large values of $x/d(\rho_\ell/\rho_g)^{1/2}$ must be due to the different C_ℓ and to experimental inaccuracies. The solid line of Fig. 2 is obtained with $C_\ell = 1$, $C_g = 0.846$, $C = 0.087$, in which case the coefficient of Eq. (17) is 6.3. Wu et al.(1984) give $C_g = 0.846 \pm 2.9\%$ and $C = 0.0868 \pm 7.9\%$. For $C_\ell = 1$, the coefficient of Eq. (17) then is $6.3 \pm 9\%$, which is in general agreement with those in the literature; e.g., Capp and George (1982) give 5.8.

Thus at sufficient distance from the injector, the axial scale of all steady jets becomes $d(\rho_\ell/\rho_g)^{1/2}$. Hinze (1975) gives references for the origin of this scale.

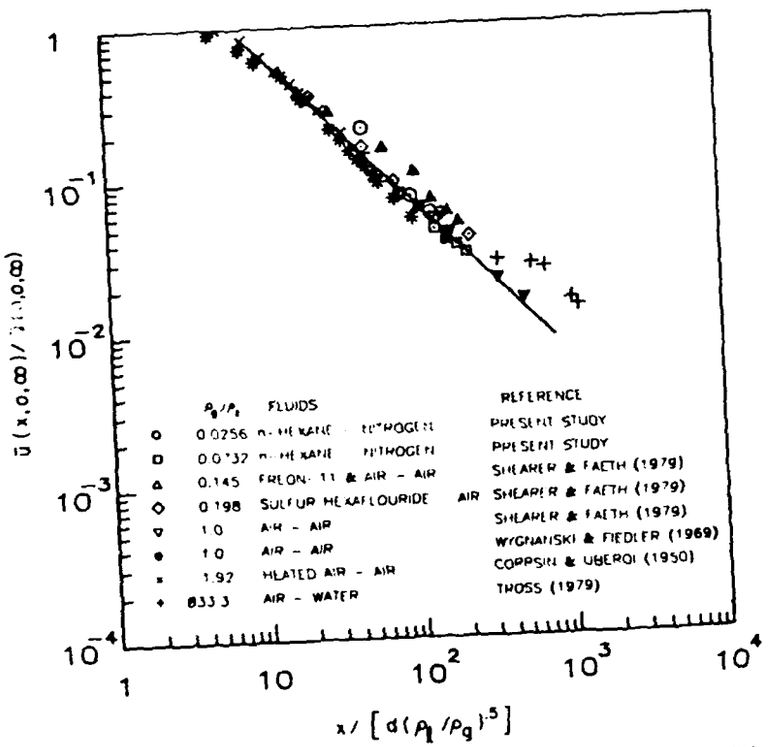

Fig. 2 Universal far field scaling for steady jets (Wu et al. 1984).

In the same axial region and in the zone of maximum radial gradient of the mean velocity, the turbulence intensity is about proportional to the centerline mean velocity $|\underline{u}'| \propto u(x,0,\infty)$ and the turbulence scale is proportional to the jet (width that is proportional to the) axial distance $\ell \propto (x-x_o)$ so that the turbulent diffusivity becomes proportional to centerline velocity and axial distance: $D_t \propto \ell |u'| \propto (x-x_o)\, u(x,0,\infty)$. Then, using Eq. (17), we get

$$D_t \propto (\rho_\ell/\rho_g)^{1/2} \frac{d}{2} \bar{v}\,(0,0,\infty) \qquad (18)$$

Thus for all "compressible" jets at sufficient distance from the injector, the diffusivity varies as the square root of the density ratio (Kleinstein 1964). Notice that the value of the proportionality constant changes depending on the injection velocity profile. From our computations, we find that its most probable value is $0.016\ (\pi C_\ell)^{1/2}$.

Comparisons are now made between the results obtained with the model described in the previous section and the laser Doppler velocimetry (LDV) drop velocity measurements of Wu et al. (1984). They measured the distribution function of the axial and radial components of the drop velocity at various radial and axial locations within steady sprays. The conditions of their experiment are given in Table 1 and computations were made for cases A-C. The three cases differ in gas-liquid density ratio and in injection velocity. Notice that the measurements were taken within 300-800 nozzle diameters from the nozzle exit.

Using only their experimental data, Wu et al. (1984) concluded that these sprays approach the above-mentioned fully developed incompressible jet limit at $x = 300d$. Thus in the figures, the corresponding quantities measured in steady incompressible jets by Wygnanski and Fiedler (1969)

Table 1 Spray conditions[a] (Wu et al. 1984)

Series	Pg,MPa	ρ_g/ρ_ℓ	Δp,MPa	$\bar{U}$, m/s	Nozzle,d(μm) -L/d	X/d
A	1.48	0.0256	11.0	127	127-4	600,800
B	4.24	0.0732	11.0	127	127-4	300,400,500,600
C	4.24	0.0732	26.2	194	127-4	400,500,600
D	4.24	0.0732	11.0	149	76-4	300,600,700,800
E	1.48	0.0256	11.0	125	76-1	300

[a] Liquid: n-hexane, ρ_ℓ = 665 kg/m^3, μ_ℓ = 3.2×10^{-4} N·s/m^2, σ_ℓ = 1.84×10^{-2} N/m; gas: nitrogen; room temperature.

Fig. 2 Universal far field scaling for steady jets (Wu et al. 1984).

are given for reference and comparison. Wygnanski and Fiedler measured the gas velocity in air jets using hot wire anemometry (HWA), Wu et al. measured the drop velocities in sprays by LDV, and we computed both gas and drop velocities in the same sprays. In our computations, the assumption was not made that the gas and drop velocities are the same and the distinction is maintained in the discussion of the results. However, similarities exist, as will become apparent.

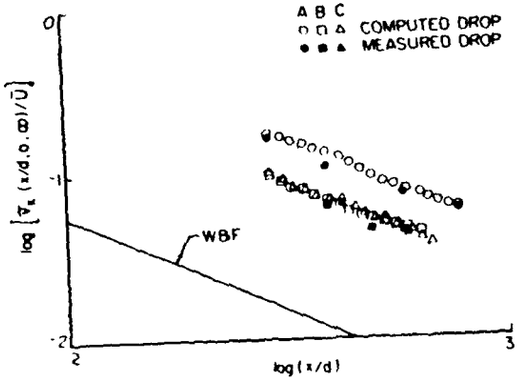

Fig. 3 Measured (Wu et al. 1984) and computed mean centerline drop velocity.

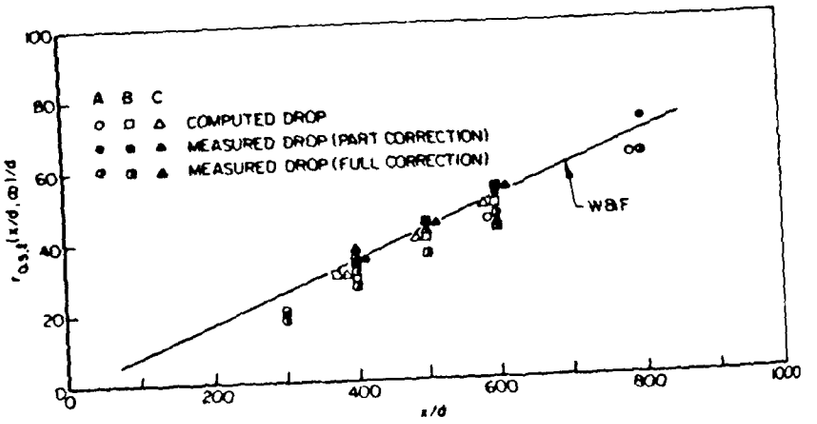

Fig. 4 Measured (Wu et al. 1984) and computed jet half radius based on the mean drop velocity.

Fig. 5 [illegible] = 665 kg/m³, $\mu_\ell = 3.2\times10^{-4}$ N. s/m², σ_ℓ = 1.84×10^{-2} N/m; gas: nitrogen; room temperature.

First the mean quantities and then the fluctuations are compared.

For applications, the two most important parameters are the steady-state centerline velocity and the angle of the spray. For constant pressure injections into unconfined quiescent gases, the tip velocity is about 70% of the steady-state centerline velocity (Whitehouse and Sareen 1974; Kuo and Bracco 1982a) and behind the head vortex the spray quickly attains its steady configuration, including its steady angle. Thus, the ability to reproduce steady centerline velocity and angle also implies the ability to predict the global transient behavior. Figures 3 and 4 show good agreement between the computed and measured values. In Fig. 4 $r_{0.5,\ell}$ is the half-radius as determined by the drop velocity. The most likely value of this half-radius is between the fully and the partially corrected data, where the computed values fall. The corresponding half angle is 4.95 deg ± 0.025 deg as compared with 4.95 deg ± 0.04 deg for incompressible jets (Wu et al. 1984).

Agreement of centerline velocity and jet width does not necessarily imply agreement over the entire cross section. However, Fig. 5 shows that such agreement does exist. The mean value of the axial component of the drop velocity is reproduced adequately for all cases and axial and radial locations. This figure and an examination of the data also show that the computed average axial drop velocity is only a few percents greater than the computed average axial gas velocity. (The stochastic computation of the drop leaves an indetermination about the exact values of all drop quantities that brings about large uncertainties about small differences.) Finally, Fig. 6 shows that at the axial locations of the comparisons both computations and measurements indicate that self-preserving profiles have been reached by the mean axial velocities of drops and gas and that these profiles are indistinguishable from that of incompressible jets. (In Fig. 6 also notice for future reference that the measurements show drops at larger radial distances than the computations.)

Having recovered the structure of incompressible jets as far as the mean quantities are concerned, we can compare the predicted diffusivity with the constant diffusivity that is sufficient to characterize the global behavior of fully developed turbulent jets. Figure 7 shows that the computed diffusivity varies radially and axially but for $x > 300d$ and for the region with the sharpest mean velocity gradients, it tends to the constant value of Schlichting (1979) after scaling it by the factor $(\rho_\ell/\rho_g)^{1/2}$; i.e. in Eq. (18), the proportionality constant is 0.0285 for $C_\ell = 1$ and with $v(0,0,\infty)$ replaced by $\bar{U}$.

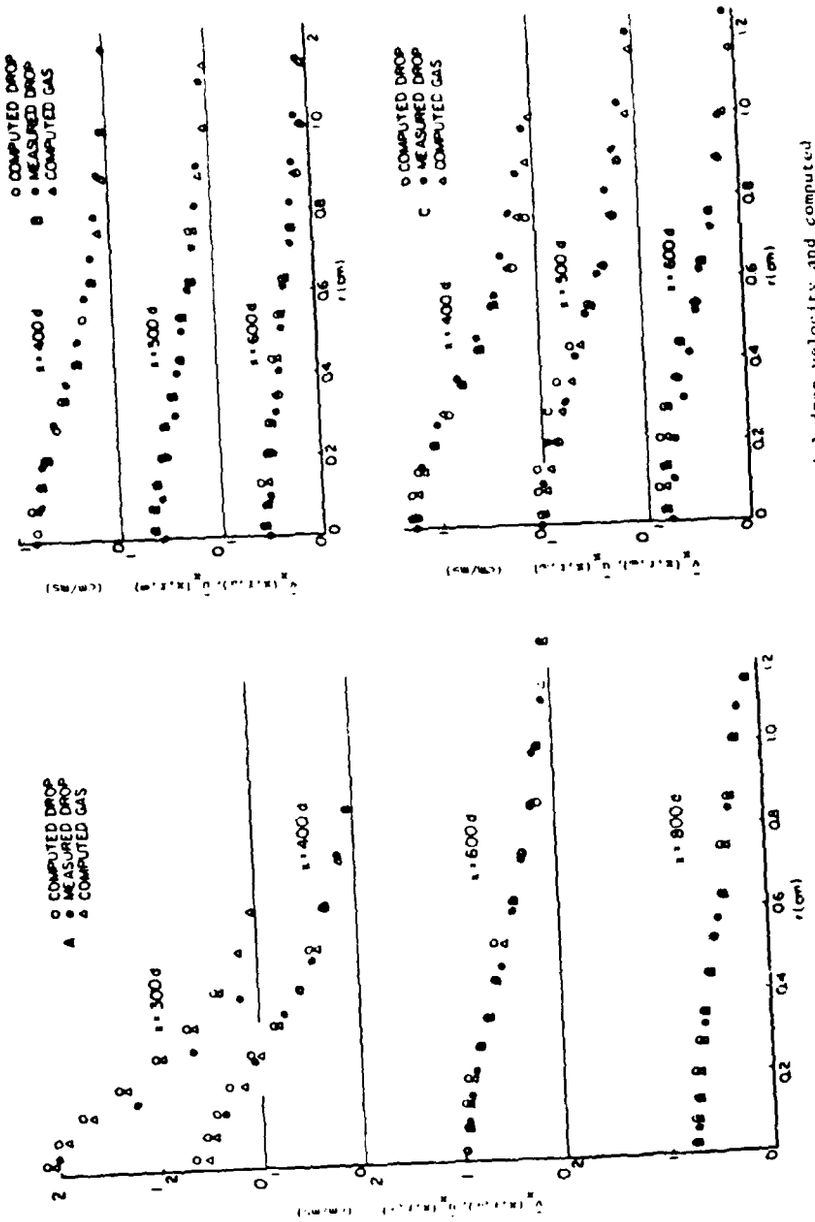

Fig. 5 Measured (Wu et al. 1984) and computed mean axial drop velocity and computed mean axial gas velocities for sprays A, B, and C of Table 1.

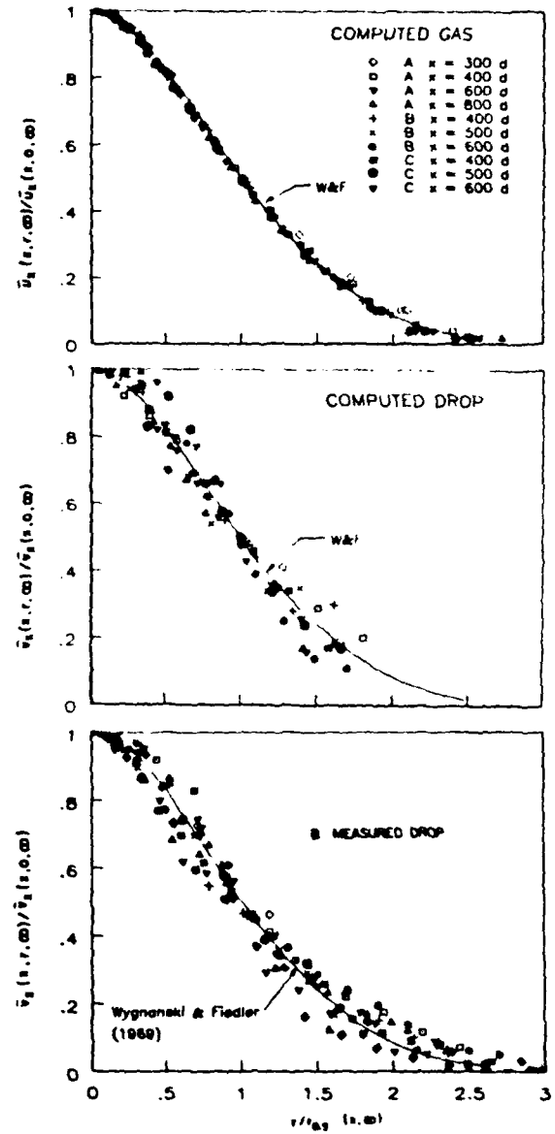

Fig. 6 Measured (Wu et al. 1984) and computed self preserving profiles of mean axial drop and gas velocities for sprays A-C of Table 1.

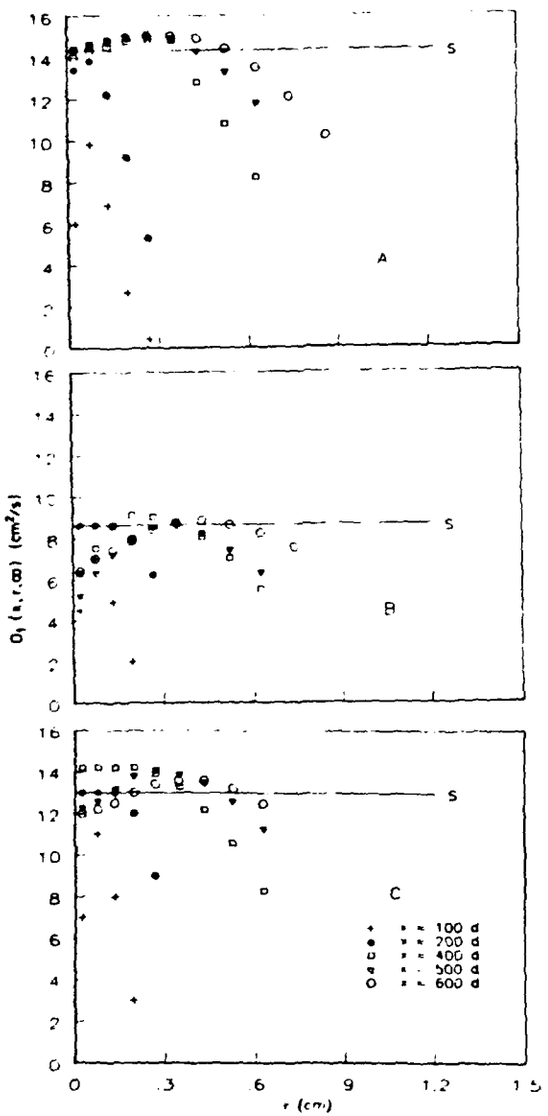

Fig. 7 Computed radial and axial distribution of the gas diffusivity for sprays A-C of Table 1.

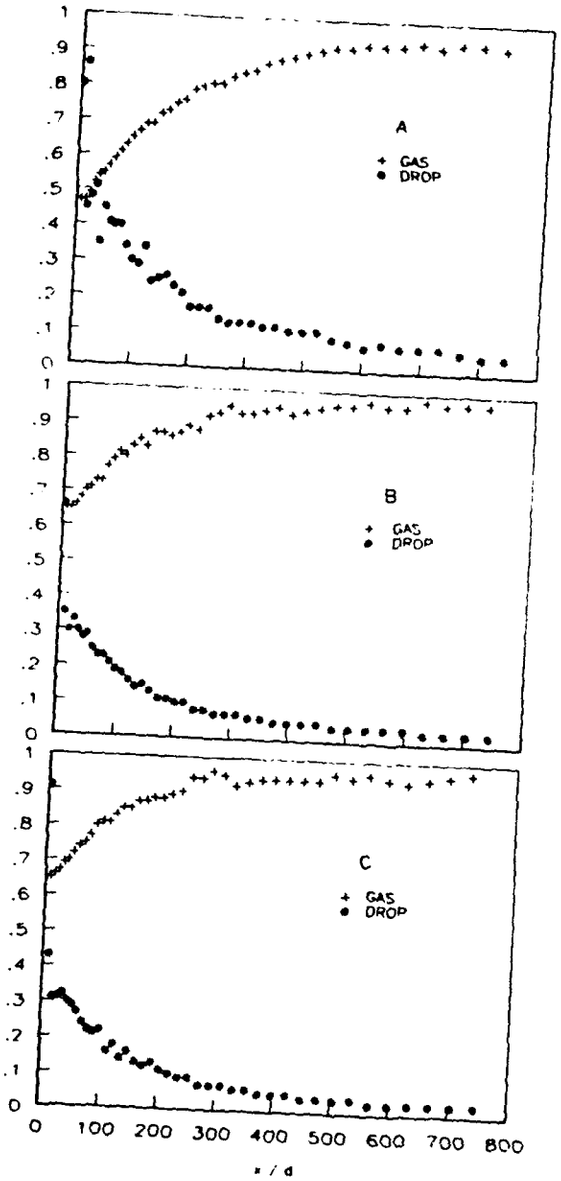

Fig. 8 Computed gas and liquid fractions of the axial momentum for sprays A-C of Table 1.

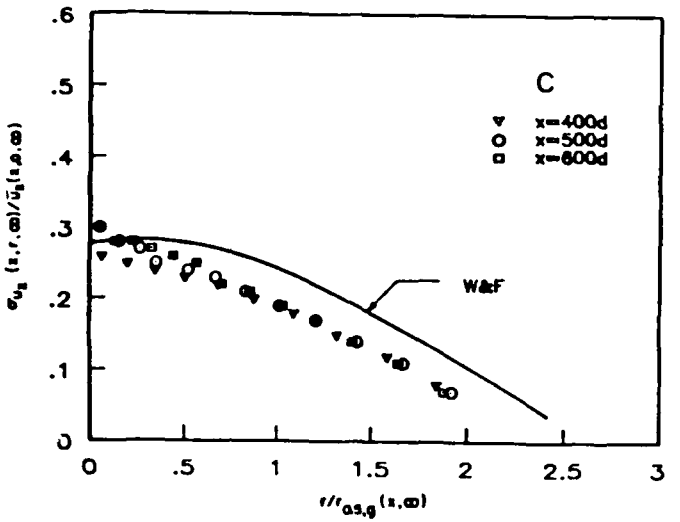

Fig. 9 Computed normalized turbulence intensity of the gas at various radial and axial locations for Case C of Table 1.

Thus, all indications are that for these sprays and x > 300d the mentioned limit, in which the entrained gas entrains more gas and controls the structure of the jet, practically has been reached. Indeed for x > 300d, no less than 87% of the axial momentum is with the gas (Fig. 8).

Parenthetically, it is noted that the magnitude of the jet diffusivities of Fig. 7 is similar to that predicted for the air in the combustion chamber of Diesel engines (Grasso and Bracco 1983). It suggests that engine sprays may also be directly affected by the turbulence of the charge.

Having considered average quantities, we can now examine the fluctuations. Figure 9 shows the computed normalized gas turbulence intensity for one of the three sprays. It is seen to have reached its fully developed limit and to agree reasonably well with that measured by Wygnanski and Fiedler (1969). Presently we will point out that classical HWA turbulence intensity measurements in incompressible round jets are not necessarily very accurate, particularly at the edge of the spray where they tend to underestimate the turbulence intensity.

Figures 10-12 show the computed relative fluctuation amplitude (normalized standard deviation), skewness, and flatness of the axial component of the drop velocity at various axial and radial locations for the three sprays. Figure 13 plots the measured data of Wu et al. (1984) for

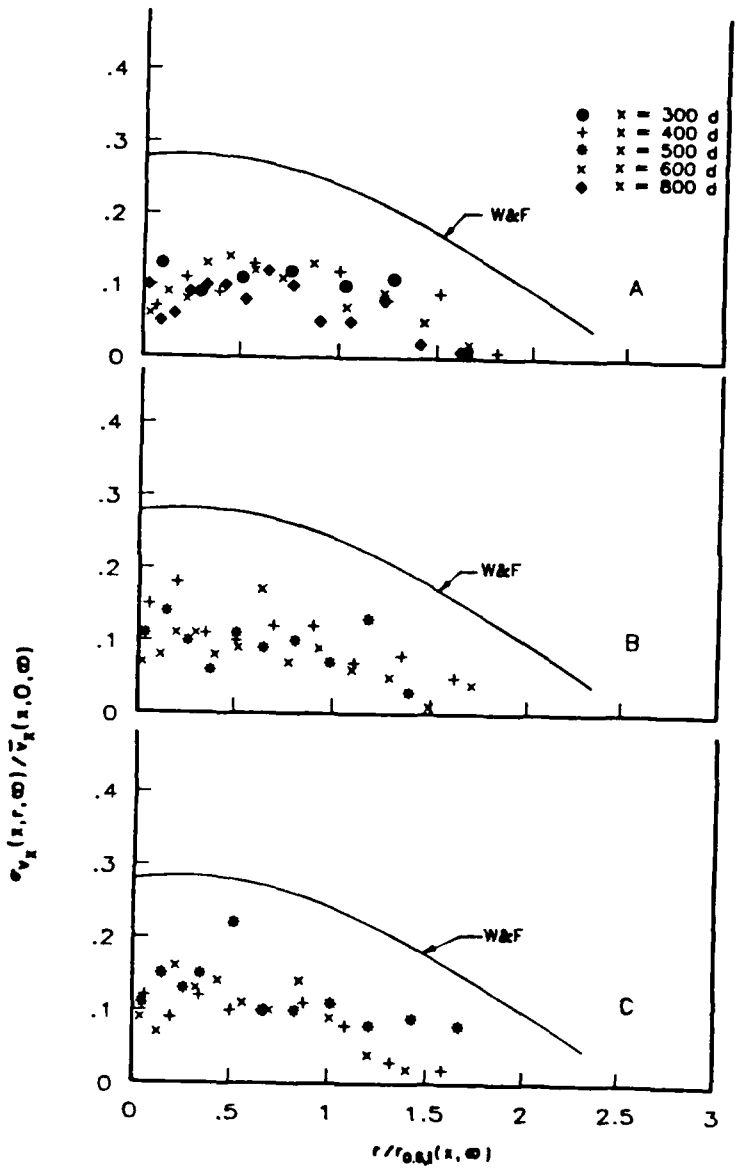

Fig. 10 Computed normalized standard deviation of the axial component of the drop velocity for sprays A-C of Table 1.

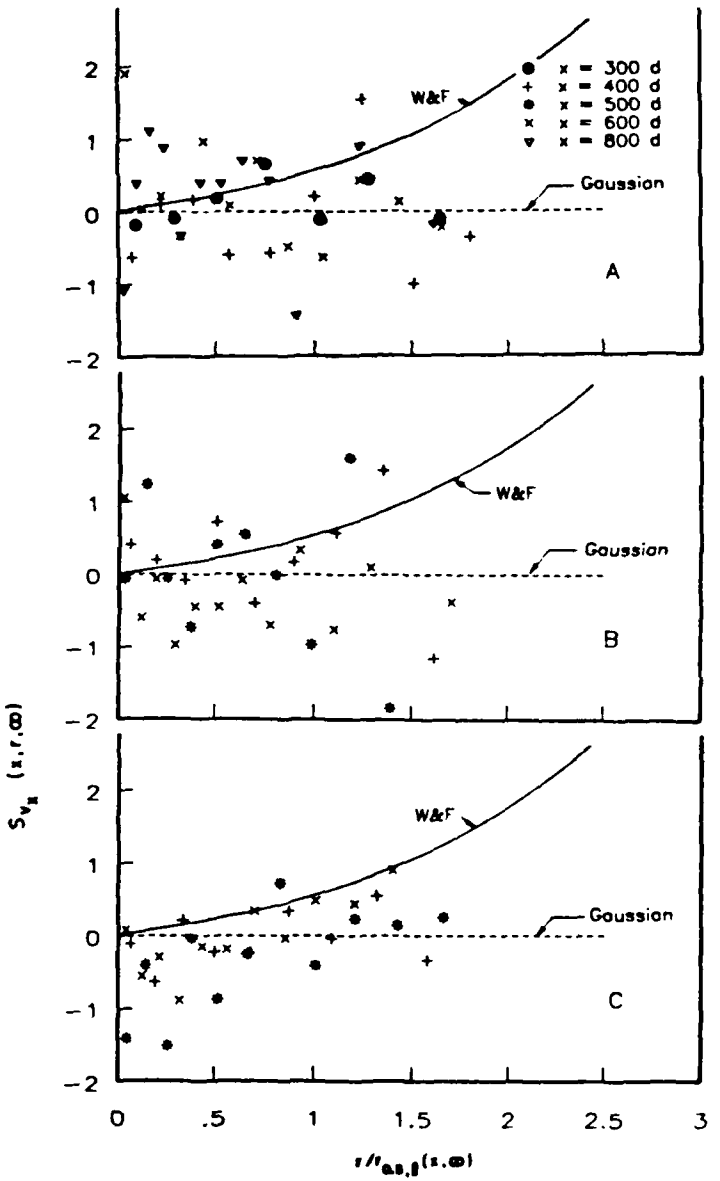

Fig. 11 Computed skewness of the axial component of the drop velocity for sprays A-C of Table 1.

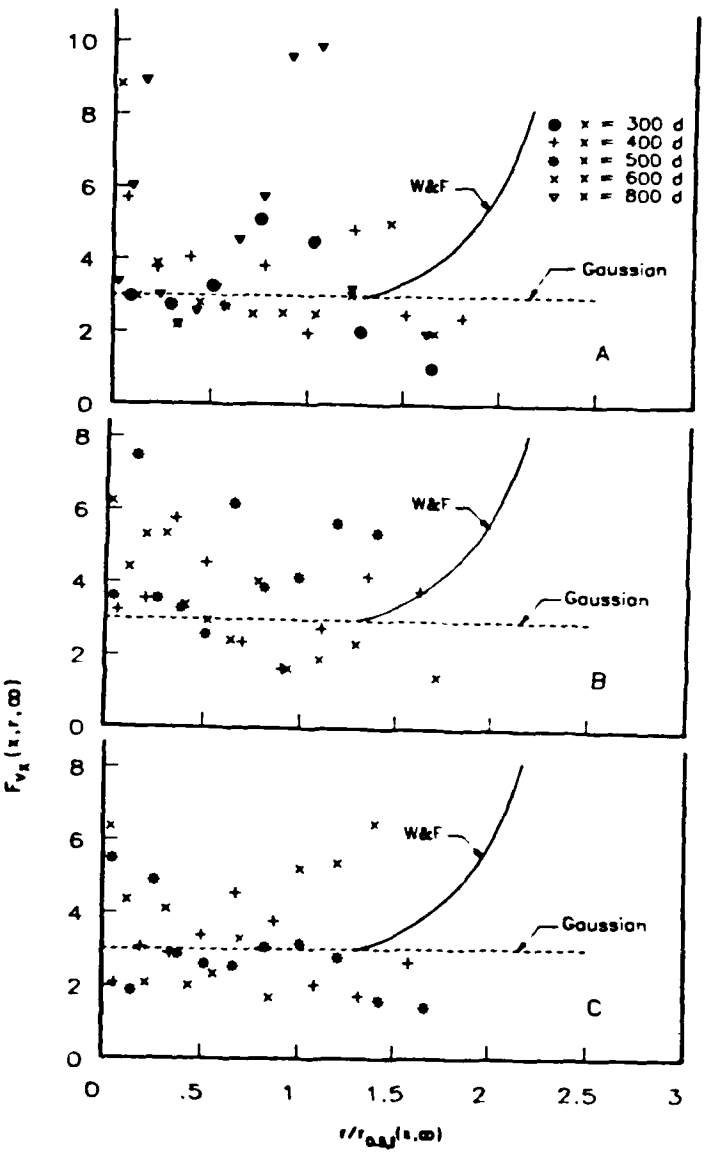

Fig. 12 Computed flatness of the axial component of the drop velocity for sprays A-C of Table 1.

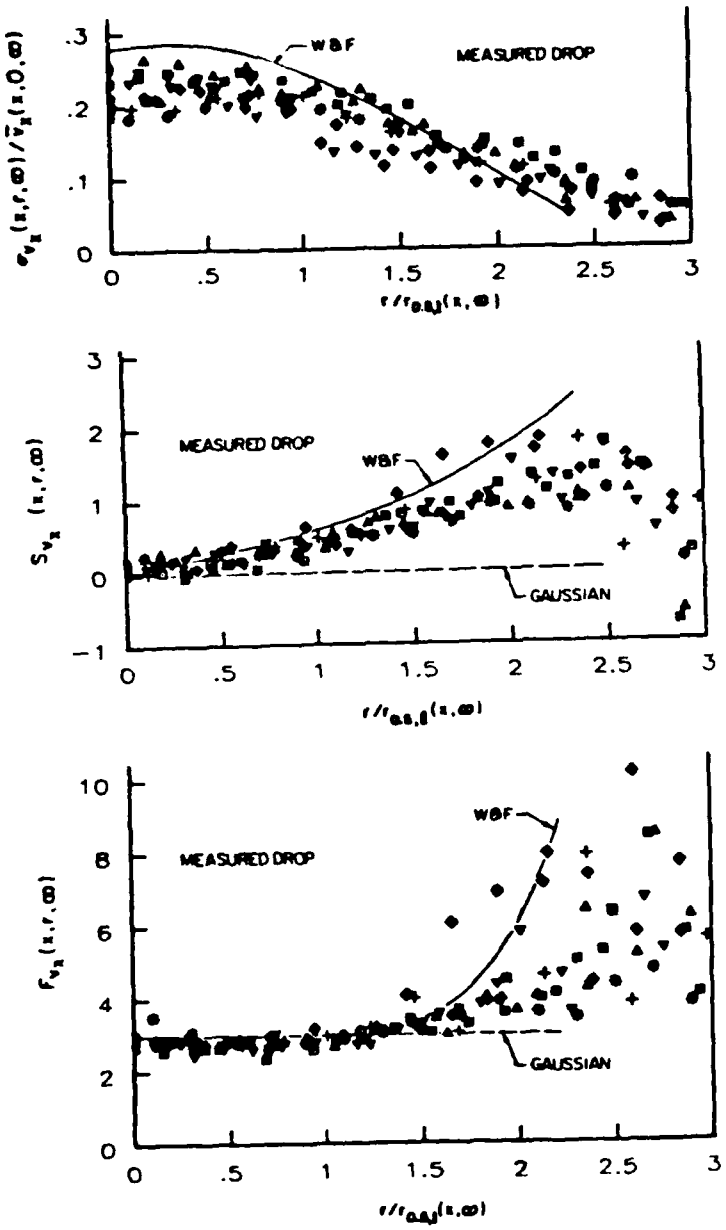

Fig. 13 Measured (Wu et al. 1984) normalized standard deviation, skewness, and flatness of the axial component of the drop velocity for sprays A-C of Table 1.

the same quantities. Also shown are the corresponding fluid quantities measured by Wygnanski and Fiedler (1969) in incompressible jets and those pertaining to Gaussian distributions. Both computed and measured data show considerable scatter, but the amplitude of the computed drop velocity fluctuation is about one half of that measured. However, the shape of the two distributions appear to be the same. Also, whereas the measured and computed mean drop quantities were shown to agree with those of incompressible jets, the measured drop fluctuations appear to disagree.

Wu et al. (1984) considered the influence of directional error in HWA and velocity biasing error in LDV and concluded that both classical HWA data and recent LDV data can be affected by large errors outside the half radius, particularly the fluctuations. When the possible sign and magnitude of the errors is considered, a tendency to better agreement is found. The accuracy of classical HWA measurements of fluctuations in incompressible jets had already been questioned (List 1982). We are inclined to conclude that the disagreement between the measured drop data and the incompressible jet data is due largely to experimental errors and that the amplitude of the fluctuation of the drop velocity should be equal to or smaller than that of the gas in the region where the gas dominates.

We are still left with the disagreement between the computed and the measured drop fluctuation amplitude. In the computations the scattering of the drop by the gas turbulence is determined by Eq. (13). A drop is assumed to feel the velocity of an eddy for a time that equals the residence time of the drop in the eddy. If the correlation time τ_c is much shorter than the drop relaxation time, $\tau_d = \rho_\ell r^2/4.5\,\mu_g$, then the drops cannot respond to the gas velocity fluctuations, exhibit smaller fluctuations and remain closer to the axis of the spray. This trend was checked with a computation of spray C in which the turbulent component of the gas velocity felt by the drop was changed at each Δt of the numerical integration, i.e., τ_c was reduced to the minimum value that can be computed (normally $\Delta t/\tau_c < 10^{-3}$). As expected, the standard deviation of the drop velocity decreased and became a half of that computed with Eq. (13) (collisions, whether or not followed by coalescence, scatter the drops and put a floor on σ_v). Also the drops did remain even closer to the axis than in Fig. 6. Thus, both trends indicate that it is necessary to account for the scattering effect of turbulence and that the coupling must be increased beyond that given by the present model.

skewness, and flatness of the axial component of the drop velocity for sprays A-C of Table 1.

At the other extreme, when the correlation time is much greater than the drop relaxation time, the drops follow the eddies and σ_{v_x} tends to σ_{u_x}. That is, the drops behave as the seeding particles for LDV turbulence measurements. This limit is approached as the distance from the injector increases, since τ_c continues to increase as x^2 whereas τ_d levels off when collisions become infrequent.

In the computations the ratio of the correlation time to the drop relaxation time was in the range 0.1-10, depending on drop size, location, and time of sampling. Therefore, σ_v should respond to adjustments in the correlation time and^{x}better agreement in both drop fluctuation amplitude and drop population at the edge of the spray should be possible.

As a whole, when the comparisons of mean quantities and shapes of distributions at the various locations and for the three sprays are considered, one can conclude that the far field is represented adequately. Unfortunately satsifactory

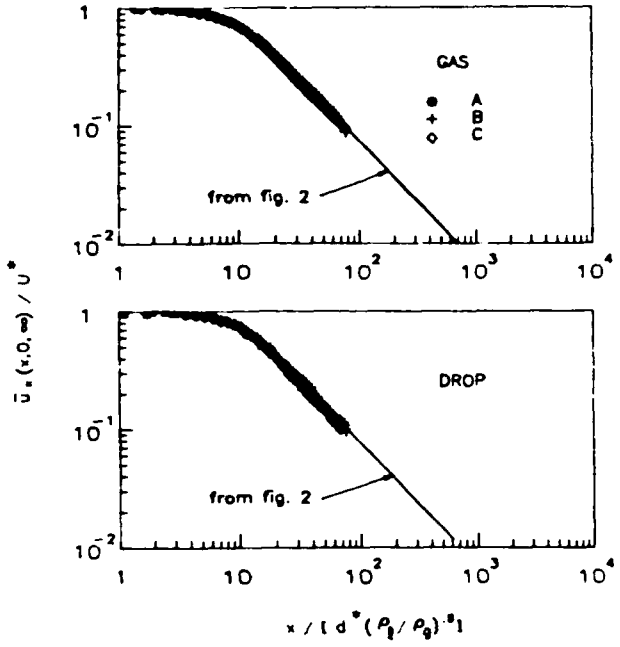

Fig. 14 Computed universal far-field scaling for gas and drops of sprays A-C of Table 1.

comparisons for $x > 300d$ assure only that the model is not in gross error for $0 < x < 300d$. Thus we will comment only briefly on what the model suggests about the structure of this inner region.

Figure 8 shows that a large fraction of the total axial momentum is transferred very rapidly by the drops to the gas, but Fig. 14 shows that the centerline velocity of the drops remains nearly constant up to $x = 7\ d^*(\rho_\ell/\rho_g)1/2$ and then starts decaying and rapidly approaches the limit of Eq. (17). In Fig. 14 the centerline gas velocity appears to be identical to the centerline drop velocity. Actually, at $x = 100d$ the mean axial drop velocity is about 10% larger than the mean axial gas velocity over the entire gross section and for all three sprays. But the difference gets progressively smaller until at $x = 300d$ the liquid velocity is only a few percentage points higher than the gas velocity, as already stated and shown in Fig. 5.

Finally, we should point out that while our model attempts to account for the effect of turbulence on the drop motion, it does not account for direct effects of the drops on the gas motion [Eqs. (5) and (6) do not include any terms due to the presence of drops]. Such effects should be important in the development region (Elghobashi and Abou-Arab 1983), but are negligible in the far field of our comparisons because the mass of the drops is small in comparison to that of the entrained gas. Even any retarding effect on the jet development is lost at sufficient distance from the nozzle.

Conclusions

Narrow full-cone high-velocity nonvaporizing isothermal sprays from steady injections into semi-infinite initially-quiescent gas were considered. The liquid-to-gas density ratio was 39 and 13.7.

Due to the rapid entrainment, the structure of these sprays becomes dominated by the ambient gas within distances of the order of hundreds of nozzle diameters. The entrained gas becomes a fully developed incompressible turbulent jet and is influenced little by the presence of the drops. The drops adjust their motion to that of the gas and local equilibrium is approached selectively.

In the fully developed region, centerline velocity and tip penetration rate are determined by the injection momentum and the gas density. To reproduce them, a simple model based on a constant diffusivity is sufficient. The diffusivity is that of incompressible jets multiplied by $(\rho_\ell/\rho_g)^{1/2}$. This is because differences in the development

process and length (i.e. in the virtual origin) become negligible at sufficient distance from the nozzle. However, care must be exercised in extrapolating these results to transient jets. Thus, for example, if the ambient gas or the injection velocity are unsteady the details of the development region can be important, depending on the ratios of various characteristic times. The model used reproduced the steady state through the computation of an impulsively started transient.

The model reproduced well the measured mean axial velocity of the drops at all locations and conditions. It also predicted correctly that within the range of the measurements mean drop and gas velocities are very nearly equal. This had been inferred directly from the measurements of the drop velocities. However, the computed amplitude of the drop velocity fluctuations was a factor of two smaller than the measured one. Nonetheless, the model was helpful in clarifying relationships between drop velocity fluctuations, gas velocity fluctuations, drop scattering by drop collisions, and location of the drops within the spray.

Unfortunately, successful reproduction of the drop far field constitutes only a weak test of the validity of the model as far as the development region and transient sprays are concerned since the main requirements to achieve it are good numerical accuracy, correct steady global far field gas diffusivity, and a valid estimate of the order of magnitude of the scattering of drops by drop collisions and gas turbulence. But spatially resolved accurate measurements in the development region and during transient operations for our type of sprays are not available and very difficult to make. Thus stricter tests of the model for such region and conditions will have to wait for the availability of appropriate experimental data.

Acknowledgments

Support for this work was provided by the U.S. Department of Energy (Contract DE-AC-04-81AL16338), the U.S. Army Research Office (DAAG29-81-K-0135), General Motors, Komatsu, and Cummins Engine. These results were presented at the 17th DISC Meeting, Los Alamos National Laboratory, N. Mex., March 1983.

References

Capp, S. P. and George, W. K. (1982) Measurements in an axisymmetric jet using a two-color LDA and bust processing. International Symposium on Applied L.D.A. to Fluid Mechanics, Lisbon, Portugal.

Dukowicz, J. K. (1980) A particle-fluid numerical model for liquid sprays. J. Comp. Phys. 33 (2), 229-253.

Elghobashi, S. E. and Abou-Arab, T. W. (1983) A two-equation turbulence model for two-phase flows. Phys. Fluids 26 (4), 931-938.

Faeth, G. M. (1983) Evaporation and combustion of sprays. Prog. Energy Combust. Sci., 9 (1/2) 1-76.

Grasso, F. and Bracco, F. V. (1983) Sensitivity of chamber turbulence to intake flows in axisymmetric reciprocating engines. AIAA J. 21 (4), 637-640.

Groeneweg, J. F. (1967) The statistical description of a spray in terms of drop velocity, size, and location. Ph.D. Thesis, University of Wisconsin, Madison, Wisc.

Hinze, J. O. (1975) Turbulence, McGraw Hill Book Co., New York.

Hiroyasu, H. and Kadota, T. (1974) Fuel droplet size distribution in Diesel combustion chamber. SAE Paper 740715.

Kleinstein, G. (1964) Mixing in turbulent axially symmetric free jets. J. Spacecr. Rockets 1 (4), 403-408.

Kuo, T.-W. and Bracco, F. V. (1982a) On the scaling of transient laminar, turbulent, and spray jets. SAE Paper 820038.

Kuo, T.-W. and Bracco, F. V. (1982b) Computations of drop sizes in pulsating sprays and of liquid core length in vaporizing sprays. SAE Paper 820133.

Kuo, T.-W. (1982) On the scaling of transient laminar, turbulent, and spray jets. Ph.D. Thesis 1538-T, Dept. of Mechanical and Aerospace Engineering, Princeton University, Princeton, N. J.

List, E. J. (1982) Turbulent jets and plumes. Ann. Rev. Fluid Mech. 14, 189-212.

O'Rourke, P. J. and Bracco, F. V. (1980) Modeling of drop interactions in thick Sprays and comparison with experiments. Institution of Mechanical Engineers, Pub. ISBN 0 85298 4693, 101-116.

O'Rourke, P. J. (1981) Collective drop effects on vaporizing liquid sprays. Ph.D. Thesis 1532-T, Dept. of Mechanical and Aerospace Engineering, Princeton University, Princeton, N. J.

Reitz, R. D. and Bracco, F. V. (1982) Mechanism of atomization of a liquid jet. Phys. Fluids, 25 (10) 1730-1742.

Schlichting, H. (1979) Boundary-layer theory, McGraw-Hill Book Co., New York.

Sirignano, W. A. (1983) Fuel droplet vaporization and spray combustion theory, Prog. Energy Combust. Sci., 9(4) 291-322.

Whitehouse, N. D. and Sareen, B. K. (1974) Prediction of heat release in a quiescent chamber Diesel engine allowing for fuel/air mixing, SAE Paper 740084.

Williams, F. A. (1962) Progress in spray-combustion analysis, Eighth International Symposium on Combustion, pp. 50-69, Williams & Wilkins Co., Baltimore.

Wu, K.-J., Coghe, A., Santavicca, D. A., and Bracco, F. V. (1984) LDV measurements of drop velocity in Diesel-type sprays, AIAA J. (to appear).

Wygnanski, I. and Fiedler, H. (1969) Some measurements in the self-preserving jet, J. Fluid Mech., 38, (3), 577-612.

APP D

STRUCTURE OF HIGH-SPEED FULL-CONE SPRAYS

Frediano V. Bracco
Department of Mechanical and Aerospace Engineering
Princeton University
Princeton, N.J. 08544

Proofs should be sent to
F.V. Bracco at the above address.
Tel. Number: 609-452-5191

To Appear in "Recent Advances in Gas Dynamics"
(C. Casci, Editor)
Plenum Publishing Corp., N.Y., N.Y.

1983

ABSTRACT

A better understanding and characterization of the formation and propagation of high velocity sprays from single hole cylindrical nozzles is of importance both fundamentally and practically. The steady and transient structure of these sprays is qualitatively similar to that of incompressible jets but the breakup of the liquid column into drops and the presence of drops introduce substantial quantitative differences. Measurements of the angle of the spray and of the size of the drops near the nozzle suggest that the breakup of the outer surface of the liquid jet is due to aerodynamic forces that lead to the rapid and selective growth of surface perturbations generated within the nozzle. The state and mechanism of disruption of the inner part of the liquid jet is less clear but sufficiently downstream only individual drops are present. Recent LDV drop velocity measurements and detailed multidimensional computations have shown that at distances of the order of hundreds of nozzle diameters so much ambient gas has been entrained by the spray that the subsequent structure of the jet is dominated by the entrained ambient gas and the fully developed incompressible jet structure and drop-gas equilibrium are approached.

NOMENCLATURE

A, B, C, C_m, C_q, C_t	Dimensionless constants of Eqs. 15, 16, 17, 1, 2, 3, respectively
C_D	Nozzle discharge coefficient
d	Nozzle diameter
d_ℓ	Drop diameter
D_t	Turbulent diffusivity
F_{v_x}	Flatness of the fluctuation of the axial component of the drop velocity, $\overline{v_x'^4}/\overline{v_x'^2}^2$
L	Nozzle length
M	Specific momentum flow rate
p	Pressure
Q	Volumetric flow rate
$r_{0.5}$	Jet half radius (half the width at half the depth)
Re_j	Liquid jet Reynolds number, $\rho_\ell \bar{V}_{inj} d/\mu_\ell$
S_{v_x}	Skewness of the fluctuation of the axial component of the drop velocity, $\overline{v_x'^3}/\overline{v_x'^2}^{3/2}$
$\underline{u}$	Gas velocity vector of components u_x, u_r
$\bar{V}_{inj}$	Mass mean injection velocity
$\underline{v}$	Drop velocity vector of component u_x, u_r
W_j	Jet Weber number, $\rho_\ell \bar{V}_{inj}^2 d/\sigma$
x	Axial distance from the nozzle exit
x_0	Virtual origin
x_1	End of intact liquid core
x_2	Beginning of fully developed entrained gas jet

r	Radial distance
Δp	Injection pressure difference
θ	Spray angle
$\theta_{0.5}$	Angle corresponding to $r_{0.5}$
μ_g	Gas viscosity
μ_ℓ	Liquid viscosity
σ	Surface tension
σ_{u_x}	Standard deviation of the fluctuation of the axial component of the gas velocity, $\overline{u_x'^2}^{1/2}$
σ_{v_x}	Standard deviation of the fluctuaton of the axial component of the drop velocity, $\overline{v_x'^2}^{1/2}$
ρ_g	Gas density
ρ_ℓ	Liquid density
τ	Characteristic time

SUPERSCRIPTS

$'$	Fluctuation
$*$	Applicable to far field of sprays

SUBSCRIPTS

CL	On the centerline, $r = 0$
e	Entrained
0	At the nozzle exit, $x = 0$

INTRODUCTION

Sprays exhibit a large variety of geometrical, dynamic, and thermodynamic configurations [1-3]. The general features of these configurations are understood but the details are not and predictions remain elusive. In this field, as in many others, the stability of complex interfaces, non-equilibrium thermodynamics, intricate reactions, and turbulence ultimately set the limits of our knowledge.

This is true even for the simplest of configurations, that is the one of interest in this review, in which a liquid is injected into a gas through a single straight hole of circular crosssection, the two media have neglegible angular momenta, and their thermodynamic states are such that vaporization and chemical reactions can be ignored. Only dynamic forces control the field and the evolution of interfaces and turbulence present the greatest difficulties.

A general idea of the structure of our sprays can be obtained by considering the similar and better understood family of incompressible jets [4-6].

Figure 1 shows the initial propagation of a turbulent incompressible jet [7] and of a spray [8]. The propagation of the incompressible jet is marked by the advancement and growth of a head vortex that is fed, from its downstream side, by the injected medium and the ambient medium that was entrained in the region between the vortex head and the nozzle. Practically, this intermediate region is in its steady state configuration. That is, the head vortex leaves a turbulent, steady, incompressible jet behind itself. In the laboratory frame, the vortex moves at a fraction of the local steady state centerline velocity. Within the steady part, the shear layer, the potential core, and its end can be seen.

The corresponding picture of a spray raises several questions. Its internal structure cannot be seen and is not known precisely because no technique has been found to probe it without altering it significantly. There is a head structure but its details are not obvious. It is expected that when the head structure is at sufficient distance from the nozzle, enough ambient gas has been entrained to set up a flow field similar to that of incompressible jets behind itself. But closer to the nozzle, the liquid core, liquid ligaments, and drops impose different configurations on the shear layer and on the head of the jet due to their different modes of momentum transfer. The length of the transition region is not known. Behind the head, however, the spray divergence angle, which is the only quantity that can be measured with relative ease, rapidly achieves its steady state value [8]. This indicates that also in sprays the adjustment to steady state occurs primarily within their head region. In the steady part of the spray of Fig. 1, as in the corresponding incompressible jet, we expect the mean axial velocity to point downstream and the mean radial velocity to point toward the axis always. Thus we call them full-cone sprays in contrast to hollow-cone sprays that exhibit mean recirculation flows along the axis and correspondingly larger spray angles.

In Fig. 1b the spray appears to start diverging immediately at the nozzle exit. Although this is the mode of breakup of interest in this review, there are other modes and some are shown [8] in Fig. 2. All other parameters being the same, at very low injection velocities a jet breaks up many diameters downstreams and forms large drops. Surface tension is the disruptive force (Fig. 2a). As the velocity is increased, the displacement of the gas by the moving undulated liquid surface generates a pressure distribution that aids sur-

face tension in amplifying surface waves (Fig. 2b). This process, which is called aerodynamic interaction, eventually becomes the main distabilizing force and leads to the formation of very small drops while being opposed by surface tension (Fig. 2c). All along an intact surface is visible and the growth of unstable surface waves is detectable. These are classical regimes of breakup of circular liquid columns and major contributions to our understanding of them were made [9] by Lord Rayleigh, C. Weber, and G.I. Taylor. They continue to be the subject of current research [10] but are not the one of interest to us here.

The regime of interest to us is obtained when the injection velocity is so high that the intact length of the outer jet surface seems to disappear and the configuration of Figs. 2d and 1b is obtained. This regime is called the atomization regime [11] and the forces that control it are more complex and less known even though it has been the subject of extensive research because of its considerable practical importance.

Thus we will concentrate on non-vaporizing, non-reactive, isothermal, atomizing, full-cone sprays, such as those of Figs. 1b and 2d, and discuss their possible structure. We will consider first the steady far field and then the breakup and development regions. For liquids such as water and hydrocarbon fuels injected at room temperature into standard or compressed air or similar gases, such sprays are found at injection velocities of the order of 10^2 m/s. The high velocity allows large mass flow rates to be obtained even with small nozzles. Their diameter is often of the order of 10^2 μm so that their initial characteristic time is of the order of 10^{-6} s. Drop diameters are of the order of 10 μm. The combination of large velocity and small size makes detailed measurements difficult in the breakup and development regions. Thus their initial transient was observed for the first time only recently [8].

THE STEADY FAR FIELD

The classical point source, boundary layer, similarity solution of Tollmien [4] for incompressible jets is a satisfactory guide to the understanding of the global structure of the far field of full cone sprays. In principle, only one constant, such as C_t that relates the effective turbulent diffusivity D_t to the specific momentum flow rate M, is left indetermined by this solution and must be evaluated from measurements. Then the width increases as x, the centerline velocity decays as 1/x, and the ratio of the entrained mass to the injected mass increases as x:

$$M = C_m \pi \bar{u}_{0,CL}^2 d^2/4 \tag{1}$$

$$Q_0 = C_q \pi \bar{u}_{0,CL} d^2/4 \tag{2}$$

$$D_t = C_t [C_m \pi \bar{u}_{0,CL}^2 d^2/4]^{1/2} \tag{3}$$

$$r_{0.5} = 8 (\pi(2^{1/2} - 1)/3)^{1/2} C_t (x-x_0) \tag{4}$$

$$\bar{u}_{x,CL} = (3 C_m^{1/2}/16\pi^{1/2} C_t) d \bar{u}_{0,CL}/(x-x_0) \tag{5}$$

$$Q_e/Q_0 = (16\pi^{1/2} C_t C_m^{1/2}/C_q)(x-x_0)/d \tag{6}$$

In the above equations the constants C_m and C_q are used to relate the specific momentum flow rate and the volumetric flow rate to the injection centerline velocity through the injection velocity profile, and x_0 is the virtual origin. (In practice the determination of C_m, x_0 and of an additional needed constant x_2 is nontrivial even for incompressible jets. We will return to this subject later.)

But at this point the growth of the entrained mass and local characteristic convection and diffusion times are of interest to us. Schlichting [4] gives C_t = 0.0161 and Eq. 6 shows that for $C_m = C_q = 1$, the entrained mass is already 10 times the injected one at 22 nozzle diameters from the virtual origin. Local

convection and diffusion times can be obtained dividing $(x-x_0)$ by $\bar{u}_{x,CL}$ from Eq. 5 and $r^2_{0.5}$ by D_t from Eqs. 4 and 3. The two times are of the same order and increase as $(x-x_0)^2$.

For our sprays the injected medium is a liquid and the entrained medium is a gas, so that the initial entrainment process can be expected to differ from that of incompressible jets. But at sufficient distance from the injector, the injected mass must become neglegible in comparison to the entrained one because past a certain distance their ratio grows as x. Downstream of such region, the momentum that leads to the entrainment of more ambient gas resides mostly with the ambient gas that was entrained earlier. That is, the structure of fully developed incompressible jets is recovered.

Imbedded in this far field there are drops that move in equilibrium with the gas. This is because the time for the drop velocity to relax to the local gas velocity, $\rho_\ell d_\ell^2/18\mu_g$, has an upper limit whereas the fluid times continues to grow as x^2. Since there is a distribution of drop sizes and of eddy times, equilibration will be selective and dependent on conditions but at some appropriate distance from the injector, all sprays become incompressible jets dominated by the entrained ambient medium and drops move within them as markers of the motion of the ambient medium.

Having accepted the existence of this limit, Eqs. 1-6 can be modified for direct application to the far field of sprays. Following Thring and Newby [12] and Kleinstein [13], we can equate the axial momentum evaluated at the nozzle exit, where the density is ρ_ℓ, to that evaluated in the far field, where the density is ρ_g and the velocity profile is fully developed, and conclude that, as far as the far field is concerned, a liquid spray is an incompressible jet with an equivalent specific momentum flow rate of $M(\rho_\ell/\rho_g)$. Then Eqs. 1-6 become

$$M^* = M(\rho_\ell/\rho_g) \tag{7}$$

$$Q_0^* = Q_0\rho_\ell \tag{8}$$

$$D_t^* = D_t(\rho_\ell/\rho_g)^{1/2} \tag{9}$$

$$r_{0.5}^* = r_{0.5} \tag{10}$$

$$\bar{u}_{x,CL}^* = \bar{u}_{x,CL}\,(\rho_\ell/\rho_g)^{1/2} \tag{11}$$

$$Q_e^*/Q_0^* = (Q_\ell/Q_0)(\rho_g/\rho_\ell)^{1/2} \tag{12}$$

$$d^* = d(\rho_\ell/\rho_g)^{1/2} \tag{13}$$

Parallel interpretations are that in the far field a spray is an incompressible jet from an equivalent nozzle diameter [12] of $d(\rho_\ell/\rho_g)^{1/2}$ or with an equivalent turbulent diffusivity [13] of $D_t(\rho_\ell/\rho_g)^{1/2}$. Notice however that the change in the virtual origin is not identified by this theory since this quantity is determined by the structure of the development region. The ratio of the turbulent diffusion time to the drop relaxation time becomes

$$\frac{\tau^*_{diff}}{\tau_{drop}} = 18\,\left(\frac{r_{0.5}}{d_\ell}\right)^2\left(\frac{\mu_g}{\rho_\ell D_t^*}\right) \tag{14}$$

Several authors have realized the existence of this limit and taken good advantage of it [14]. But only recently detailed drop velocity measurements within sprays of this family have provided direct evidence of it. We shall review these measurements briefly, but first a note of caution. In specific applications, particularly to time varying and/or closed volumes, the development region is often the one of prime interest. Indeed in many cases no more volume or time are provided than those necessary to complete some specific degree of mixing of the injected and ambient media. In the far field limit, the injected medium is but a trace within the ambient one. Thus we are not saying

or implying that the local equilibrium limit is necessarily achieved in applications. We are saying that these limits exist and are conceptually useful.

The data of Fig. 3 were taken in the sprays of Table 1 under steady injections, at distances greater than 300d, and with the gas contained in a vessel of such size that a wall-free environment was approach [15]. These sprays looked very much like those of Figs. 1b and 2d. Up to $r = r_{0.5}$, the radial profiles of the mean axial drop velocity and of the amplitude, skewness, and flatness of the fluctuation of the drop axial velocity are seen to fall within the range of the corresponding fluid quantities measured in incompressible jets by Wygnanski and Fiedler [16] by hot wire anemometry and by others [4-6, 17,18] with hot wire anemometry and laser Doppler velocimetry. The same parallel was also found for the radial component of the drop velocity, for the centerline velocity decay and for the width. Also, the drop velocity was measured with various laser power levels, thus weighing the measurements in favor of drops of different sizes, and the results were found to be independent of it for $x \gg 300d$. If the drops had not been in equilibrium with the gas, their velocity would have depended on their size. Thus indications are that for the full cone sprays of Table 1 the incompressible jet and drop-gas equilibrium limits are achieved around $x = 300d$ and for $r < r_{0.5}$. For spray E, at $x = 200d$ the measurements indicate that drops are not in equilibrium with the gas and for $x \gg 300d$ but $r > r_{0.5}$ the evidence is inconclusive because of large errors in both HWA and LDV data [15].

There is no reason to expect that all sprays of Table 1 should reach equilibrium at the same axial distance, but the data were not sufficiently numerous or sufficienty accurate to differenciate and the 300d location should

be considered indicative. By extrapolating backward the centerline velocity decay, and also checking the growth of the jet width, it was determined that x_0 = 30d for ρ_ℓ/ρ_g = 13.7 and x_0 = 100d for ρ_ℓ/ρ_g = 39.1. If the 300d range and the two values of x_0 are compared with the corresponding 50d-70d and 5d-10d values for incompressible jets [16], the reasonable conclusion is reached that full-cone sprays develop into incompressible jets but require a longer distance and that such distance is likely to be an increasing function of ρ_ℓ/ρ_g. The density ratio, ρ_ℓ/ρ_g, is seen to be the main additional parameter for the achievement and structure of the far field of these sprays.

THE STEADY NEAR FIELD

In considering the near field we will start from the outer part of the spray in the immediate vicinity of the nozzle exit. It is of interest to know what forces breakup the liquid surface in this region. From photographs, such as Figs. 1b and 2d, it appears that the jet starts diverging immediately at the nozzle exit. Higher resolution images, such as Fig. 6 which will be reconsidered later, show isolated drops and an opaque, highly-irregular, diverging fluid that could be made up of any combination of drops, ligaments, blobs, and deformed intermingled gas-liquid continua.

Hypothesis about the breakup mechanism are not lacking [1], but quantitative evidence from controlled well documented unequivocal experiments has been very scant. One difficulty is that too many events that can contribute are present simultaneously and cannot be investigated separately while still considering the same family of sprays.

For example, turbulence of the liquid was suggested as the main distabilizing agent. The Reynolds number based on the nozzle diameter is generally

greater than 10^4 but the nozzle length-to-diameter ratio is seldom greater than 6 and fully developed turbulent pipe flows are not present. Moreover increasing L/d from 10 to 80 leads to smaller divergence angles, i.e. to more stable jets [19,20]. Within the nozzle, there are turbulent wall boundary layers and the sudden change of forces within them that occurs at the nozzle exit has been suggested as distabilizing, but even in the most carefully machined metal nozzles the surface roughness is still no less than 10 μm with diameters in the range of 70 μm to 300 μm. It is not clear whether the tall ridges and deep valleys formed by surface roughness trip the flow or trap it. In any case, radiusing the exit edge with various curvatures brought about no measurable change in the initial spray angle [20]. Cavitation is invariably present at the entrance of practical nozzle of this family and has been suggested as the main distabilizing agent. But cavitation free nozzles have been found to give immediately diverging jets too [20]. Their angle was smaller, indicating greater stability, but the geometry of the cavitation-free nozzles was so different from the sharp-inlet, sharp-outlet, straight-wall geometry of standard nozzles that the entire nozzle flow field was also different.

Also suggested as possibly being responsible for the breakup are the rearrangement of the cross-section axial velocity profile, and liquid supply pressure oscillations. But none of these mechanisms alone was found adequate to explain the trends exhibited by the initial spray angle [11, 20]. However, any of them could be contributing to the break up process as explained below.

Since aerodynamic interaction is known to cause the breakup of jets at lower speeds, the suggestion that it may continue to do so at higher speeds too is a natural one. According to this view the length of jet surface over which

unstable surface waves grow becomes shorter and shorter as the speed is increased, due to the faster growth rate of the unstable waves, until it becomes of the order of a few microns and is no longer detectable. Then the jet appears to diverge immediately at the nozzle exit. This first order linear perturbation theory leaves a parameter unspecified that can be interpreted as the initial amplitude of the surface perturbations when the liquid first enters the gas. If this parameter is allowed to vary with nozzle geometry, as it would be the case if different nozzle flows establish different initial perturbation levels through some combination of the previously mentioned processes, then a supplemented aerodynamic interaction mechanism results that seems to comply in a fitting way with a rather large set of experimental information. Castleman [21] was among the early supporters of this view. Ranz [22] produced a theoretical framework for it, extending the work of Taylor [23]. And Reitz [24,11] performed a comprehensive evaluation of most major proposals and sharpened the focus on it.

The supplemented aerodynamic theory leads to the prediction [22,24,25] of the initial spray angle, the initial average drop size, and the length of the intact core. The equations are particularly simple in the limit $\frac{1}{2} Re_j^2/\rho_g We_j^2 > 1$ which is the one of practical interest in many cases of atomization. The angle is determined by combining the radial velocity of the fastest growing of the unstable surface waves with the axial injection velocity:

$$\tan \frac{\theta}{2} = \frac{1}{A} \, 4\pi \left(\frac{\rho_g}{\rho_\ell}\right)^{1/2} \frac{3^{1/2}}{6} \qquad (15)$$

where A is a constant whose value depends on the nozzle geometry and must be determined experimentally. The initial average drop diameter is assumed to be proportional to the length of the most unstable wave:

$$\bar{d}_\ell = \frac{4\pi\ B\ \sigma}{\rho_g\ \bar{u}^2_{0,CL}}\ \frac{3}{2} \tag{16}$$

where B is a constant of order one and independent of the nozzle geometry (but dependent on the reference velocity that is chosen for the break up process). And the length of the intact core is obtained by subtracting the mass of the drops from the intact liquid column as they are formed:

$$\frac{x_1}{d} = C\ (\frac{\rho_\ell}{\rho_g})^{1/2} \tag{17}$$

where C is a proportionality constant.

The prediction that in the atomization regime the initial value of the spray angle depends almost exclusively on the density ratio and the nozzle geometry is surprising, considering the many parameters that could effect it, but is generally born out by measurement. Figure 4 shows that, for a given nozzle geometry, large changes in liquid properties, injection velocity, and gas pressure bring about only very small systematic trends and that the density ratio dominates [20]. Figure 5 gives an example of the effect of nozzle geometry, all other parameters being the same [20]. In spite of the success there are limitations: The mechanism by which the nozzle geometry influences the angle is not known; although the angle is very reproducible in any given experiment, its value depends somewhat on definitions and measuring techniques; when a broad range of injection velocities is explored a mild trend is detected at lower density ratios that does not conform with the expected one [20].

Recently [26,27] the diameter of drops was measured at the edge of atomizing sprays in the immediate vicinity of the nozzle exit using photographs such as that of Fig. 6. The average diameter is given in Fig. 7 for the con-

ditions of Table 2. When compared with Eq. 16, the measured values exhibit the correct trends with respect to injection velocity, liquid properties and nozzle geometry (it should have no effect and doesn't) but the incorrect one with respect to gas density. Moreover the measured diameters are about a factor of 3 greater than expected. However it would appear that a reasonable explanation for the disagreements exists [27]. The drops that could be and were measured are at the outer edge of the spray and not at their formation sites to which Eq. 16 applies. Due to the high drop number density in the region, it is unreasonable to expect that each drop clears the congested area and comes out without colliding with other drops. When collisions and coalescence are considered, with a model that will be mentioned presently, the discrepancies tend to disappear. It is true, however, that one set of measurements and computations cannot possibly be considered sufficient to close this complex subject.

Finally the data of Hiroyasu et al [19] support the prediction of Eq. 17 with respect to injection velocity and gas density. However the technique they used, based on measurement of the electrical resistance between the nozzle and a screen that could be moved axially, detects any continuous liquid connection between the nozzle and the station of the screen. A ligament or a mixture of liquid and gas would give the same signal as a solid liquid core free of gas. Thus some uncertainty about the structure of the core persists.

Individually any one of the quoted experiments may not provide adequate support for the supplemented aerodynamic theory of atomization. But together they form a rather consistent picture. By comparison, the support for alternative theories is very meager.

THE TRANSIENT

Because of its importance in Diesel engines, many measurements have been reported of the velocity of the tip of atomizing jets [28] and it is generally agreed that it is about 70% of the steady state centerline velocity. But details are anything but clear as indicated, in the first instance, by the lack of consistency in the reported curve fits for the tip velocity. In fact, the transient of round jets has received very little detailed attention.

There seems to have been only one study of the transient of laminar incompressible jets [29] and it concludes with wrong time and length scales for it.[30] Recent measurements [31] of transient incompressible jets were limited in value by complicated nozzle conditions. Recent numerical studies [30] of the transient of laminar, turbulent and spray jets gave reasonably complete information about laminar jets, because there are no uncertain physical parameters for such jets, but only indicative information about turbulent and spray jets, because there are too many uncertain parameters for them.

The diffusive nature of jets makes the identification of their most advanced position a matter of definition and a function of the experimental technique. However it would appear that all jets scale up in time at least approximately. That a scaling exists is shown by pictures, such as those of Fig. 1, and by the many correlations derived from them. That the scaling of sprays is complex, or just an approximation, is indicated by the small probability of the existence of exact similarity solutions of their constitutive equations.

Indeed if we reconsider Fig. 1b and if we define the arrival of the spray as the time at which the centerline velocity first achieves a selected percent

of its steady state value, then we can identify different stages in the propagation that are controlled by different processes and therefore are likely to scale in different ways.

For distances up to several tens of nozzle diameters there is likely to be a compact liquid core that moves at the injection velocity. Its most forward surface, however, encounters the resistance of the ambient gas. A stagnation point can be conceived with gas forcing the liquid to flow radially away from it and then backward. Thus the observed tip velocity will be a function of the injection velocity, the density ratio, and the actual structure of the core.

Eventually the compact core disappears and ligaments and/or drops encounter the ambient gas first. Since drops and gases exchange forces differently than liquid columns and gases, the apparent tip velocity need not scale as it did earlier. At sufficient distance from the nozzle, most of the jet momentum is with the entrained gas and a gaseous head vortex moves into the gaseous environment and exchanges forces with it in a manner which is again different from that of drops and liquid columns. Thus the scaling is likely to be different at different stages of the tip propagation.

Reitz filmed the initial propagation of atomizing jets [8] but he was concerned with an overall description of the process and a broad set of conditions and his data are insufficient to determine accurate correlations for the initial tip speed. Far from the injector, the tip velocity is about 70% of the velocity given by Eqs. 11 and 5 (with x_0 neglected with respect to x or estimated using the data of Wu et al [15]). There is no dependable information for the scaling of the intermediate region and its merging with the other two.

AD-A165 655 STRUCTURE OF HIGH-SPEED SPRAYS(U) PRINCETON UNIV NJ 2/2
DEPT OF MECHANICAL AND AEROSPACE ENGINEERING
F V BRACCO FEB 85 ARO-18333.7-EG DAAG29-81-K-0135
UNCLASSIFIED F/G 21/4 NL

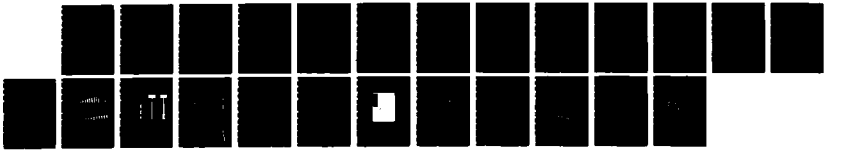

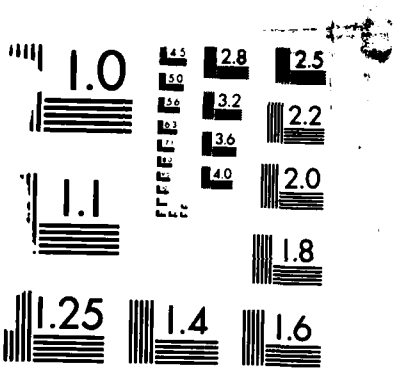

MICROCOPY RESOLUTION TEST CHART
NATIONAL BUREAU OF STANDARDS 1963 A

COMPUTATIONS

A good test of the degree of our understanding of the structure of these sprays is the extent to which we can predict their details.

Navier-Stokes equations for two-phase flows are the appropriate conservation equations [32] but cannot be solved with adequate resolution for the entire flowfield either analytically or numerically [33]. Local averaging and the adoption of semiempirical equations to represent the effects of the neglected details are necessary. Even so no attempt has been made to compute the flow within the nozzle to predict the initial perturbations required by the aerodynamic theory of breakup to account for the effects of the nozzle geometry.

Many difficulties remain even if one considers starting the computations at the nozzle exit from some arbitrary initial perturbations of the liquid gas interface. Not predicted by the linear stability theory, and therefore unknown, are the size and size distribution of the unstable growths at breakup and the time between successive ruptures. Away from the nozzle exit plane, as the generating surface moves closer to the axis of the jet, there are questions as to what gas field is seen by the liquid interface. The velocity of the entrained gas is closer to that of the generating surface. Thus it would appear that the breakup process should become coupled to the structure of the two-phase flow field that exists between the presumed intact core and the unperturbed outer gas. As the relative velocity between liquid and gas decreases inside the jet, larger drops or ligaments or blobs should be formed; just as different breakup modes, and larger drops are found when the injection velocity is decreased, as in going from Fig. 2d to Fig. 2a. Also, coalescence of the liquid fragments can be expected where formation occurs due to the locally large value

of the liquid volume fraction. The net outcome may be the small difference between large formation and coalescence rates. Thus it is clear that Eqs. 15-17 may provide some information about the outcome of the breakup, but in no way do they give all that is necessary.

Faced with so many unknowns, even the most advanced of current spray computations [34], are initiated at some distance from the nozzle from selected drop size and velocity distributions. Then Eqs. 15-17 are used to give limits, average values, and functional dependences. The results should become independent of the details of the initial conditions at large distances from the nozzle. This tends to be the case, for example, for the computed size of the drops when drop collisions and coalescence are included because a higher rate of coalescence is found from smaller initial drops than from larger ones. Since, as previously discussed, the far field is dominated by the entrained gas, the only necessary conditions for the accurate computation of far field mean quantities are knowledge and conservation of axial momentum and proper gas phase turbulent diffusivity [35]. Even those minimal requirements are not met without some care. In general it is difficult accurately to compute the injection momentum of an actual spray even when its mass flow rate is known, because the injection velocity profile is not known (C_m in Eq. 1 is not known even if C_q in Eq. 2 is known). k-ε models can be tuned to give the far field diffusivity of incompressible jets if such diffusivity were known accurately. But this is not the case as shown, for example, by C_t varying within ±10% when different sets of experimental data are used [15]. Successful computations of fluctuations, such as those of the drop velocity, require that the model be accurate also at smaller scales. The comparisons [35] of Fig. 8 and 9 show adequate

reproduction of mean axial velocities but the amplitude of the drop axial velocity fluctuation is underestimated by a factor of two. Several reasons could be advanced for the specific disagreement of Fig. 9 but, ultimately, current quantitative knowledge of the coupling between drop motion and turbulence gas eddies is incomplete [14,36]. A broad review of the many approaches used in modeling sprays and other two-phase flows is given by Faeth [14].

SUMMARY

What is known about the structure of non vaporizing, non reactive sprays from single hole cylindrical nozzles can be summarized with the help of Fig. 10.

At sufficiently high injection velocity the jet is found to diverge immediately at the nozzle exit where fine drops are observed. The outer surface of the liquid is disrupted by the interaction with the ambient gas that leads to the rapid and selective growth of surface waves whose initial amplitudes are controlled by events that occur within the nozzle. This view allows one to predict the initial angle of the spray. The parallel prediction of the size of the drops thus formed also compares favorably with measurements if collisions and coalesce of the drops after their formation are included.

The disruption of the liquid column eventually reaches the axis of the jet, i.e. is complete, because only isolated drops are found downstream. However the geometry, structure, and mode of breakup of the core of the jet are not known, but there are indications that the length of the intact core, x_l, may approach 100 nozzle diameters (versus 10, for incompressible jets).

While the internal breakup continues, gas from the environment is entrained rapidly, the entrained gas eventually becomes dominant and achieves the structure of fully developed incompressible jets. Within it, drops tend to reach

equilibrium but selectivity since both drop and eddy sizes are distributed. The fully developed equilibrium distance, x_2, is several hundred nozzle diameters (versus several tens, for incompressible jets). The virtual origin of this fully developed far field, x_0, is of the order of tens of nozzle diameters (versus order of nozzle diameters, for incompressible jets).

The precise relationship between x_0, x_1, and x_2 and shape of the corresponding boundaries is not known because the structure of the transition region is not known. But the three lengths increase with increasing liquid-gas density ratio.

The propagation velocity of the tip, or head, of these sprays is a fraction of their steady state centerline velocity. In the fully developed equilibrium region this fraction is about 70% but in the development region it is not known. Since the steady state centerline velocity scales in an established way in the fully developed equilibrium region, so does the tip velocity. Experimental information suggests that the steady state centerline velocity and the tip velocity scale also in the development region, at least approximately. But these scaling functions are determined by the structure of the development region and therefore are not known precisely.

ACKNOWLEDGEMENTS

Support for this review was provided by the Army Research Office (DAAG 21-81-K-0135) and the Department of Energy (DE-AC-04-81AL16338).

REFERENCES

1. E. Giffen and A. Muraszew, The Atomization of Liquid Fuels, John Wiley and Sons Inc., N.Y., N.Y. (1953).

2. W.R. Marshall, Jr., Atomization and Spray Drying, AIChE Monograph Series, 50 (2)(1954).

3. N. Dombrowski and G. Mundy, Spray Drying, Biochemical and Biological Engineering Science, 22, Academic Press, N.Y., N.Y. (1968).

4. H. Schlichting, Boundary-Layer Theory, McGraw-Hill Book Co., N.Y., N.Y. (1968).

5. J.O. Hinze, Turbulence, McGraw-Hill Book Co., N.Y., N.Y. (1975).

6. G.N. Abramovich, The Theory of Turbulent Jets, The M.I.T. Press, Cambridge, Massachusetts (1963).

7. W. Rizk, Experimental Studies of the Mixing Processes and Flow Configurations in Two-Cycle Engine Scavening, Proc. Inst. Mech. Eng., 172, 417-437 (1958).

8. R.D. Reitz and F.V. Bracco, Ultra-High-Speed Filming of Atomizing Jets,

Phys. Fluids, 22, 1054-1064 (1979).

9. V.G. Levich, Physicochemical Hydrodynamics, Prentice-Hall, Englewood Cliffs, N.J. (1962).

10. R.E. Phinney, The Breakup of a Turbulent Liquid Jet in a Gaseous Atmosphere, J. Fluid Mech., 60, 689-701 (1973).

11. R.D. Reitz and F.V. Bracco, Mechanism of Atomization of a Liquid Jet, Phys. Fluids, 25, 1730-1742 (1982).

12. M.W. Thring and M.P. Newby, Combustion Length of Enclosed Turbulent Jet Flames, 4th Symposium on Combustion, Williams and Wilkins Co., Baltimore, MD, 789-796 (1953).

13. G. Kleinstein, Mixing in Turbulent Axially Symmetric Free Jets, J. Spacecraft, 1, 403-408 (1964).

14. G.M. Faeth, Evaporation and Combustion of Sprays, Progress in Energy and Combustion Science, 9, 1-76 (1983).

15. K.-J. Wu, A. Coghe, D.A. Santavicca, and F.V. Bracco, LDV Measurements of Drop Velocity in Diesel-type Sprays, to appear in the AIAA Journal.

16. I. Wygnanski and H. Fiedler, Some Measurements in the Self Preserving Jet, J. Fluid Mech., 38, 577-612 (1969).

17. S. Corrsin and M.S. Uberdi, Further Experiments on the Flow and Heat Transfer in a Heated Turbulent Air Jet, NACA TR998 (1950).

18. S.P. Capp and W.K. George, Jr., Measurements in an Axisymmetric Jet Using a Two-Color LDA and Burst Process, Int. Symp. on Appl. of LDA to Fluid Mech., Lisbon, Portugal (1982).

19. H. Hiroyasu, M. Shimizu, and M. Arai, The Breakup of High Speed Jet in a High Pressure Gaseous Atmosphere, ICLASS-82, Madison, WI (1982).

20. K.-J. Wu, C.-C. Su, R.L. Steinberger, D.A. Santavicca, and F.V. Bracco, Measurements of the Spray Angle of Atomizing Jets, J. of Fluids Engineering, 105, 406-413 (1983).

21. R.A. Castleman, Jr., The Mechanism of Atomization Accompanying Solid Injection, NACA Report No. 440 (1932).

22. W.E. Ranz, Some Experiments on Orifice Sprays, Can. J. Chem. Eng. 36, 175-181 (1958).

23. G.K. Batchelor (Editor), Collected Works of G.I. Taylor, Cambridge Univ. Press, Cambridge, Mass. (1958).

24. R.D. Reitz, Atomization and Other Breakup Regimes of a Liquid Jet, Ph.D. Thesis No. 1375, Department of Mechanical and Aerospace Engineering, Princeton University, Princeton, N.J. (1978).

25. R.D. Reitz and F.V. Bracco, On the Dependence of the Spray Angle and Other Spray Parameters on Nozzle Design and Operating Conditions, SAE Paper No. 790494 (1979).

26. K.-J. Wu, Atomizing Round Jets, Ph.D. Thesis No. 1612, Department of Mechanical and Aerospace Engineering, Princeton University, Princeton, N.J. (1983).

27. K.-J. Wu, R.D. Reitz, and F.V. Bracco, Drop Sizes of Atomizing Jets, to be published.

28. N. Hay and P.L. Jones, Comparison of the Various Correlations for Spray Penetration, SAE Paper No. 720776 (1972).

29. S. Abramovich and A. Solan, The Initial Development of a Submerged Laminar

Round Jet, J. Fluid Mech, 59, 791-801 (1973).

30. T.-W. Kuo and F.V. Bracco, On the Scaling of Transient Laminar, Turbulent, and Spray Jets, SAE Paper No. 820038 (1982).

31. P.O. Witze, The Impulsively Started Incompressible Turbulent Jet, SANDIA 80-8617 (1980).

32. F.A. Williams, Combustion Theory, Addison-Wesley Publ. Co., Reading, MA (1965).

33. F.V. Bracco, Introducing a New Generation of More Detailed and Informative Combustion Models, SAE Transactions, 84, 3317-3340 (1975).

34. P.J. O'Rourke and F.V. Bracco, Modelling of Drop Interactions in Thick Sprays and a Comparison with Experiments, I Mech E, ISBM 0 85298 469 3, 101-116 (1980).

35. L. Martinelli, R.D. Reitz, and F.V. Bracco, Comparisons of Computed and Measured Dense Spray Jets, 9th Int. Coll. on Dyn. of Explosions and Reactive Systems, Poitiers, France (1983). Proceedings to appear in the AIAA Progress in Astronautics and Aeronautics Series.

36. S.E. Elghobashi and T.W. Abou-Arab, A Two-Equation Turbulence Model for Two-Phase Flows, The Physics of Fluids, 26, 931-938 (1983).

Table 1: Spray Conditions for the Drop Velocity Measurements of Figs. 3, 8, and 9 (from Ref. 15)

Series	P_g (MPa)	ρ_g/ρ_ℓ	Δp (MPa)	$\overline{V}_{inj}$ (m/s)	Nozzle d(μm)-L/d	X/d
A	1.48	0.0256	11.0	127	127-4	600,800
B	4.24	0.0732	11.0	127	127-4	300,400,500,600
C	4.24	0.0732	26.2	194	127-4	400,500,600
D	4.24	0.0732	11.0	149	76-4	300,600,700,800
E	1.48	0.0256	11.0	125	76-1	300

Liquid : n-hexane, $\rho_\ell = 665$ kg/m^3, $\mu_\ell = 3.2 \times 10^4$ N·s/m^2, $\sigma_\ell = 1.84 \times 10^2$ N/m. Gas : nitrogen. Room temperature.

Table 2: Spray Conditions for the Drop Size Measurements of Figs. 6 and 7 (From Refs. 26, 27)

Series	Nozzle L-d (μm)	P_g (MPa)	ρ_g (kg/m^3)	Liquid	Δp (MPa)	$\bar{V}_{inj}$ (m/s)	C_D	Re_j x10^{-4}	We_j x10^{-4}	No of Drops
1	335-4	1.48	17.0	n-C6H14	1.38	59.4	0.92	4.14	4.26	119
2	335-4	2.86	33.0	n-C6H14	1.38	52.4	0.81	3.65	3.32	109
3	335-4	1.48	17.0	n-C6H14	3.45	79.2	0.78	5.51	7.58	116
4	335-4	2.86	33.0	n-C6H14	3.45	92.8	0.91	6.46	10.41	111
5	335-4	1.48	17.0	n-C6H14	6.90	99.0	0.69	6.89	11.85	107
6	335-4	2.86	33.0	n-C6H14	6.90	111.0	0.77	7.73	14.89	117
7	335-10	1.48	17.0	n-C6H14	3.45	79.2	0.78	5.51	7.58	119
8	127-4	1.48	17.0	n-C6H14	3.45	78.1	0.77	2.06	2.79	114
9	335-4	1.48	17.0	n-C14H30	3.45	81.2	0.86	0.95	6.31	103

FIGURE CAPTIONS

FIG. 1 Development of: a) a turbulent incompressible jet [7] (water in water, $Re_D = 4\ 10^4$); and b) an atomizing spray [8] (50% glycerol + 50% water into N_2)

FIG. 2 Some regimes of breakup of liquid jets [8]

FIG. 3 Mean axial drop velocity and amplitude, skewness, and flatness of the fluctuation of the axial drop velocity for the atomizing sprays [15] of Table 1.

FIG. 4 Initial angle of atomizing jets versus density ratio with fixed nozzle geometry. Injections of glycerol-water, water, hexane, tetradecane into N_2, H_e, X_e, Ar at liquid pressures of 500-13,300 psi and D = 254, 343, and 610 μm. Room temperature [20].

FIG. 5 Initial angle of atomizing jets versus nozzle length-to-diameter ratio: ○ from Ref. 20; × from Ref. 19.

FIG. 6 Edge of spray and droplets in the immediate vicinity of the nozzle exit for an atomizing jet [26-27].

FIG. 7 Average diameter of drops in the immediate vicinity of the nozzle exit for the atomizing jets of Table 2: ○ measured; ● expected trends from the supplemented aerodynamic theory [26-27].

FIG. 8 Measured[15] mean axial drop velocity and computed [35] mean axial drop and gas velocities for Spray A of Table 1.

FIG. 9 Measured [15] amplitude of the fluctuation of the axial drop velocity and computed [35] amplitudes of the fluctuations of the axial drop and gas velocities for Spray C of Table 1.

FIG. 10 Schematic structure of atomizing jets.

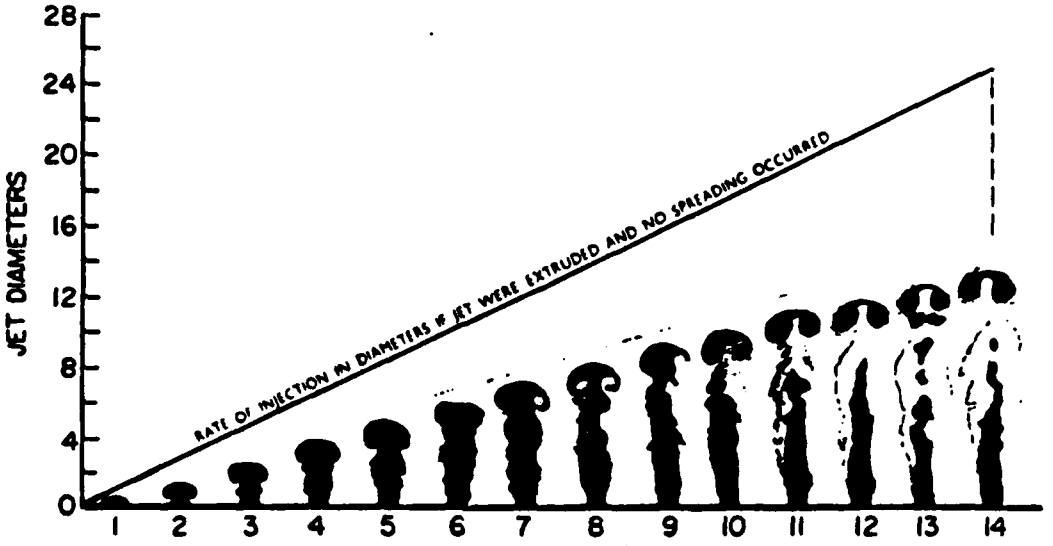
JET DIAMETERS
28
24
20
16
12
8
4
0
RATE OF INJECTION IN DIAMETERS IF JET WERE EXTRUDED AND NO SPREADING OCCURRED
1 2 3 4 5 6 7 8 9 10 11 12 13 14

(a)

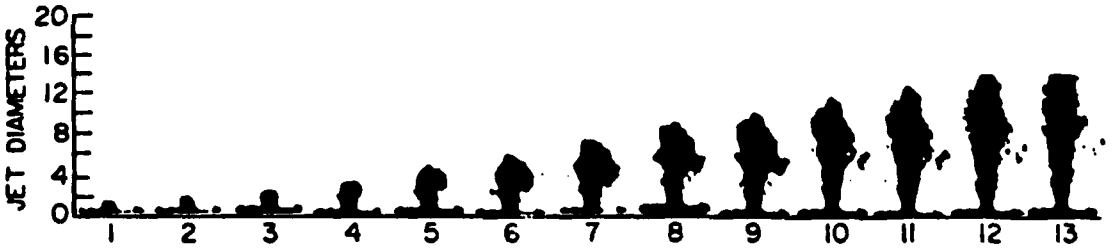
JET DIAMETERS
20
16
12
8
4
0
1 2 3 4 5 6 7 8 9 10 11 12 13

(b)

FIG.
Bracc

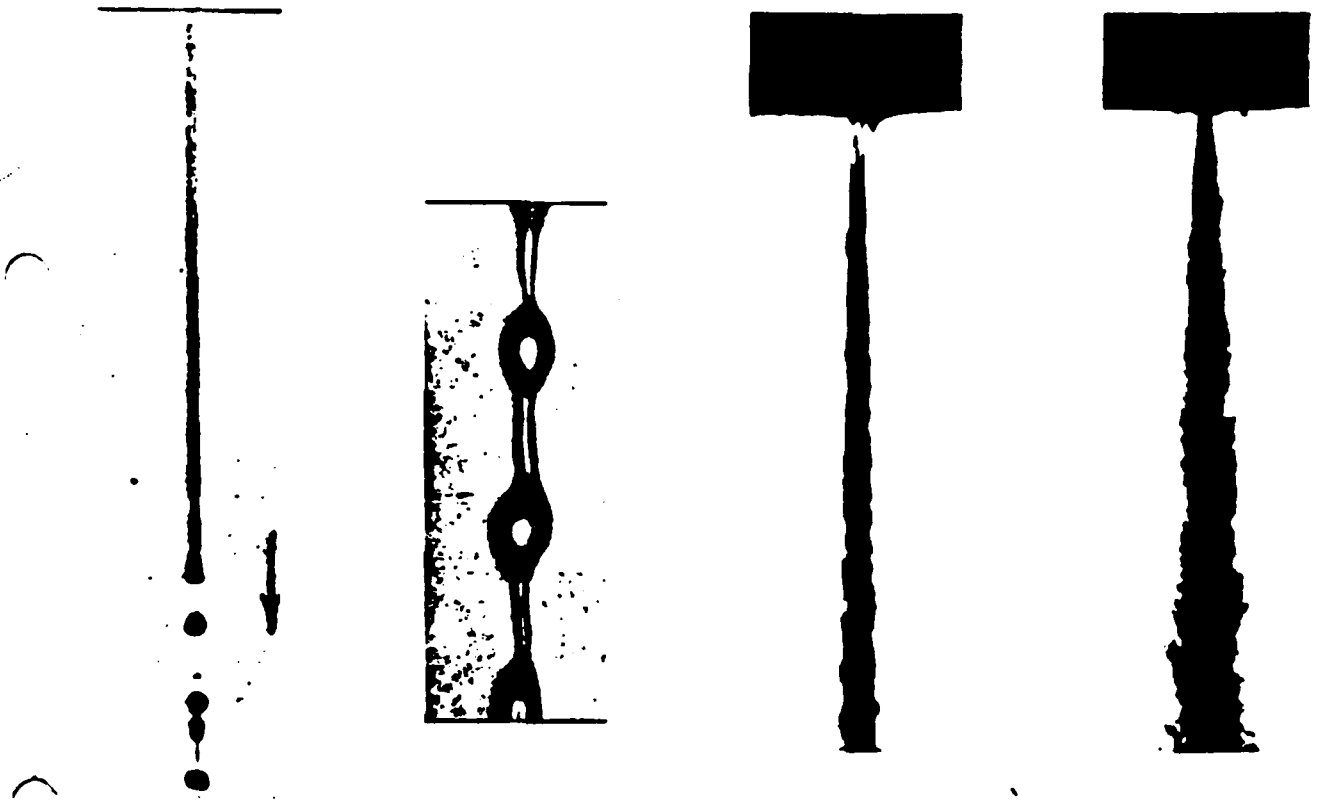

FIG. 2
Bracco

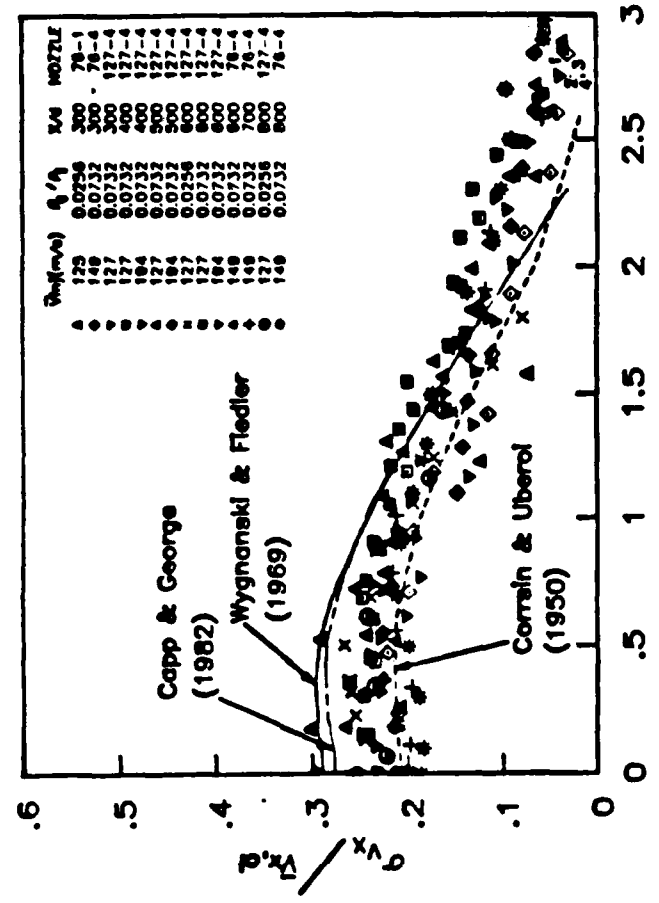
Capp & George (1982)
Wygnanski & Fiedler (1969)
Corrsin & Uberoi (1950)
r / r0.5

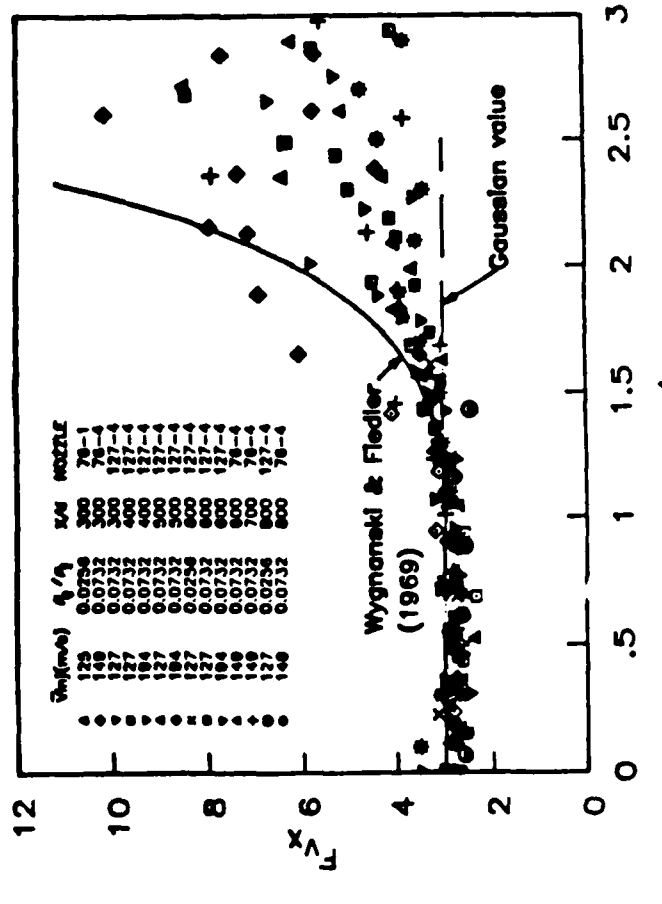
Wygnanski & Fiedler (1969)
Gaussian value

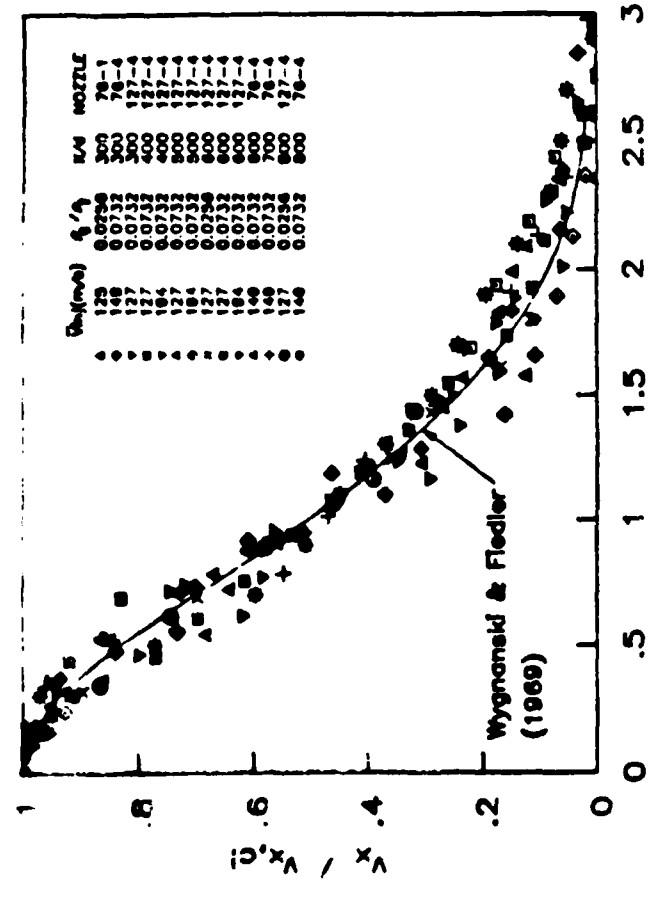
Wygnanski & Fiedler (1969)
r / r0.5

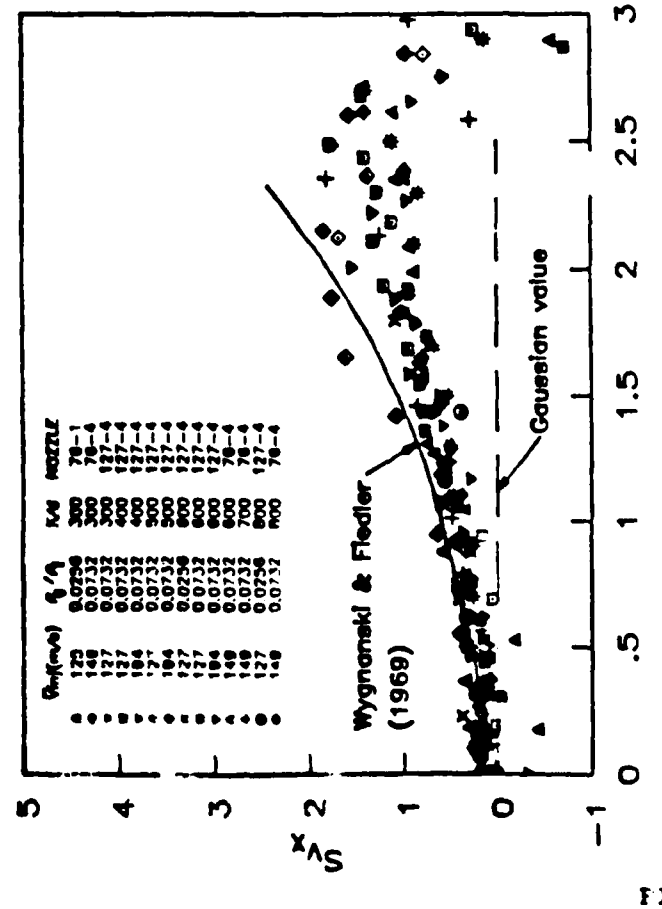
Wygnanski & Fiedler (1969)
Gaussian value

FI
By

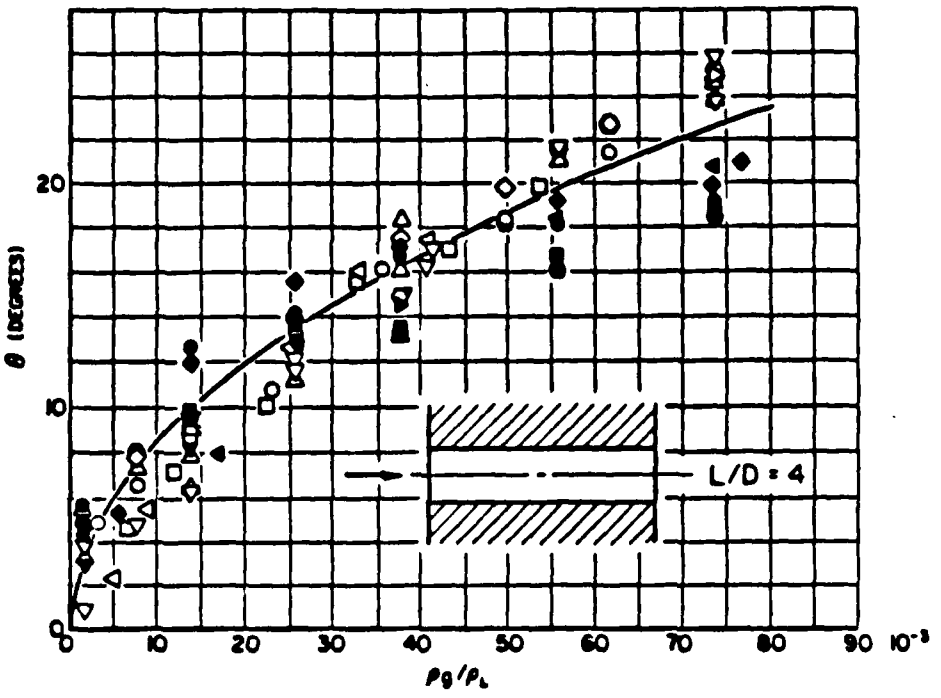

FIG. 4
Bracco

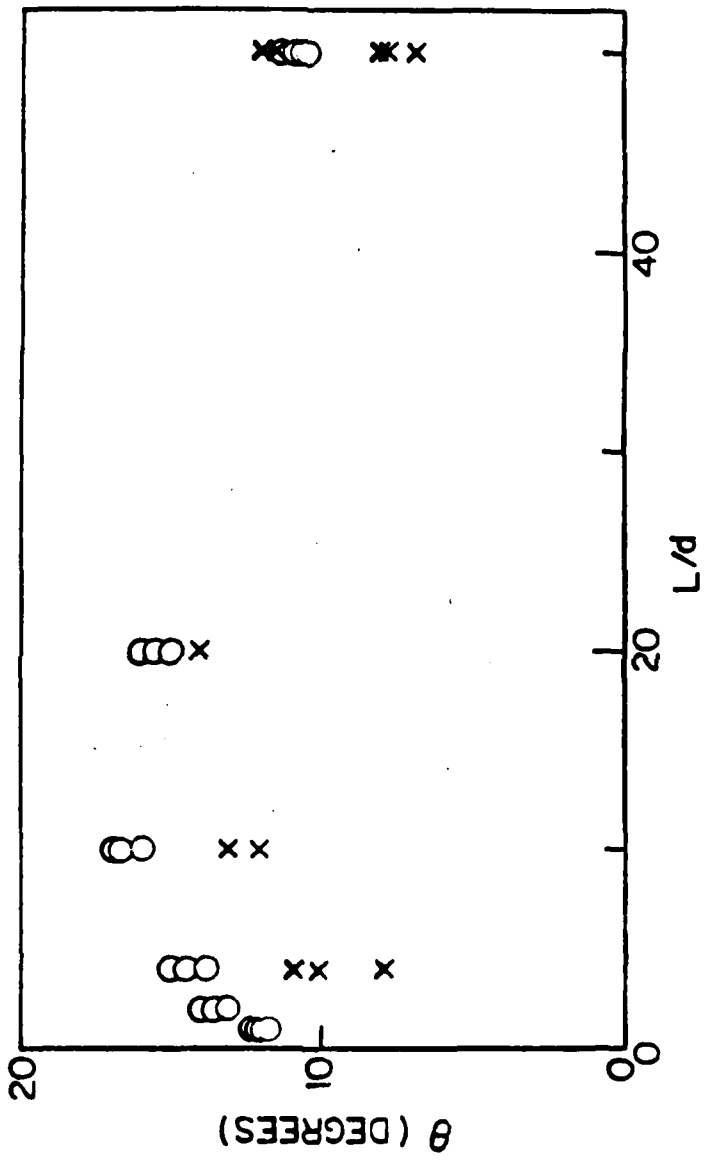

FIG. 5
Braccc

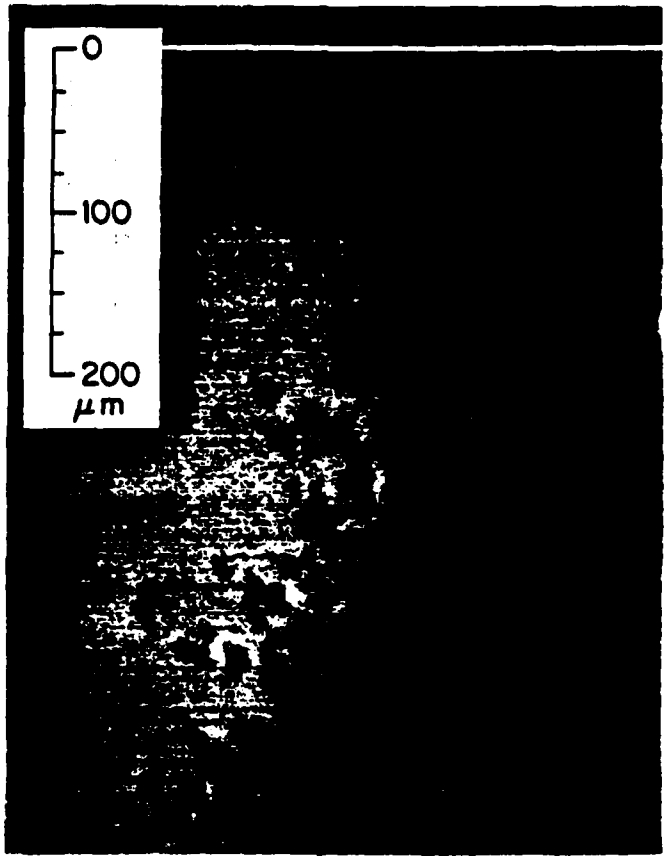

FIG. 6
Bracco

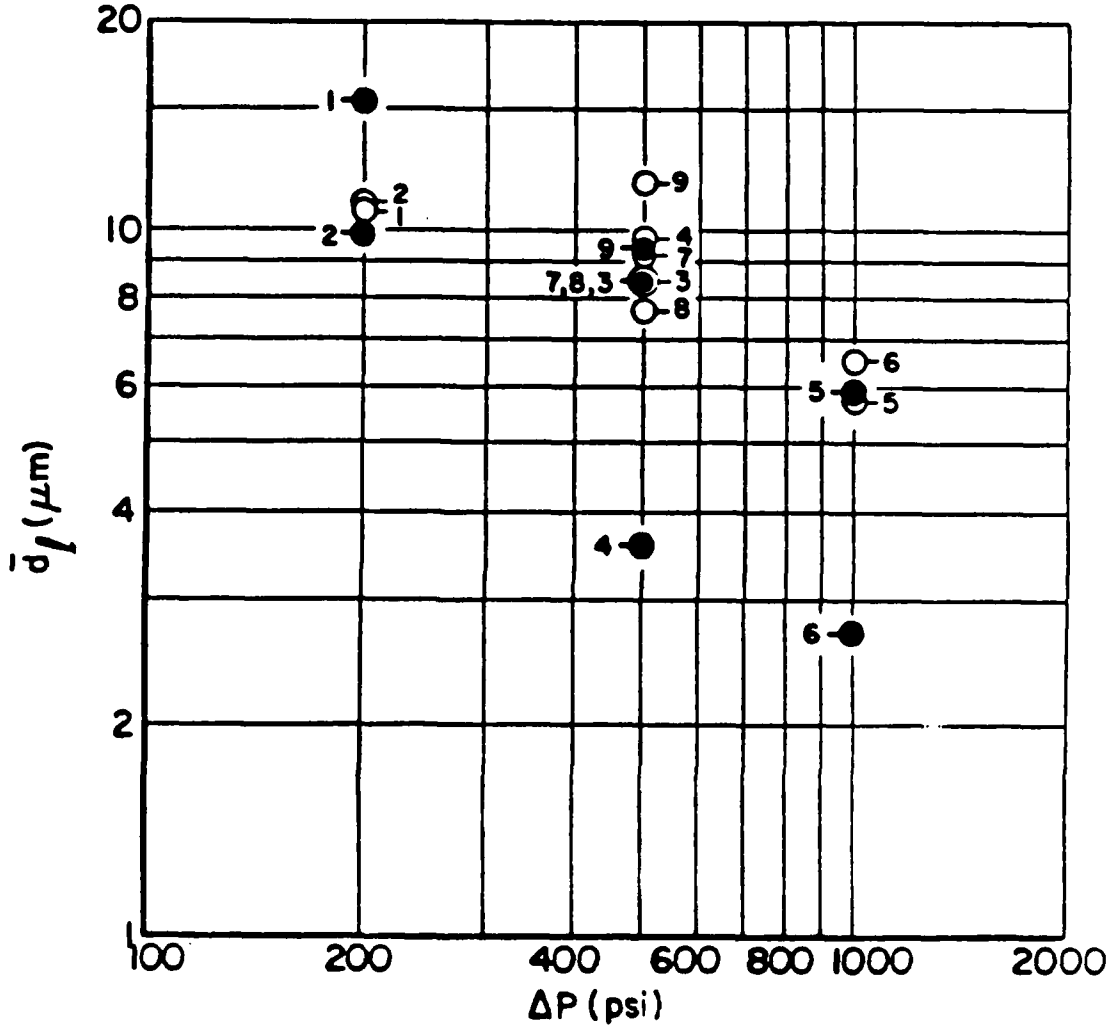
20
10
8
6
4
2
100
200
400
600
800
1000
2000
ΔP (psi)
$\bar{d}_f$ (μm)
1
2
2
1
9
9
4
7
7,8,3
3
8
6
5
5
4
6

FIG. 7
Bracco

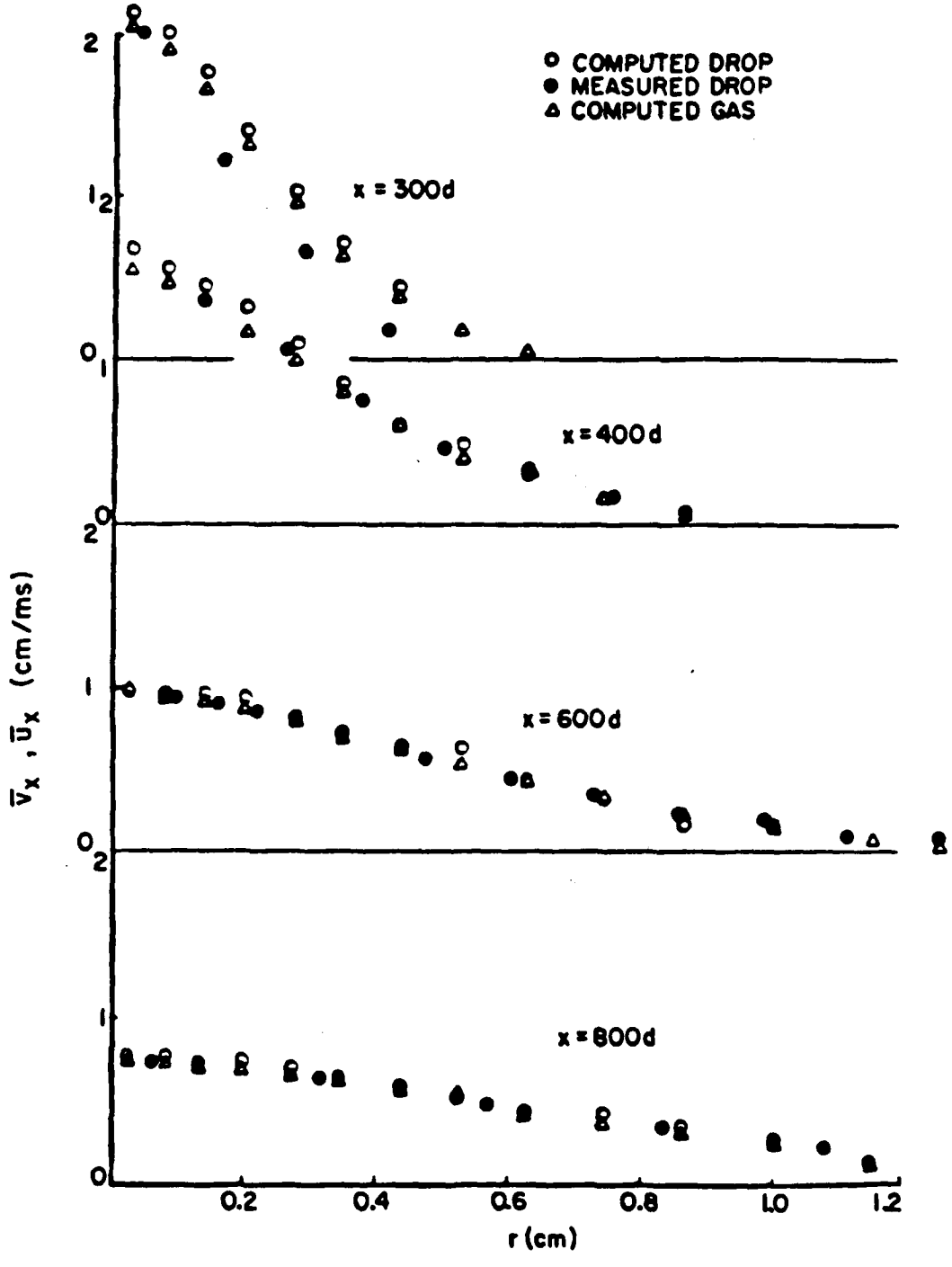
COMPUTED DROP
MEASURED DROP
COMPUTED GAS
x = 300d
x = 400d
x = 600d
x = 800d
$\bar{v}_x$, $\bar{u}_x$ (cm/ms)
r (cm)
0.2
0.4
0.6
0.8
1.0
1.2

FIG. 8
Bracco

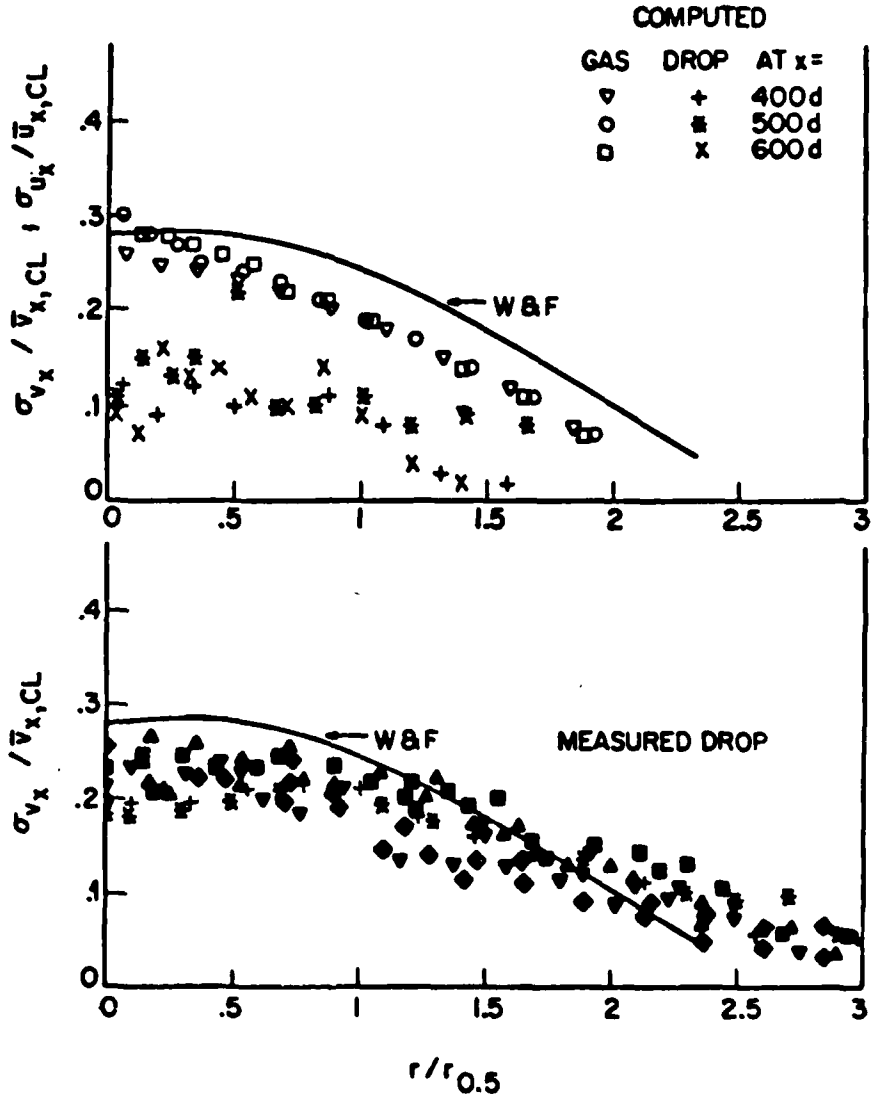
COMPUTED
GAS DROP AT x=
400d
500d
600d
W&F
MEASURED DROP
$\sigma_{v_x} / \bar{v}_{x,CL}$; $\sigma_{u_x} / \bar{u}_{x,CL}$
$\sigma_{v_x} / \bar{v}_{x,CL}$
$r/r_{0.5}$
0
.1
.2
.3
.4
.5
1
1.5
2
2.5
3

FIG. 9
Bracco

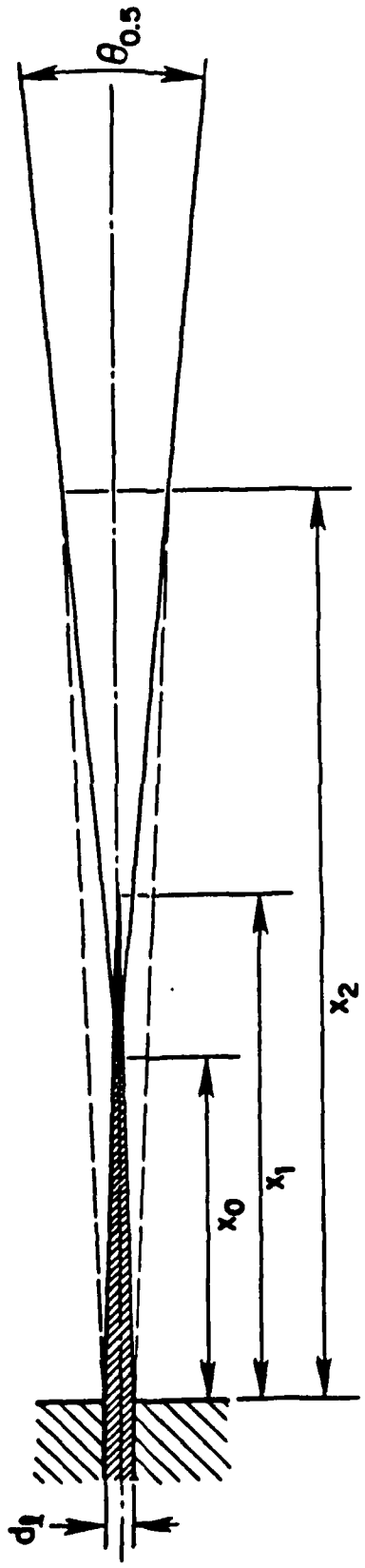

FIG. 10
Bracco

DTIC

END

4-86